Statistical analysis and prediction of climate impacts on sugarcane yield in southeastern Africa

By

Thulebona Wellington Mbhamali

A dissertation submitted in
fulfilment of the degree of Master of Science

Department of Geography and Environmental Studies
Faculty of Science and Agriculture at the
UNIVERSITY OF ZULULAND
KWADLANGEZWA

APRIL 2018

ENDORSEMENT

Supervisor:	Prof. Mark R. Jury
	Department of Physics
	University of Puerto Rico Mayaguez
Co-Supervisor:	Dr. Nkanyiso B. Mbatha
	Department of Geography and Environmental Studies
	University of Zululand

DECLARATION

I, Thulebona Wellington Mbhamali, solemnly affirm that this full dissertation is submitted for the degree of Master of Science in Geography (MSc Geography) in the Faculty of Science and Agriculture, University of Zululand, KwaDlangezwa, KwaZulu-Natal, South Africa, 2018.

I confirm that this research project is my own work, although supervisors have provided guidance. It has not been submitted before for any other qualification, part of a degree, or examination at this or any other institution of higher learning.

..………………………. ……………………….

Thulebona Wellington Mbhamali

Date

ACKNOWLEDGEMENTS

I would like to express my heartfelt gratitude to the following individuals and institutions, supervisors, and meteorological and sugarcane yield data sources for playing a tremendous role in providing me with scholarly resources and data which assisted me to effectively complete the dissertation:

- Prof. Mark R. Jury, Professor of Meteorology in the Department of Physics at the University of Puerto Rico Mayaguez and Research Fellow at the University of Zululand, for supervising the dissertation. With his input the dissertation achieved a successful result, and he is deserving acknowledgement.
- Dr. Nkanyiso B. Mbatha, Senior Lecturer in the Department of Geography and Environmental Studies, University of Zululand, who participated in the supervisory board, with constructive criticism and support during the research study, which helped towards its completion. Therefore, his invaluable contribution will not go unnoticed.
- All colleagues in the Department of Geography and Environmental Studies at the University of Zululand for encouragement and support during difficulty and hard times of the study.
- Mr. S Xulu and Mr. KG Makwela for helping me with the delimitation and description of the study area.
- I acknowledge several datasets, tools of analysis, models and data sources used in this study: GPCC V8, CRU TS4.1, scPDSI datasets derived via KNMI Climate Explorer, CPC for SOI data, NCEP/NCAR data for mapping meteorological parameters, SASA and FAO for sugarcane yield data, the PDSI for analysis of water balance as a proxy of sugarcane yield, DWS for pan evaporation data, CRU, University of East Anglia for temperature data, the IRI Climate Library for NDVI vegetation fraction, and the Morlet wavelet spectral analysis used to determine rainfall and sugarcane yield cycles.

DEDICATION

This dissertation is dedicated to my late father (Mr Michael K. Mbhamali), my mother (Mrs Phumzile T. Mbhamali) and my three children, Khono (son), Cogent (daughter) and Nqaba (son).

NOTE

Some parts of this work were presented at the 33rd and 34th annual conferences of SASAS hosted by the University of Venda 21-22 September 2017 and the University of KwaZulu-Natal 20-21 September 2018, respectively. The extended abstracts are listed in the conference proceedings and available at: https://www.sasas.org.

ABSTRACT

Sugarcane production is chiefly influenced by climate, but there are also farming operations that diminish the sugarcane yield. The study concentrated on discovering the statistical relationship between the climate and subsequent sugarcane yield by statistical analysis of monthly and annual data averaged over the area 31-23°S and 28-33°E in the period from 1970-2016 with respect to FAO data and 1988-2010 for SASA data.

R procedures were employed to derive statistical associations between sugarcane yield and climate variables and indices. Time series analysis was performed, including Mann-Kendall tests for trend detection, Pearson correlation and MLR for exploring the statistical links between yield and climate parameters. Moreover, the spatio-temporal correlations and regressions were performed between the sugarcane yield index and relevant local crop drivers such as rainfall and temperature, and the global sea surface temperatures and winds through online tools.

The results demonstrated a downward trend in sugarcane yield over SE Africa as signalled by $z \approx -4$ for FAO time series and $z \approx -2$ for SASA yield data at 95% level. Time series analysis showed high influence of local climate indices such as PDSI (e.g $r \approx +0.7$) with global sugarcane yield, and the value increased to $r \approx +0.80$ locally (e.g in South Coast region).

A positive correlation for rainfall ($r > +0.5$) and negative for temperature ($r < -0.5$) conditions in the preceding December to May with the harvested sugarcane yield in the spatial analysis was observed. Hence, it is understood that high temperatures induced by offshore air flow and low pressure tend to suppress sugarcane yield, and correspond with rainfall below 1000 mm/yr. The surface air temperature is by far the most important indicator of sugarcane yield in ESwatini while PDSI explains most of the yield variation in South Africa. The findings show that climate influences on sugarcane yield cover 40-80% of variance, and that the decline and variability of sugarcane production has distinct climatic factors. Meridional wind flow over the western Indian Ocean and anticyclonic circulation in the Mozambique Channel manifest themselves as key climatic features for sugarcane production over SE Africa. Recommendations for ways to mitigate and adapt to climate variability are given to benefit the sugar industry in southeastern Africa. In addition, a statistical model to predict sugarcane yield over the study area was developed through MLR algorithms extracted from large-scale climate drivers.

Key words: Climate impacts, PDSI, Temperature, Precipitation, ENSO, Sugarcane yield

LIST OF FIGURES

LIST OF TABLES

ACRONYMS AND ABBREVIATIONS

AL – Angola Low

APSIM – Agricultural Production Systems Simulator

APSRU – Agricultural Production Systems Research Unit

AVHRR – Advanced Very High Resolution Radiometer

BUH – Botswana Upper High

CMIP3 – third Coupled Model Intercomparison Project

CMIP5 – fifth Coupled Model Intercomparison Project

CO – Carbon Monoxide

CO_2 – Carbon Dioxide

CPC – Climate Prediction Centre

CRU – Climate Research Unit

CSIRO – Commonwealth Scientific Industrial Research Organisation

DAAC – Distributed Active Archive Center

DJF – December-January-February

DMI – Dipole Mode Index

DSYI – Detrended sugarcane yield index

DWS – Department of Water and Sanitation

E – Evaporation

ECMWF– European Centre for Medium-Range Weather Forecasts

ENSO – El Niño Southern Oscillation

ERA-Interim – Emergency Response Activities

ERSST – Extended Reconstructed Sea Surface Temperature

FAO – Food and Agriculture Organisation

GDP – Gross Domestic Product

GPCC – Global Precipitation Climatology Centre

H – High Pressure

HadSLP2 – Hadley Centre Sea Level Pressure

I – Infiltration

IOD – Indian Ocean Dipole

IPCC – Intergovernmental Panel on Climate Change

IRI – International Research Institute of Climate Library

JJA – June-July-August

KNMI – Royal Netherlands Meteorological Institute

KNMI-CE – Koninklijk Nederlands Meteorologisch Instituut Climate Explorer

KZN – KwaZulu-Natal Province
LOESS – Locally Estimated Scatterplot Smoothing
MAM – March-April-May
MAP – Mean Annual Precipitation
MATLAB – Matrix Laboratory
MERRA2 – Modern-Era Retrospective for Research and Applications, Version 2
MJO – Madden–Julian–Oscillation
MLR - Multiple Linear Regression
MODIS – Moderate Resolution Imaging Spectroradiometer
NASA – National Aeronautics and Space Administration
NCAR – National Center for Atmospheric Research
NCEP – National Centers for Environmental Prediction
NDVI – Normalized Difference Vegetation Index
NESDIS – National Environmental Satellite, Data, and Information Service
NOAA – National Oceanic and Atmospheric Administration
OLR – Outgoing Longwave Radiation
ONI – Ocean Niño Index
P – Precipitation
PCC – Pearson Correlation Coefficient
PDSI – Palmer Drought Severity Index
QBO – Quasi-Biennial Oscillation
r – Correlation
R – Programming Language
R – Runoff
R^2 – Correlation coefficient
RSSC – Royal Swaziland Sugar Corporation
S_1 – Initial Soil Water
S_2 – Final Soil Water
SA – South Africa
SAF – Society of American Foresters
SAH – South Atlantic High
SASA – South African Sugar Association
SASAS – South African Society of Atmospheric Sciences
SASRI – South African Sugarcane Research Institute
SEIO – Southeast Indian Ocean
SHF – Sensible Heat Flux

SIH – South Indian High
SLP – Sea Level Pressure
SOI – Southern Oscillation Index
SON – September-October-November
SST – Sea Surface Temperature
STAR – Satellite Applications and Research
Swazi – ESwatini
TS – Time Series
UCAR – University Corporation for Atmospheric Research
UN – United Nations
USGS – United States Geological Survey
V – Version
VHP – Vegetation Health Product

CONTENTS

CHAPTER 1

INTRODUCTION AND BACKGROUND

1.1 Introduction

This study focuses on the sugarcane growing regions of eastern South Africa and ESwatini. The research was intended to boost scientific understanding of climatic factors affecting sugarcane yield, extending previous work undertaken (Inman-Bamber, 1995; Dube, 1998; Bezuidenhout & Schulze, 2006; Schulze & Kunz, 2010; Jones, *et al.,* 2015). This study fills gaps in knowledge on the degree of association and its extent between different meteorological parameters (rainfall, soil moisture, surface air temperature, SHF, evaporation, surface pressure and geo-potential height, SST and wind) and sugarcane yield.

The study period is from 1970 to 2016, subject to sugarcane yield and meteorological data available in the study area. During this time there was a variety of climatic conditions, from the severe droughts of 1983 and 1992, to the floods of 1984 and 2000.

1.2 Background

The southeast coast of South Africa is characterised by dependable rainfall (Weldon & Reason, 2014; Chikoore, 2017), but with a degree of variability that affects crop yield (Jury, 2002). Rainfall is a heterogeneous and intermittent meteorological parameter (Everingham, *et al*., 2002), but soil moisture and vegetation integrate and moderate its influence (Pielke, 2001). Variations in crop production may be useful indicators of climatic anomalies that involve departures of rainfall and temperature from long-term averages (FAO, 2015).

Sugarcane is grown in 70 countries, mainly in latitudes below 25° (Knew, 2015). In northern KwaZulu-Natal sugarcane (*Saccharum officinarum L.*) of the *Poaceae* family *(*grass) is commercially grown using mechanised industrial methods that are marginally profitable. In KwaZulu-Natal high altitudes regions such as the Midlands, rain-fed sugarcane is harvested some 18 to 24 months later. This is partially due to the cool and relatively dry climate (Inman-Bamber, 1995; van den Berg & Singels, 2013). In areas near the coast (North and South Coast regions), the sugarcane is rain-fed, but further inland in the northern KwaZulu-Natal (e.g. in Pongola), Mpumalanga, and eSwatini sugarcane is completely irrigated under hot and dry weather conditions. Some irrigation schemes are also reported in the Zululand region. The crop cycle is longer at higher elevations with cooler weather conditions (Keeping & Meyer, 2006), and this is analogous to the SASA review of 2012 (van den Berg & Singels, 2013).

The sugarcane production and yield (tons per hectare) are chiefly influenced by climatic factors. There are also farming operations (planting, weeding, fertilising, pests, harvesting methods, and the *mosaic* virus) that diminish sugarcane yield (Viswanathan, *et al*., 2007; Adams & Carstens, 2012).

The South African Weather Service derives climate outlooks, including crop yield forecasts (Bezuidenhout & Schulze, 2006), which are based on numerical models. Crop modelling and seasonal climate forecasts help farmers to prepare adaptation and mitigation strategies during extreme weather conditions such as drought. In addition to numerical models, there are statistical or probabilistic models that forecast the annual sugarcane production (Promburom, *et a*l., 2001; Potgieter, *et al*., 2003). These forecasts increased the value of total production of the sugar industry by $4.2 M/yr in 2004 (Bezuidenhout, 2005).

Efforts to introduce seasonal climate forecasts for improved risk management in agriculture, particularly of perennial crops such as sugarcane, started in the 1990s (Hansen, *et al*., 1998; Everingham, *et al*., 2002). The prediction of seasonal rainfall depends on teleconnections between ocean heating and atmospheric circulations (Chikoore, 2005). This can enhance agricultural management and aid in proactive preparations such as improving sugarcane varieties which can resist drought.

The use of climate and weather information to guide daily and seasonal agricultural schedules is now common in South Africa’s commercial farming communities. When a dry or wet season is predicted, farmers can switch crop types and area planted (Ummenhofer, *et al*., 2015).

1.3 Statement of the problem

The Umfolozi Sugar Mill had approximately 50 000 small-scale sugarcane growers during the early 2000s. The number dropped to 21 110 in the 2014/15 season with only 12 507 growers actually submitting sugarcane to the mill (Dubb, 2015). This reduction was partially due to the weak economic value and marginal profitability of sugarcane and also because of drought conditions that affected sugarcane production (Dubb, 2015; SASA, 2015). According to Dube (1998), drought conditions in the 1982/83 and 1992/93 seasons had similar impacts on sugarcane yield, and a huge decrease in sugarcane production was experienced across the Mpumalanga and KwaZulu-Natal Provinces during that period.

Scientific studies using future climate projections indicate disparate trends in the yield of sugarcane in southern Africa and in Brazil some studies suggest increase (Marin, *et al*., 2013; Jones, *et al*., 2015), while some suggest decrease (Deressa, *et al*., 2005; Knox, *et al.,* 2010; Chandiposha, 2013). In the description of sugarcane models, it is not well specified which meteorological variables were fitted into the models, and presumably there could be under-fitting problems.

Weather and climate information has been extensively used for maize yield projections, but not so much for sugarcane (Jones & Thornton, 2003; Mkhabela, *et al.,* 2005; Tadross, *et al.,* 2005; Abraha & Savage, 2006). These studies show that the rainfall, temperature and agro-climate of the preceding season are significant for maize-growing in southern Africa.

In this study, the extent to which climate affect sugarcane yield was explored using the statistical methods such as correlation and regression. A new model for sugarcane-PDSI was developed, which linked the known climate features for sugarcane production with various climate variables and indices which have never used for sugarcane modelling. This was done in order to improve and address under-fitting in previously used models. This was achieved through step-wise regression, cross correlation and screening. Moreover, the study stimulates the ambition and desire to study the application of climate science in sugarcane production using data from public databases such as FAO and KNMI-CE.

1.4 The main aim of the study

The main aim of this study was to investigate the influence of climatic variables on sugarcane yield in eastern South Africa and ESwatini from 1970 to 2016. The main focus was exploration of the degree of association between climate and yield and the extent to which past climate affects yield. The study was conceptually limited to climate impacts, as outlined in previous studies that relate hot weather conditions and frequent dry spells (Selvaraju & Baas, 2007; Tadross, *et al.,* 2011; Field, 2012) to reduced vegetation growth (Bradshaw-Rouse & Judith, 2015). Non-climatic factors were considered, but they were not a focus of this research.

1.5 Objectives of the study

The specific objectives of the study were:

a) To investigate climate patterns and trends in the sugarcane production area (31-23°S and 28-33°E) from 1970 to 2016.
b) To document global and regional climate impacts in the sugarcane yield over the eastern part of South Africa and ESwatini.
c) To develop a statistical technique to predict sugarcane yield from large-scale climate drivers.
d) To evaluate future projections of climate relevant to sugarcane production using IPCC CMIP5 model simulations from 1970-2050.

1.6 Key research questions

a) To what extent do climatic factors affect annual sugarcane yield in the eastern part of South Africa and ESwatini?
b) What are other key climate features for sugarcane growing, in addition to rainfall and temperature over southeast Africa?

1.7 Hypothesis statements

The eastern seaboard of SE Africa (31-23°S and 28-33°E) experiences austral summer rainfall from November to March (Dube, 1998). In some years, rainfall is diminished, such as 1992/1993, 2014/15 (Dubb, 2015) and 2015/16, so sugarcane yields are suppressed. It is hypothesised that:

a) Meteorological conditions that inhibit rainfall in eastern South Africa and ESwatini will cause a subsequent decline in annual sugarcane yield, which detrimentally affects the local economy.

b) Years of strong El Niño events and severe droughts are followed by low sugarcane yields. Regional controls on the uptake of Pacific climate signals also include the Indian Ocean Dipole and Quasi-Biennial Oscillation.

1.8 Delimitation of the study area

The study area comprises of ESwatini and two major sugarcane producing provinces (Mpumalanga and KwaZulu-Natal) in South Africa that are vulnerable to rainfall variability (Gbetibouo & Hassan, 2005; SASA, 2013) with the area 31-23°S and 28-33°E as illustrated in Figure 1.1.

KwaZulu-Natal Province is geographically located in the southeast of South Africa with an area of 94 361 km^2 which covers 7.7% of the total South African area, with a central point of 29° 36’ 4.35’’S and 30° 22’ 54.93’’E. The population is estimated at 10 456 900 people with an unemployment rate of approximately 25% (SSA, 2013). It is partly rural and has twelve sugarcane mills: Umzimkhulu, Sezela, Eston, Noodsburg, UCL Company, Maidstone, Gledhow, Darnall, Amatikulu, Felixton, Umfolozi and Pongola (Funke, 2013).

Mpumalanga Province also produces sugarcane and has a population of 4 128 000 people. It has an unemployment rate of approximately 30% (SSA, 2013). It covers 6.3% (76 495 km^2) of the total South African area, lying in the northeast of the country (Mayosi, *et al*., 2012). The province central point is 25° 28’ 41.3’’S and 30° 59’ 21.8’’E. It has two large sugarcane mills: Malelane and Komati (Funke, 2013).

ESwatini, an independent country located east of Mpumalanga and west of Maputo in Mozambique, has four sugar mills: Mhlume, Simunye, Ubombo, and Nsoko-Msele Integrated in the eastern Lowveld. There are approximately 207 731 people and 5 945 square kilometres in the sugarcane growing parts, while ESwatini has a total population of 1 018 449 people and covers 17 363 square kilometres (WHO, 2013). ESwatini was also incorporated in the study area because of its high sugarcane production and different farming methods that include more irrigation. Thus some differences between sugarcane productions in these two countries were expected.

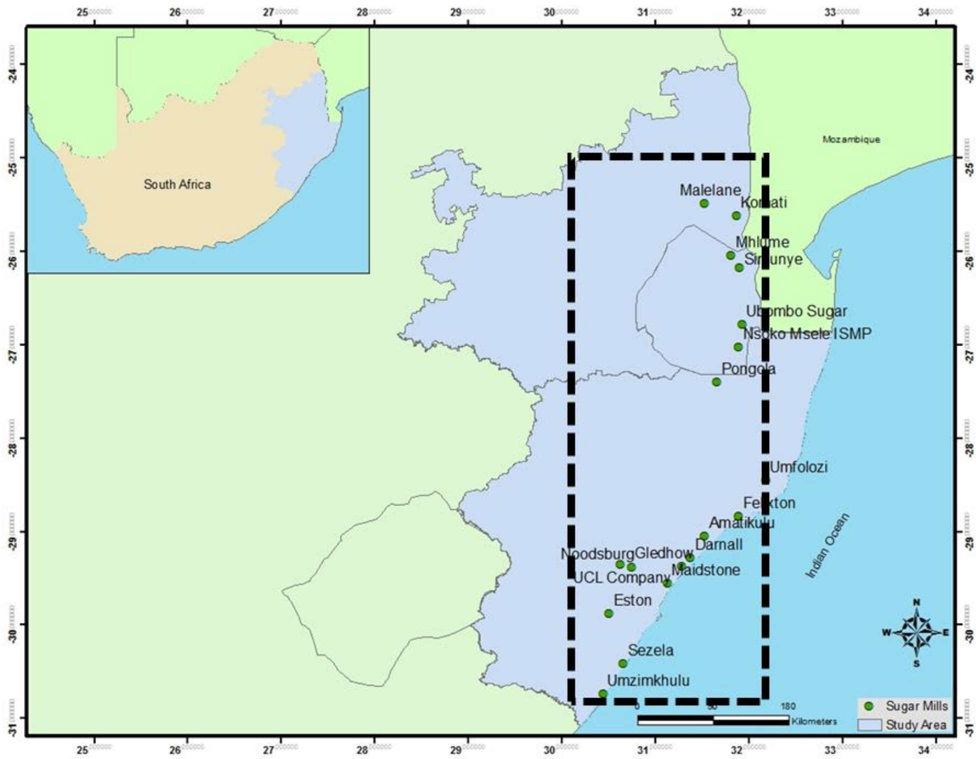

Figure 1.1: Map of southeastern Africa and the sugarcane growing region. Individual sugar mills are green dots. The dashed box encompasses the area used for averaging time series.

1.9 Significance of the study

The sugarcane Industry in South Africa employs both skilled and unskilled labour directly and indirectly in rural communities estimated at 350 000 people in 2013, and in excess of 3 000 people in ESwatini. The region contributes about 18% of the total South African Gross Domestic Product - GDP (Manuel, 2008). The study area is characterised by a rainfall gradient varying from dry west to moist east owing to elevation and proximity to the warm waters of the Mozambique Channel. Although Mpumalanga is small, its agricultural outputs are high, partially because of uptake of climate information by large-scale growers (Maponya & Mpandeli, 2012).

In the South African sugarcane growing region the number of small-scale sugarcane farmers has declined (Dubb, 2015; Jones, *et al*., 2015). The value of sugar has decreased relative to monetary inflation and this may impact the economy and social stability of the region (Egoume-Bossogo, 2003). Small-scale non-mechanised production costs tend to exceed the market value.

Naturally, for farmers to remain profitable, given the low margins for sugarcane, large commercial farms must employ strategic planning and mechanised production to maintain viability. This dissertation aimed to provide insight for strategic planning, with the hope that this will infiltrate to the small-scale farmers. The study fills gaps in scientific knowledge and renews efforts that started over 18 years ago. The study evaluated those findings and considered whether the climatic trends and cycles are similar or different to earlier values.

The impacts of drought on sugarcane have been generalised (Dubb, 2015), so the study has determined the climate effects on the sugarcane yield, considering specific drivers such as El Niño Southern Oscillation (ENSO) as represented by sea surface temperature (SST) and sea level pressure (SLP). Moreover, decisions of sugarcane farmers should be informed by past, current and future climate, and crop drivers (temperature, rainfall, evaporation) in addition to economic considerations outside the scope of this dissertation.

1.10 Organisation of the dissertation

Chapter 1 provides the introduction and background with reference to the impacts of climate on sugarcane yield, the problem statement, the main aim, and specific objectives of the study, delimitation of the study area and the significance of the study.

Chapter 2 describes a literature survey of earlier studies which have been conducted on similar and related topics, e.g. the impact of ENSO and climate change on agriculture, aqua-crop soil moisture simulation, and non-climatic factors such as pests and diseases.

Chapter 3 outlines the research methodology, which includes data sources and methods of analysis employed. The use of NCEP/NCAR, KNMI-CE, CRU4, GPCC8, MERRA2, HadISST, HadSLP2 and ECMWF ERA-interim is explained in this chapter.

In Chapter 4, the results from time series analysis of local and global climate effects on local sugarcane yield from 1988-2010 for different agro-climatic regions of the SA sugar industry and global sugarcane yield data (from 1970-2016) are scrutinised.

Chapter 5 presents the results and discussion on climatic trends, cycles and patterns and their relationship with sugarcane yield over SE Africa for the period 1970 to 2016.

Chapter 6 documents the results and discussion with reference to the global impacts of ENSO on the sugarcane yield in the study area for the period 1970 to 2016.

Chapter 7 gives the results on climate variability, long-term climate, and observed and projected climate trends. Future projections of rainfall, temperature and P-E derive from IPCC model simulations.

Chapter 8 comprises a summary and synthesis of the key research findings, recommendations for farmers and the overall conclusion.

1.11 Summary

Chapter one has detailed the background on the application of climate science to sugarcane production in the eastern part of southern Africa. This chapter provided the background, problem statement, main aim, specific objectives, research question, and delimitation of the study and its significance, and the structure of the dissertation. The study also considered the consensus of local and global climate studies on sugarcane yield and trends in future (Deressa, *et al*., 2005; Knox, *et al*., 2010; Chandiposha, 2013; Marin, *et al.,* 2013; Singels, *et al*., 2014; Dubb, 2015).

CHAPTER 2

LITERATURE REVIEW

2.1 Introduction

Sugarcane (*Saccharum officinarum* L.) is a C_4 crop which is grown in both tropical and subtropical agro-ecological zones, mainly for the production of sugar and bioenergy. Plants and crops are spatially distributed according to climate (temperature and rainfall) responses. Hence, C_3, C_4 and CAM plants are reported to have different abilities for temperature acclimation of photosynthesis (Yamori, *et al.* 2014).

Sugarcane yield and production have been reported to be directly and ultimately affected by crop drivers such as evapotranspiration, rainfall, temperature, and pests and diseases (Zhao & Li, 2015; Everingham, *et al*., 2003).

2.2 Characteristics of a rainy season

The onset and cessation of the rainy season and intermittent dry spells affect sugarcane production through the daily and seasonal agricultural schedules. Rainfall with high intensity (>9 mm/hr) is likely to wash away the organic matter and leave the soil less fertile, thus reducing the productivity of the land (Fraser, *et al*., 1999).

2.2.1 Rainfall intensity

Rainy season characteristics are important to farmers in southern Africa who depend on rain-fed agriculture. Crop yields are vulnerable to rain shortfall and variability, which threaten food security (Ropelewski & Halpert, 1987, 1989).

Below average rainfall in southern Africa relates to tropical east Pacific warm episodes such as 1983 and 1992 (Goodman, *et al*., 2000).The average rainfall of > 1000 mm/yr is expected during Pacific cold episodes such as during the 2000 season (Kogan, 2000), and rainfall trend inclines or fluctuates to the wet episode.

2.2.2 Rainfall duration

According to Mason and Joubert (1997), rainfall can surge in southern Africa to 100 mm/day (Guzzetti, *et al*., 2004), which leads to flooding of crops owing to intensified surface runoff. Southern Africa can also experience prolonged dry spells.

The rainy season in southern Africa is confined to the summer half of the year, namely, the 6-7 months from October-April, excluding the Mediterranean region (Western Cape). This determines the growing season of 80% of sugarcane in South Africa under rain-fed conditions (Halpert & Bell 1996; Jones & Singels, 2015).

2.3 ENSO impacts on sugarcane

In Brazil the ENSO affects sugarcane production, which decreased 5-10% during the El Niño years of 1983 and 1998 (Cirino, *et al*., 2015). In La Niña years the sugarcane production is benefited in Queensland, Australia (Kuhnel, 1993). These responses drive changes in supply and demand, and thus global commodity market prices for sugarcane.

In addition, the rainfall is influenced by large-scale climate drivers such as the Pacific El Niño-Southern Oscillation (Riffkin & Evans, 2004). Everingham, *et al*. (2003) investigated the relationship between ENSO and sugarcane productivity levels in Australia. They found significant negative correlations between sugarcane yield and the Southern Oscillation Index (SOI) in the year before harvesting.

Singels and Bezuidenhout (1999), reported that El Niño (the negative phase of ENSO) is linked to reduced rainfall and sugarcane yields over South Africa's sugar production regions. However, it should be noted that this does not happen for all El Niño years. ENSO does not have a strong impact on rainfall throughout the whole season, and the rainfall-ENSO relationship is characterised by a strong spatio-temporal variability over the subtropical sugar belt of SE Africa (Nicholson & Kim, 1997).

2.4 Climate change and agriculture

Gbetibouo and Hassan (2004) estimated the economic impact of climate change on the major South African crops using the Ricardian model. The model was based on agricultural data for sugarcane, maize, wheat, sorghum, soybean, groundnut and sunflower. The study revealed that field crops are more sensitive to increased temperatures than to precipitation, and thus to greenhouse warming.

The impact of climate varies across continents and within countries (Mendelsohn, *et al*., 2002). Resources in semi-arid zones tend to survive better through drought events because mitigation, adaptation, resilience and preparedness are already in place. Gbetibouo and Hassan (2004) indicated that the western and interior provinces of South Africa (Limpopo, Western Cape, Northern Cape, North West, Free State) saw agricultural net revenue increase with a 2 °C rise in temperature. Whereas, the eastern provinces (KwaZulu-Natal, Mpumalanga and Eastern Cape) experience diminished agricultural profits in warmer weather, possibly due to coping strategies (Darwin, 1999; Gbetibouo & Hassan, 2005).

Various crop growth models are used to relate climate and farm production. The Ricardian model does not take into consideration soil water and variations in the sugarcane market price (Cline, 1996). The Agricultural Production System Simulator is better able to simulate crop yield (Nape, 2011).

Flooding can wash away the top soil and nutrients, leaving the land barren, and taking fertilisers downstream to cause eutrophication and water pollution. Crops respond to flooding in different ways. For example, maize can survive flooding up to four days in an average air temperature of 16 °C, for two days if the average temperature is 21 °C, and roughly one day above 27 °C. Soybean can resist flooding if soil saturation is less than six days (Pedersen, *et al*., 2004).

Jones *et al.* (2015) revealed that the use of reliable simulated climate change impacts on sugarcane yield could positively benefit the sugar industry such that adaptation measures could be in place and/or farming systems might be changed to increase sugarcane yield in future. Previous studies in climate change simulations suggested sugarcane yield increase in irrigated sugarcane over southeastern Africa (Singels, *et al*., 2014; Jones, *et al*., 2015). Rain-fed sugarcane yield increase under altered future climate (2050s) was observed over southern Brazil (Marin, et al., 2013). These papers indicate the necessity for enhanced irrigation to obtain high sugarcane yield, and that average temperature departures are the determinant of cane yield variability.

2.5 Seasonal forecasting and agriculture

2.5.1 Simulating crop yield

Nape (2011) employed the Agricultural Production Systems Simulator (APSIM) to provide technical insights into maize production in the Modder River Catchment in the Free State, central South Africa, based on seasonal rainfall 1950-1999. APSIM is a software system which allows modules of crops and field production, residue decomposition, soil water, nutrient flow, and erosion to be reconstructed to simulate various production systems, and soil and crop management using conditional rules (McCown, *et al*., 1996). The APSIM was validated through the recommended management practices using the observed environmental and maize yield data from 1981 to 2005. The model has been used in other applications in southern Africa (Ncube, *et al*., 2007, 2009).

The Commonwealth Scientific Industrial Research Organisation (CSIRO) and the Agricultural Production Systems Research Unit (APSRU) were the founders of APSIM in 1991 (Keating, *et al*., 2003). The findings suggest that to meet the food demand associated with rapid world population growth expected to reach 9 billion by 2050 the agricultural production must be maximised (Nape, 2011). Climate variability is the main factor which makes agricultural production volatile. The APSIM is used in regions which are more prone to climate change and variability to assist farmers with regard to decision-making and management planning strategies (White, 2000).

2.5.2 Seasonal forecasts and decision-making

Weather and climate information has been extensively used for maize yield projections (Jones & Thornton, 2003; Mkhabela, *et al*., 2005; Tadross, *et al*., 2005; Abraha & Savage, 2006), hence maize yield depicts an upward trend. These studies show that the rainfall, temperature and agro-climate of the preceding season are significant for maize-growing in southern Africa.

Everingham, *et al.* (2002) studied the value chain model of the sugar industry in Australia. The study identified statistical predictors that were significant for understanding the impact of climate on crop production, such as the Southern Oscillation Index (SOI) and sea surface temperatures (SSTs), and local crop-drivers such as temperature, evaporation, solar radiation and rainfall. The intention was to maximise the effectiveness of rainfall forecasts in irrigation water demand management (Russell, 1990; Wegener, 1990).

2.6 Influence of non-climatic factors on sugarcane (diseases and pests)

Eldana saccharina is a native pest in Africa, and sugarcane is the fundamental host. It is found to aggravate the occurrence and harshness of stalk rots (Walker, 1865; Atkinson & Nuss, 1989). It was first discovered by Walker in 1865 in Sierra Leone, West Africa. He studied the differences in the *Eldana saccharina* outbreak in sugarcane in various parts of Africa. The outbreak remained the result of existing variety of biotypes of these species in the continent (Walker, 1865). These pests are found to have decreased the yield of sugarcane in South Africa, particularly in KwaZulu-Natal Province (Martin & Wismer, 1989; Viswanathan & Rao, 2011).

2.7 Summary

The literature which is relevant to climate impacts on sugarcane yield and production has been reviewed. It is evident from the literature that ENSO does not have influence on sugarcane yield in the whole 24-month life span of *Saccharum officinarum* L. (Everingham *et al*., 2003). There are scenarios whereby multiple variables are correlated one year before harvest. Previous studies showed that weather and climate information are useful in agriculture planning for minimising the loss in profit and preventing food insecurity, and guiding decision-making and policy formulation. Developing countries are more vulnerable to climate change impacts as there is little funding to finance mitigation and adaptation strategies (Chandiposha, 2013; Zhao & Li, 2015). Highly developed countries may not participate in sugarcane growing, because of its low value in comparison to ecotourism. Sugarcane yield is not only decreased by climatic factors. Matthieson (2007) reported that sugarcane pests flourish in increased temperatures which decrease the sugarcane yield. Harvesting methods and agricultural policy formulation and decision-making also play a role in the year-to-year variation of the sugarcane yield. Many earlier studies provide context for statistical methods to relate crop production to climate. Scientific studies using future climate projections indicate disparate trends in the yield of sugarcane in southern Africa and in Brazil. Some studies suggest increase (Marin, et al., 2013; Jones, et al., 2015), while some suggest decrease (Deressa, et al., 2005; Knox, et al., 2010; Chandiposha, 2013).

CHAPTER 3

RESEARCH METHODOLOGY

3.1 Introduction

In this study, data were obtained for local crop drivers (rainfall, temperature, evaporation and soil moisture), regional climate drivers (SST patterns, SLP, ENSO and IOD indices), and sugarcane yield over eastern South Africa and ESwatini. The analysis made use of reanalysis model-derived, satellite, and *in-situ* data available from climate websites such as Royal Netherlands Meteorological Institute Climate Explorer (KNMI-CE), National Centers for Environmental Prediction/National Center for Atmospheric Research (NCEP/NCAR), and the International Research Institute (IRI) for Climate and Society. The primary goal of chapter 3 in this current study is to describe data, their sources, methods of data analysis and processing employed in this study.

3.2 Data and sources

The area-averaged (31-23°S and 28-33°E) time series come from monthly 1° station-based Global Precipitation Climatology Centre Version 8 (GPCC8) rainfall and Climate Research Unit TS4.1 (CRU4) surface air temperatures, climate indices such as the Southern Oscillation Index, and sugarcane yield over eastern South Africa and ESwatini as described below.

3.2.1 Rainfall (GPCC8)

The station-based monthly rainfall for computation of monthly and annual time series derives from the GPCC8 (Caloiero, et al., 2018; Schneider, *et al*., 2018) that is available through the CE-KNMI website. An area average was calculated over eastern South Africa and ESwatini (23-31°S, 28-33°E, *cf*. Figure 1.1) for the period from 1970-2016. The rainfall data was formulated into a Standardised Precipitation Index.

3.2.2 Palmer Drought Severity Index (PDSI)

UCAR self-calibrated PDSI has been extensively used for identifying and monitoring drought events (Dai, *et al.,* 2004). PDSI is precipitation (P) minus potential evaporation (E), where E is the function of temperature and soil moisture content over time in a given location (van der Schrier, *et al*., 2013; Osborn, *et al.,* 2017). It should be understood that PDSI is from station-based parameters, and its values range between +10 (wet) and -10 (dry). The magnitude of the absolute value of PDSI shows the severity or extent of dryness and wet. The self-calibrated PDSI (scPDSI) were used for exploring sugarcane-climate links (correlations and regressions) in Chapters 4, 6 and 7. Thereafter, it was compared with MERRA2 P-E (reanalysis data) for validation, so that P-E could be analysed for long-term change because PDSI has no projections in CMIP5.

3.2.3 Air temperature (CRU4) and Relative humidity (RH %)

The monthly CRU4 station-based surface air temperature anomalies (Harris, *et al*., 2014), was employed to construct an area-average temperature time series. The NCEP reanalysis relative humidity (500 hPa) was obtained from KNMI-CE for the period from 1970 to 2016 to examine water vapour over the study area. Alderfasi and Nielsen (2001) derived crop-water-stress through temperature and relative humidity datasets. In this study soil moisture index was devised as described next.

3.2.4 Surface evaporation

Class-A and S-tank are evaporators which are usually filled with water such that they represent a waterbody, and then mounted on the surface in agro-meteorological stations and daily water loss (evaporation) is recorded daily. Surface evaporation data from these instruments were used to examine the role of water loss from soil and vegetation in the sugarcane yield. These observed and quality controlled data were extracted from the Department of Water and Sanitation (DWS) website. Meteorological data from the sugar mills such as rainfall, air temperature and evaporation help determine daily agricultural schedules, and feed into the data assimilation systems comprising the reanalysis products. This data was integrated with MERRA2 SHF to compute a new and distinct index for estimating soil water loss.

3.2.5 MERRA2 SHF

Monthly MERRA2 (Bosilovich, *et al*., 2015) sensible heat flux (SHF) reanalysis fields starting in 1980 were utilised in correlation analyses. The SHF describes the surface turbulent heat flux as a proxy for potential evaporation.

3.2.6 NCEP OLR, GPH and soil moisture

Monthly interpolated satellite Outgoing Long-wave Radiation (OLR) from the National Oceanic and Atmospheric Administration (NOAA) was available from 1976 to 2013 (Liebmann & Smith, 1996; Chikoore, 2017), and was used as a proxy for rainfall and temperature. Data from NCEP reanalysis provided field information on meteorological variables such as geo-potential height-GPH at 850 hPa and soil moisture, and these fields were used to study climatic influences on sugarcane growth, and to quantify for spatial variability of sugarcane over SE Africa.

3.2.7 P-E

Precipitation minus evapotranspiration (P-E) is a model-derived drought index which derives from the equation of surface water budget. The surface water budget can be expressed as:

$$\Delta S = P - E - R - I \qquad (3.1)$$

where ΔS (changes in storage) are associated with the balance of the input P (precipitation) and outputs E (evaporation), R (runoff) and I (infiltration). Hence, employing the scale-analysis and considering the assumption that: R and I influences are $< 10\%$ of P fraction (Chikoore, 2017), the principal drivers of the surface water budget become $P - E$. The negative values of this index indicate drought conditions, and the severity of the drought event can be quantified using the magnitudes of the index $(P - E)$. In this study it was used for projecting future drought conditions over SE Africa, and projections derive from CMIP5 of the IPCC in KNMI-CE.

3.2.8 Normalized Difference Vegetation Index (NDVI)

NDVI refers to a measure for capturing how much more near-infrared light is reflected as compared to visible red. NDVI is calculated by:

$$NDVI = \frac{NIR - R}{NIR + R} \qquad (3.2)$$

where *NIR* and *R* are spectral bands of reflectance in near-infrared (450-500 nm) and red (600-700 nm) parts of the electromagnetic spectrum (Chikoore, 2005; Mbatha & Xulu, 2018). High reflectance from the satellite sensor is linked to green vegetation and lower reflectance is associated with brown vegetation. In agriculture it is used to show differences between bare soil from grass or forest, thus identifying plants under stress, and to differentiate types of crop and their stages. The Global Inventory Modelling and Mapping Studies (GIMMS) NDVI dataset which was used for correlation of satellite vegetation and sugarcane yield derives from KNMI-CE for the period from 1981 to 2006. A further AVHRR NDVI time series was drawn from the International Research Institute (IRI) for Climate and Society. NDVI was used for mapping the vegetation colour and fraction over southeastern Africa (31-23°S and 28-33°E) in the period 1981 to 2013. NDVI data used in this study has been pre-corrected for satellite drift as described in previous studies (James & Kalluri, 1994; Tucker, *et al.*, 2005).

3.2.9 Large-scale climate drivers

Global and remote influences account for up to 30% of climate variability in southern Africa (Hastenrath & Heller, 1977; Brookfield & Parsons, 2005; SAWS, 2016). Therefore, indices such as the IOD (Indian Ocean Dipole), QBO (Quasi-Biennial Oscillation), and MJO (Madden Julian Oscillation) were tested with respect to sugarcane yield.

3.2.9.1 Sea level pressure (SLP) and wind fields

Sea level pressure (SLP) at 850 hPa data was available via KNMI-CE for the period 1970-2016. The HadSLP2 reanalysis interpolation system is described in Allan and Ansell (2006). HadSLP2 is the improved version of the Hadley Centre's monthly historical mean sea level pressure (MSLP) dataset. HadSLP2 is computed using various terrestrial and marine collated data.

The study used vector winds and vertical motion from ECMWF and NCEP reanalysis (Dee, *et al*., 2011; Szczypta, *et al*., 2011; Kanamitsu, *et al*., 2002). The atmospheric levels examined were 850, 500, and 200 hPa.

3.2.9.2 Southern Oscillation Index (SOI)

The Climate Prediction Center (CPC) Southern Oscillation Index (SOI) was employed to identify the phases and intensity of the Pacific El Niño-Southern Oscillation (ENSO), and they were drawn from KNMI-CE for the period 1970 to 2016. The SOI data was used as defined in the study of monthly weather review by Ropelewski and Jones (1987). The National Weather Service (NWS) defined SOI as the standardised Sea Level Pressure (SLP) difference between the Tahiti and Darwin MSLP (NWS, 2015).

3.2.9.3 Niño4 and DMI

This monthly ENSO index is calculated through averaging SST anomalies (SSTA) (Rayner, *et al.,* 2003) in the central equatorial Pacific (5°N-5°S and 160°E and 150°W), and SSTAs that exceed $\pm$0.5 °C are used to define La Niña and EL Niño signatures (Rayner, *et al*., 2003). The Niño4 time series derives from averages of Met Office Hadley Centre SST datasets (HadISST) available in KNMI-CE. In this present study it was useful for scrutinising ENSO influence (remote forcing) on sugarcane yield from 1970-2016.

The Dipole Mode Index (DMI) is used to signal the Indian Ocean Dipole (IOD). The IOD is defined as the difference between SST patterns from the west tropical Indian Ocean (WTIO) and the southeast equatorial Indian Ocean (SEIO), and is related to ENSO. DMI is calculated by subtracting the SSTs in WTIO and SEIO, and has a reliable record since 1960. The DMI was drawn from KNMI-CE; it is well defined in Masson, *et al*. (2012).

3.2.9.4 SST patterns

The monthly NOAA reconstructed Sea Surface Temperature (SST) version 4 (Rayner, *et al*., 2003), has been interpolated to 1 degree, and was available from 1970 to 2016, based on data from ship, buoys and infrared satellites. This was used to compute the seasonal composites and correlations, and to extract statistical predictors of PDSI.

3.2.9.5 ERA-int Meridional wind

Meridional wind refers to southerly (positive values) and northerly (negative values) of the wind. The meridional wind used in this study derives from ERA-int reanalysis field extracted at 850 hPa in KNMI-CE. ERA-int wind data are computed from ECMWF forecast models and data assimilation systems. These datasets are detailed in McGregor, *et al.* (2013).

3.2.10 Sugarcane yield data

In South Africa the sugar industry has 14 sugar mills, where sugar estates, large-scale growers (LSGs) and small-scale growers (SSGs) submit cane for milling (van den Berg & Singels, 2013). Sugarcane yield data for individual mills was derived from the SASA database for 12 sugar mills (uMzimkhulu, Sezela, Eston, Noodsburg, UCL Company, Maidstone, Gledhow, Darnall, Amatikulu, Felixton, Umfolozi and Pongola) in Kwazulu-Natal, and 2 sugar mills (Malelane and Komati) in Mpumalanga. These sugarcane yield data from the above sugar mills were grouped and averaged according to their respective agro-climatic regions (e.g. Northern Irrigated, Zululand, Midlands, North Coast and South Coast) in the study of van den Berg and Singels (2013). Hence, the regional yield data for SA regions were obtained (from the abovementioned authors) and analysed for trends for the period 1988-2010.

The regional yield data from van den Berg and Singels (2013), were compared with FAO data to confirm validity. The regional yield data was slightly different from FAO yield data in the beginning and towards the end of the time series for the period 1988-2010 (Table B.1), but closely tracked the variations. Hence the primary index for analysis is the FAO yield because it is continuous for the study record (1970-2016). The detrended sugarcane yield index (DSYI) has been detrended and adjusted for variance.

National sugarcane yield data was extracted from the United Nations (UN) Food and Agriculture Organisation's (FAO) database for the period 1970-2016. The South Africa and ESwatini sugarcane yields were amalgamated into one index using the weighted sum of their mean yield from 1970 to 2016 according to production, whereby South Africa contributed 84% influence and ESwatini contributed 16%. The yield was linearly detrended to eliminate global warming and production effects and focus on year-to-year fluctuations. A consistent variance was maintained through the record, dividing by a linearly diminishing standard deviation value.

Comparisons were made with monthly meteorological data considering that the influence of climate effects such as rainfall and temperature should lead the yield by 3-6 months. Generally, sugarcane grows from June to the following May (>+1 year) subject to elevation, and it is harvested between March/April and December. For the satellite vegetation index there is little lead-time or lag of 1-2 months, and NDVI and sugarcane yield correlations are done for each season (DJF, MAM, JJA, and SON).

3.3 Methods of data analysis and processing

Monthly and seasonal climate fields and time series were processed to investigate the patterns of rainfall, temperature, and atmospheric and oceanic climate indices with respect to sugarcane yield. The multiple linear regression for testing the variable importance, and Pearson correlation analysis were done with the use of R procedures to investigate the relationship between key climatic variables, indices and the sugarcane yield data. In addition, point-to-field regression and correlation analyses were performed in KNMI-CE to explore the statistical link and its extent between key climatic fields and the sugarcane yield time series.

3.3.1 Mann-Kendall Test

The Mann-Kendall test is used to calculate the monotonic trends in a time series, and here this technique is used as described in previous studies (Mann, 1945; Kendall, 1975; Gilbert, 1987). The Mann-Kendall test is non-parametric and rank based, and is often used for detecting monotonic trends in the time series of geophysical data (environmental sciences, climate and hydrological data). Non-parametric techniques are robust and resistant to time series with outliers (Lanzante, 1996), hence in this study it was paramount to employ this technique. According to Kendall (1975) and Pohlert (2016), the Mann-Kendall test statistic is calculated as follows:

$$S = \sum_{k=1}^{n-1} \sum_{j=k+1}^{n} sign(X_j - X_k) \qquad (3.3)$$

and

$$sign\ (x) = \begin{Bmatrix} +1 & if\ x > 1 \\ 0 & if\ x = 0 \\ -1 & if\ x < 1 \end{Bmatrix} \qquad (3.4)$$

The mean magnitude of the statistic S is denoted by $E(S) = 0,$ and the variance (σ^2) is calculated from the equation:

$$\sigma^2 = \left\{ n(n-1)(2n+5) - \sum_{j=1}^{p} t_j\,(t_j - 1)(2t_j + 5) \right\} /18 \qquad (3.5)$$

where t_j represents the number of data-points in j^{th} tied group, and p indicates the number of the tied group in the data. It should be noted that the large-operator summation in the equation above is not used in any instance other than tied groups of the time series. This reduces the influence of extreme values in tied groups in the ranked statistics. When assuming that the time series is random and independent, the statistic S virtually exhibits the normal distribution, given that the z-transformation equation below is employed:

$$z = \begin{cases} \dfrac{S-1}{\sigma} & if\ S > 1 \\ 0 & if\ S = 0 \\ \dfrac{S+1}{\sigma} & if\ S < 1 \end{cases} \tag{3.6}$$

The value of the statistic S is related to the Kendall tau (τ), which is expressed as:

$$\tau = \frac{S}{D} \tag{3.7}$$

and

$$D = \left[\frac{1}{2}n(n-1) - \frac{1}{2}\sum_{j=1}^{p} t_j\left(t_j - 1\right)\right]^{\frac{1}{2}} \left[\frac{1}{2}n(n-1)\right]^{\frac{1}{2}} \tag{3.8}$$

With reference to the z-transformation equation outlined above, this study considered a 5% confidence level, by which the null hypothesis of no trend was rejected if $|z| > 1.96$. The test also provides the Mann-Kendall tau (τ) that measures the correlation, which shows the extent and degree of association between two or more variables. The Mann-Kendall test defined above was used to detect trends in sugarcane yield, and this was done using the R procedures.

The Mann-Kendall test defined above only detects whether the monotonic trend is upward or downward. However, to quantify for the onset of the trend and approximate the potential trend turning points (PTTPs) in a time series, the Sequential Mann-Kendall (Seq.MK) test is robust (Sneyers, 1990; Chatterjee, *et al*., 2014; Casa, 2018). This technique (Seq.MK) is used as defined in Chatterjee *et al*. (2014). Where the Seq.MK is applied in a series x_i , and it detects the PTTP of a long-term data. The Seq.MK test statistics is calculated by ranked-values of y_i of the original time series $(x_1, x_2, x_3 \dots, x_n)$. The test allows a comparison between $y_i(i = 1,2,3 \dots, n)$ and $y_j(j = 1,2,3 \dots, 1 - i)$. Then, the t_i statistic is expressed as:

$$t_i = \sum_{j=1}^{i} n_i \tag{3.9}$$

The mean of t_i distribution could be computed as:

$$E(t_i) = \frac{i(i-1)}{4} \tag{3.10}$$

and if the variance is

$$Var(\mathrm{t_i}) = \frac{i(i-1)(2i+5)}{72} \tag{3.11}$$

Now, if t_i, $E(t_i)$ and $Var(t_i)$ are known, sequential values of a standardised variable known as $u(t_i)$ can be calculated for each value of t_i statistic as:

$$u(t_i) = \frac{t_i - E(t_i)}{\sqrt{Var(t_i)}} \tag{3.12}$$

Although the forward sequential (Prog) values ($u(t_i)$) of the standardised time series derive from the original data ($x_1, x_2, x_3 \dots, x_n$), and the backward sequential (Retr) values $(u'(t_i))$ are approximated using the same approach but beginning with the last value of the original time series. In the plot of $u(t_i)$ and $u'(t_i)$ curves their intersection shows the PTTP, and the trend is considered significant when $u(t_i)$ and $u'(t_i) \geq \pm 1.96$. Here, the Sequential Version of the Mann-Kendall Trend Test Statistic was used to detect trends and approximate potential trend turning points. It should be noted that the intersection of $u(t)$ and $u'(t)$ curves indicates the approximate PTTPs. If the intersection is within ± 1.96 at 5% level the PTTPs could be inferred.

3.3.2 Taylor diagrams

These diagrams are used to graphically represent the concise statistics, which fit in the correlation coefficient (r), the root mean square difference (RMSD) for two or more variables, and their standard deviations plotted in one diagram which represents them in a two dimensional (2-D) scheme (Taylor, 2001).

In this study, these statistics presented a summary of how each pattern resembles the other in a 2-D diagram, providing the ability to perform comparative assessment of how the simulated sugarcane yield mimics the actual sugarcane yield. Generally, these diagrams use two variables, called 'reference' field (observed behaviour) and 'test' field (modelled behaviour). In this study the 'reference' field (observation) is simulated yield and the 'test' field is the actual yield (LSG/LG, SSG/SG and TOT/Total) because three fields are linked to one field and this has no adverse impacts on the desired outcomes. It should be understood that these diagrams are useful for multivariable comparisons and not for just two variables. These diagrams were devised using the Matrix Laboratory (MATLAB). The statistics summarised in Taylor diagrams include, the correlation coefficient (r) between observed (S^{obs}) and predicted (S^{pred}) data, *RMSD* and standard deviation (σ) were calculated as shown below (Taylor, 2001; Yaseen, *et al.,* 2018):

$$r = \frac{\sum_{i=1}^{i=N}\left[(S_i^{obs} - \overline{S^{obs}}\right).(S_i^{pred} - \overline{S^{pred}})]}{\sqrt{\sum_{i=1}^{i=N}(S_i^{obs} - \overline{S^{obs}})^2.\sqrt{\sum_{i=1}^{i=N}(S_i^{pred} - \overline{S^{pred}})}}} \tag{3.13}$$

where $-1 \leq r \leq +1$, and

$$RMSD = \sqrt{\frac{1}{N}\sum_{i=1}^{i=N}(S_i^{obs} - S_i^{pred})^2} \tag{3.14}$$

The $RMSD$ was expressed as a relative root mean square difference $(RRMSD)$ as shown below:

$$RRMSD = 100 \cdot \frac{RMSD}{\overline{S^{obs}}} \tag{3.15}$$

and N is the number of data points in the test period, S_i^{obs} is the i^{th} observed S value, $\overline{S^{obs}}$ is the mean observed S magnitude, S_i^{pred} is the i^{th} predicted value of S and $\overline{S^{pred}}$ is the average value of the observed S in the data. In addition, the standard deviation (σ) used in this study was expressed as below:

$$\sigma = \sqrt{\frac{\sum(S - \overline{S})^2}{N}} \tag{3.16}$$

3.3.3 Pearson correlation and multiple linear regression

The Pearson correlation method uses the Pearson correlation coefficient (PCC) to show the statistical links between variables, and their extent and direction (positive or negative) of two variables. In this study it was used to investigate rainfall, temperature, PDSI, SLP, SST patterns, SOI, Niño4 and sugarcane yields over southeastern Africa. In this present study, multiple linear regression (MLR) analysis described the relationship between a dependant variable and one or more independent variables using the equation:

$$y = \beta_0 + \beta_1 x_1 + \beta_2 x_2 + \cdots \beta_n x_n + \in \tag{3.17}$$

where y is the dependant variable (sugarcane yield), $x_1, x_2, \ldots x_n$ denote the independent variables (rainfall, temperature, PDSI, SLP, SST patterns, SOI, Niño4), β_0 is the intercept from the model output, $\beta_1, \beta_2, \ldots \beta_n$ are the coefficients of x terms and $\in$ is the standard error. In this study it was used to quantify and test the importance of each independent variable to sugarcane yield over the study area. These methods (Pearson correlation and MLR) are also explained in the study of NDVI and drought impact by Mbatha and Xulu, (2018).

3.3.4 KNMI-CE correlation analysis

The correlation of sugarcane area-averaged (31-23°S and 28-33°E) time series was done in a lagged pair-wise manner to determine the degree of association between climate variables and sugarcane yield from 1970-2016 (46 years). With 2-yr persistence in the sugarcane yield time series, an absolute correlation value >0.5 is needed to achieve statistical significance at 90% confidence. While the sugarcane index is annual, comparisons with the meteorological sugarcane area-averaged time series were made by month or season. For correlations and CCWT analysis, (*see* Chapters 5 and 6 of this study), the linear detrending methods as defined in Qian, *et al.* (2018) were employed to remove linear trends for avoiding false correlations.

3.3.5 Composite analysis

This method is a sampling technique based on the conditional probability that an event will reoccur given that it was seen to do so in the past. This method is superior to a case study approach (Levey, 1993). The composite-mean and composite-difference techniques are defined in previous studies (Jury & Pathack, 1993; Levey & Jury, 1996).

The composite-mean analysis was used to study the climatology of climate variables over southern Africa. This was important for determining key weather systems for sugarcane production over the study area.

The composite-difference was used to analyse and compare climatic differences between years of high and low sugarcane yields and PDSI. Years of high sugarcane yield as defined by the detrended sugarcane yield index are: 1971, 1972, 1975, 1976, 1997, 1998, and 2000; while the low yields were observed during: 1980, 1983, 1992, 1993, 1994, 1995, and 2012.

The years with high PDSI are: 1987, 1988, 1995, 1996, 1997, 1999, 2000 and 2001; while the years with low PDSI are: 1982, 1991, 1992, 1993, 1994, 2003, 2004 and 2015. It should be noted that PDSI was ranked according to December values because this month marks the onset of the important season for sugarcane growing in the study area.

3.3.6 Wavelet analysis

The power of Morlet 8 wavelet transform was used as described in key studies and wavelet guidelines for users (Foufoula-Georgiou, 1995; Torrence & Compo, 1998).

The technique has the ability to analyse data with non-stationary power at numerous frequency domains (Daubechies, 1990), and it has been widely used in geophysical sciences for studying tropical convection (Weng & Lau, 1994), and ENSO (Wang & Wang, 1996).

The Continuous Complex Wavelet Transform (CWT) was invented by Morlet (1983) and is explicitly defined in Torrence and Compo (1998) and Jury and Melice (2001) in the study of rainfall and river flow. The wavelet φ to be used in each study depends on the signal to be analysed. In this study, the signal was well defined, hence a localised in frequency space wavelet was desirable - the Continuous Complex Wavelet Transform devised by Morlet (1983), was employed to determine the temporal characteristics of area-averaged rainfall and sugarcane yield in southeast Africa. This wavelet is calculated as:

$$\varphi(t) = \pi^{-1/4} e^{-t^2/2} e^{i\omega_0 t} \qquad (3.18)$$

where $= \sqrt{-1}$, and the non-dimensional ω_0 =5.4**.** The wavelet is defined in phases and modulus manner, which is describe by the inverse of the scale and frequency**.** The relationship between the scale a and frequency f was explained by Meyers, *et al.* (1993) as shown below.

$$f(a) = \frac{\omega(a)}{2\pi} = \frac{1}{4\pi}\left(\frac{\omega_0}{a} + \frac{2+\omega_0^2}{\omega_0}\right) \qquad (3.19)$$

3.3.7 Sugarcane-PDSI forecast technique

A backward-step-wise multiple linear regression was employed to develop a forecast system. Sugarcane has a long-cycle (12-24 months), and depends on many parameters other than climate, and using sugarcane yield as a predictand could be misrepresentative of the desired outcomes. Hence, the summer (Dec-Mar) Palmer Drought Severity Index (PDSI), which is precipitation minus potential evaporation, was used as a ‘’target’’ for prediction and as a proxy for sugarcane yield. Predictors in the prior spring (Aug-Nov) were extracted from correlation maps with respect to Dec-Mar PDSI.

Subsequently these were regressed onto the time series, and less influential predictors were removed until a final model was reached with the least number of predictors. To check for over-fitting and co-linearity, the multi-variate algorithm should have a standardised coefficient for each predictor of value < 1 and be of the same sign as the pair-wise association.

3.3.8 Long-term climate trend analysis

The study assessed historical and future climate projections for SE Africa using the Coupled Model Inter-comparison Project (CMIP5) of the Intergovernmental Panel on Climate Change (IPCC) model simulations from KNMI-CE under an RCP4.5 scenario from 1970-2050. The CMIP5 IPCC model certainty has improved (Xu, *et al*., 2013). Yearly anomalies of CMIP5 data were extracted from KNMI-CE ETCCDI records. The observed trends in soil moisture and SST patterns, and the projected rainfall and temperature trends were smoothed by applying the 18-months and a 2-year Locally Estimated Scatterplot Smoothing (LOESS) low-pass filter, respectively. This was performed in the KNMI-CE on-line analysis tool. Linear regression trends were fitted in the simulated time series. In the trend equations the negative slopes (gradients) indicate a declining trend, positive slopes indicate an inclining trend, and R-squared (R^2) shows how data points are distributed over time.

3.4 Summary

Datasets employed in this dissertation, their sources, and methods of analysis and processing have been described in this chapter. Station-based GPCC8 rainfall, CRU4 temperature, scPDSI and sugarcane yield serve as the main datasets investigated in this study. The SST, SLP, SOI, DMI and Niño4 datasets have been used to examine the influence of the ENSO on sugarcane yield in the eastern part of South Africa and ESwatini. The regional sugarcane yield data for different agro-climatic regions (Northern Irrigated, Zululand, Midlands, North Coast and South Coast) of the SA sugar industry were obtained from van den Berg and Singels (2013) for the period 1988-2010 and analysed for trends. The total yields for the SA industry were compared to those reported in the South African Sugar Industry Review in 2012 (van den Berg and Singels, 2013). The significant sources of meteorological data are KNMI-CE, NCEP/NCAR, and IRI. Local and national sugarcane yields were obtained from SASA and FAO, which are in the public domain, and the regional yield data was obtained from van den Berg and Singels (2013) and analysed for trends. Most station observations are interpolated, together with ancillary data, into gridded reanalysis fields to provide complete spatial and temporal coverage. Data was extracted and analysed using online tools (correlation, regression, composite and wavelet analyses) in climate websites, R procedures and MATLAB. The key methods employed are: Mann-Kendall test, correlation, regression, composite and wavelet analyses. In addition, the overview of the study is presented below (*see* Figure 3.1), which reflects on the key aspects of the methodology, and summarises the whole study.

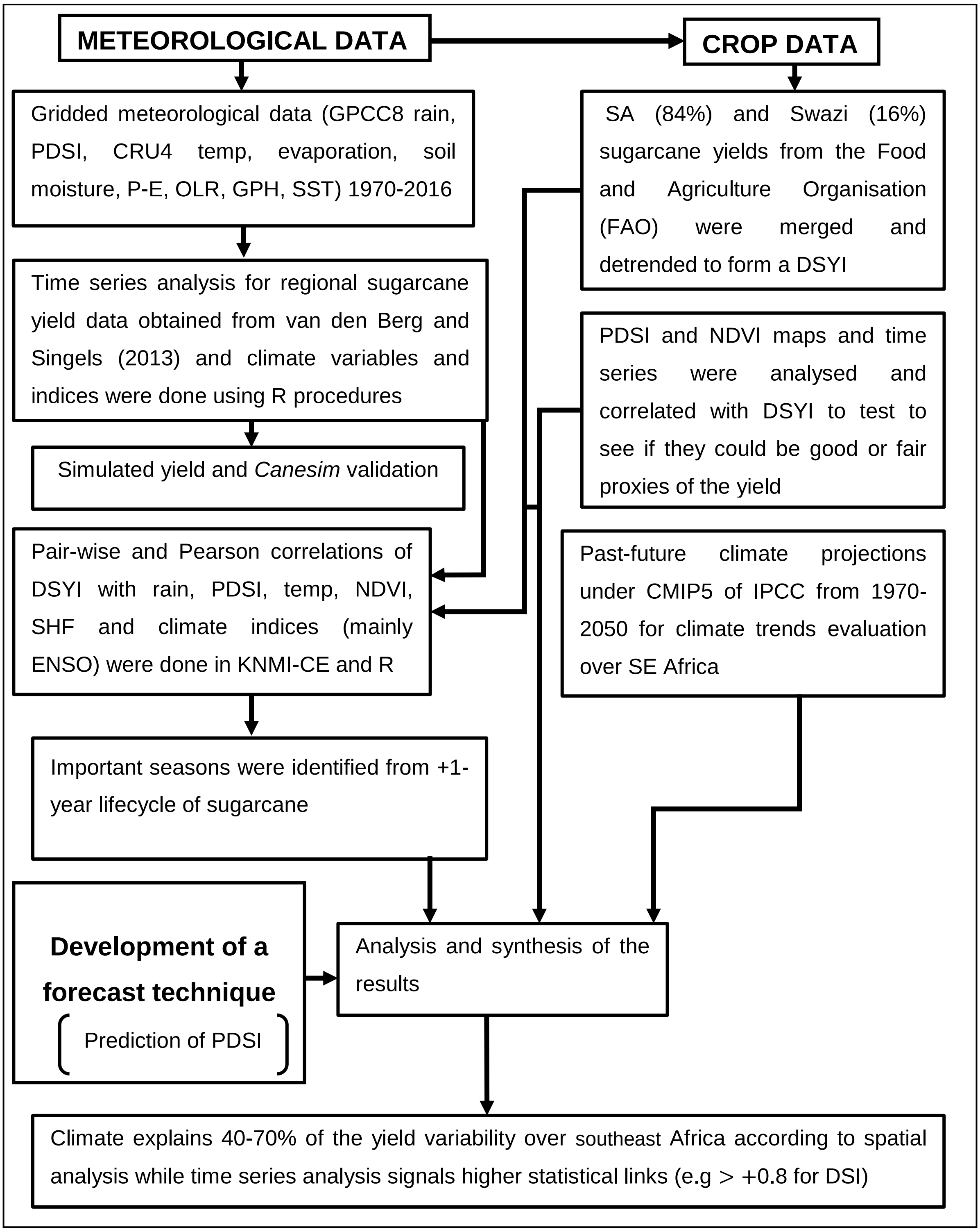

Figure 3.1: Conceptual framework of the study.

CHAPTER 4

TIME SERIES ANALYSIS OF CLIMATIC VARIABLES AND YIELDS

4.1 Introduction

The main aim of this chapter is to report on the time series analyses and statistics of local sugarcane yield and climate from different agro-climatic regions of South Africa's sugar industry (Northern Irrigated, Zululand, Midlands, North Coast and South Coast) and long-term global sugarcane yield data for South Africa and ESwatini from the Food and Agriculture Organisation (FAO). The FAO does not distinguish between rain-fed and irrigated yields, but their crop data are continuous and easily available, as described in chapter 3. Hence, the main index (DSYI) for analysis derives from FAO data but comparison with regional sugarcane yield data was done for confirming validity. Regional yields data for the aforementioned agro-climatic regions of SA have been used previously for SASA annual review (van den Berg & Singels, 2013). It should be noted that the results presented in this chapter mainly consist of long-term yield data from the FAO and, to a lesser extent, SASA data. In addition, the results for each region are discussed within the text but presented at the end of the thesis as appendices. This was due to their length as they could not be afforded a space within the main text.

4.2 Seasonal cycle of rainfall

For calibration of previous studies, the seasonal cycle of rainfall over SE southern Africa (31-23°S and 28-33°E) has been studied and the results are shown below (*cf*. Figure 4.1). During the dry season there are slight departures of monthly means from the long-term mean.

The rainfall over southeastern Africa rises in November and diminishes in March, after peaking in January due to triggering events such as tropical cyclones and north-west cloud bands. During winter (June-August) the temperature inversion is strong and the winds are westerly and very dry.

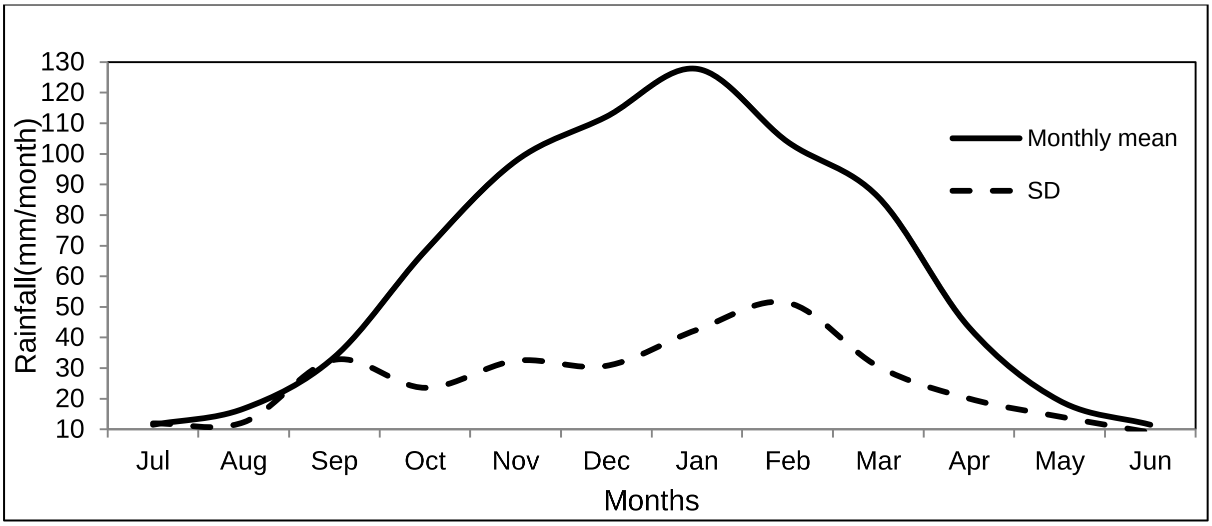

Figure 4.1: Seasonal cycle of mean GPCC V8 rainfall over the SE Africa for the period from 1970 to 2016. NB: the solid-black series indicates monthly mean rainfall and dashed time series represent standard deviations.

In summer, the Kalahari high is weak and the winds are easterly, so moisture from the warm southwest Indian Ocean penetrates the interior, causing heavy rainfall. Although the season appears short, the coastal belt north of Durban receives light rainfall at intervals during winter.

4.3 The inter-annual variability of climate and sugarcane yield

The inter-comparison between regional climate variables (rainfall, temperature and PDSI) and sugarcane yield was done to explore the resembling characteristics on their annual variation over southeastern Africa from 1970-2016. The meteorological variables (rainfall, temperature and PDSI) studied here were area-averaged from five agro-climatic regions (Northern Irrigated, Zululand, Midlands, North Coast and South Coast) of South Africa's sugar industry.

The area-averaged time series show that rainfall has no trend but is fluctuating or alternating from dry to wet in the study period 1970-2016 (Figures 4.2a and b), which is analogous to Tadross, *et al.* (2011).

According to the results in Figures 4.2a and b the sugarcane yields resemble the rainfall pattern, being high after wet phases and low after dry phases, with a lead-time of 3-6 months. In some years there is excessive rainfall due to tropical cyclone activity and waterlogging, and associated pests flourish and damage sugarcane, thus suppressing the yield.

Drought tends to suppress sugarcane yield, such as the case of the 1992/93 and 1994/95 seasons where minimum values (41.7 ton/ha for South Africa and 90.8 ton/ha for ESwatini) were reached (Figure 4.2a, b and Figure 4.3a, b).

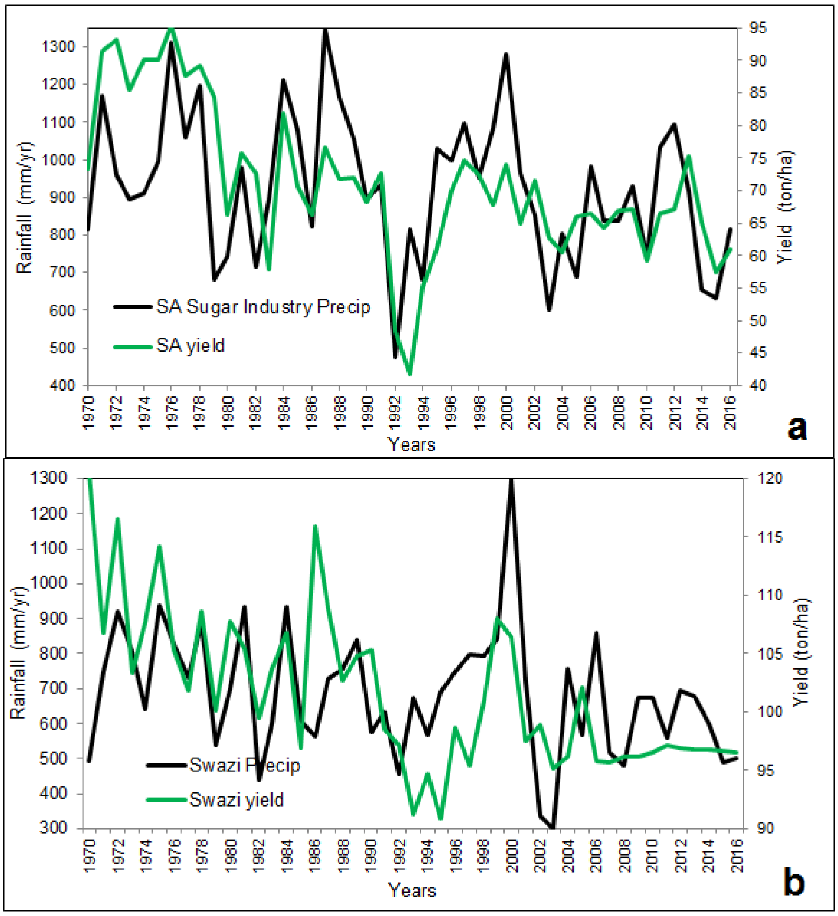

Figure 4.2: Inter-comparison between rainfall (mm/yr) and FAO sugarcane yields for the period 1970-2016 a) South Africa, area-averaged rainfall has been extracted from different sugarcane growing areas, then annual-averaged over time b) ESwatini rainfall vs sugarcane yield, rainfall was extracted over eastern ESwatini.

There are some instances where annual rainfall is reduced but the annual yield does not drop, such as the case of the 2002/03 season with rainfall of 500 and 300 mm/yr for South Africa and ESwatini, respectively. The yield was 62.6 and 98.9 ton/ha for South Africa and ESwatini, respectively.

This was possibly due to increased irrigation and other non-climatic controls. Yet, irrigation is not always an option. For example, in ESwatini in 2016 when the Ingwavuma River dried up during winter, the sugarcane wilted and nearby farmers cut the failed crops to feed their livestock since there was no grass. There are slight differences in yield response to climate influences in the study area because

ESwatini sugarcane is 100% irrigated and the storage dams provide a buffer during the dry season.

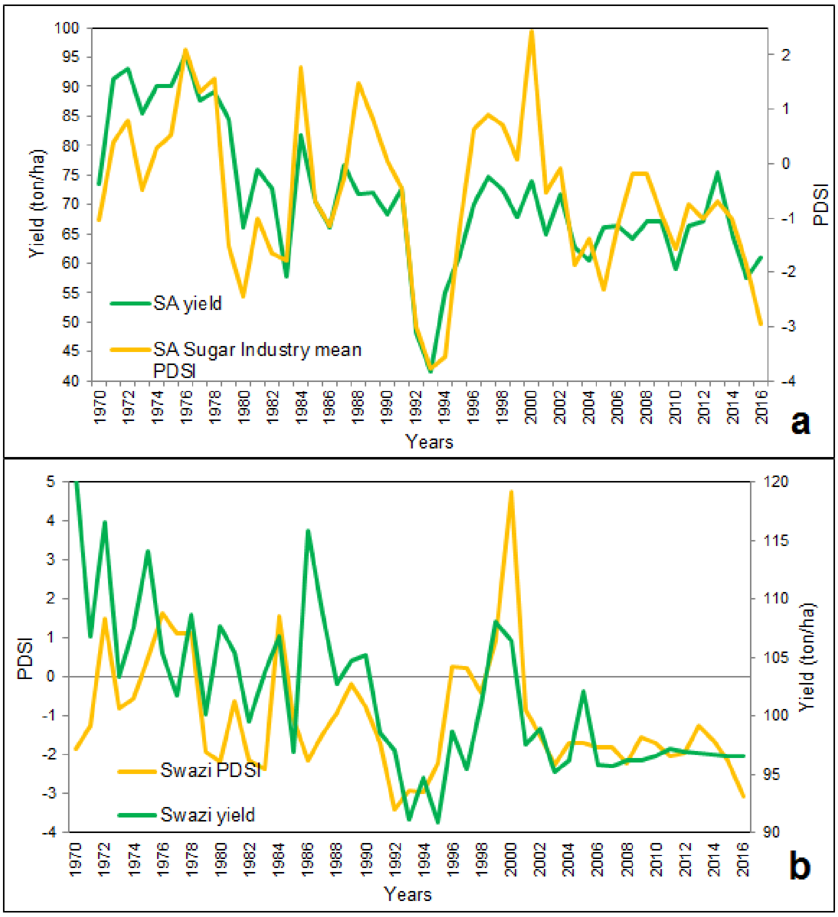

Figure 4.3: Annual variability of sugarcane with respect to the Palmer Drought Severity Index (PDSI) for the period 1970-2016 over a) South Africa and b) ESwatini.

Surface temperature anomalies depict an upward trend and variability over the years. Yield responds negatively to temperature changes according to the results in Figures 4.3a and b, as illustrated below. Years of high surface temperature anomalies are followed by a low annual sugarcane yield. High temperatures trigger potential evaporation; the rate at which soil water is lost exceeds replacement which brings aridity. The gradual temperature increase is part of global warming due to rising greenhouse gases (Peng, *et al*., 2004).

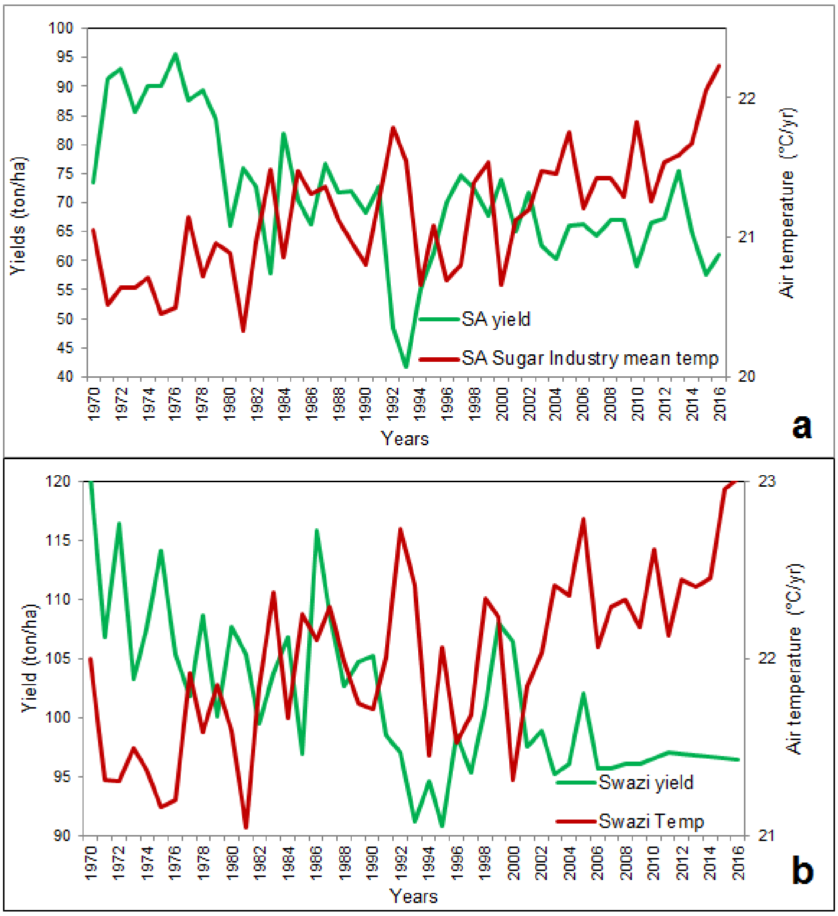

Figure 4.4: Annual variations of annual area-averaged air temperature against sugarcane yield from 1970-2016 over a) South Africa b) ESwatini.

There is some incommensurable and heterogeneous behaviour detected in the above inter-comparisons (Figure 4.2a, b; 4.3a, b; and 4.4a, b). Sugarcane yield varies according to rainfall with its unclear trend, temperature is increasing and causing yields to decline. PDSI seems to explain much of the sugarcane variability over time, and this necessitates performing other statistical tests to find statistical associations between these climatic variable and yields to make meaningful judgements.

4.4 Sensible heat flux and Evaporation

Crops directly depend on soil moisture rather than actual precipitation. The predictor of evaporation (soil water loss) was computed by averaging MERRA SHF, and observed S-tank and A-pan evaporation, as illustrated below (Figure 4.5).

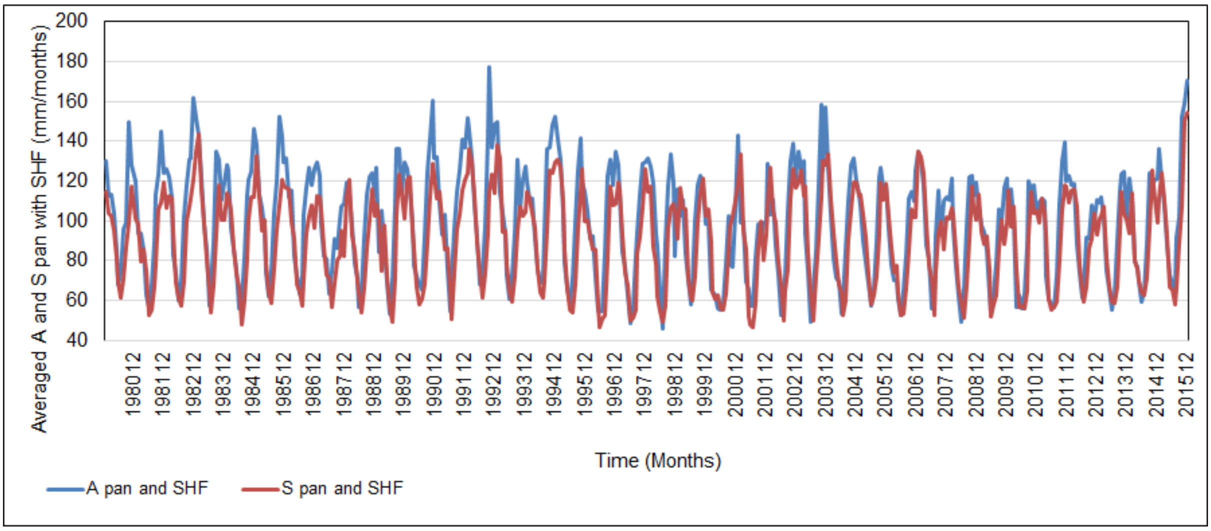

Figure 4.5: Averaged S Class Pan evaporation and MERRA model sensible heat flux in the surface and A Class Pan evaporation and MERRA reanalysis sensible heat flux (mm/month) in the eastern part of South Africa and ESwatini for the period 1980 to 2015.

The MERRA2 reanalysis sensible heat flux (SHF) and the observed S-tank evaporation follow each other and have a seasonal cycle that peaks in spring each year. The soil water budget can be expressed as:

$$S_2 = S_1 + (P - E - R - \mathrm{I}) \quad (4.1)$$

where changes in soil water (Final (S_2) – Initial (S_1) soil moisture) are driven by the input of P-Precipitation subtracted by E-Evaporation, R-Runoff and I-Infiltration. During warm dry weather conditions, the sensible heat flux increases during the day-time and, as a proxy for E, removes soil water and advects it vertically to the atmosphere through turbulent mixing by wind (Tyson & Preston-Whyte, 2000). When the rate of soil water loss exceeds the rate of replacement, then soil moisture drought could occur and the yields are expected to drop.

The indicators of evaporation (soil water loss) derive from a combination of monthly averaged observed S-tank evaporation and MERRA-2 reanalysis SHF. This is used to estimate the amount of soil water loss (Pidwirny, 2006). High values of this index indicate a high amount of soil moisture loss. Potential evaporation that controls soil moisture is distinct from the input of moisture to the atmosphere through crops and vegetation via evapotranspiration. The relationship connecting these concepts is that the crop water needed for growth is equal to the potential minus actual evaporation.

4.5 Temporal variations of sugarcane yield in South Africa

The number of sugarcane growers in South Africa is approximated from different studies. There is agreement that the majority are small-scale growers (SSGs) who constitute about 95% of the total sugarcane growers, but only produce 8% of sugarcane in South Africa (van den Berg & Singels, 2013). A huge decrease of SSGs was envisaged in KwaZulu-Natal during 2014/15 season (Dubb, 2015). This section provides inter-annual variability and time series analysis of sugarcane yields in different regions of South Africa.

4.5.1 Large-scale growers (LSGs)

The Northern Irrigated region recorded high sugarcane yields (90 ton/ha) for large-commercial growers (LSGs). However, the North Coast region experienced a lower yield through the record (less than 70 ton/ha for the period from 1988-2010) than the other 4 growing regions (*see* Figure 4.6). A strong dip in the sugarcane yield time series during 1992/93 was detected throughout the sugar industry, and this is linked to 1992/93 drought conditions (Dube, 1998). This was also observed in the FAO sugarcane yield time series (Figures 4.2a, 4.3a and 4.4a) and satellite vegetation was also suppressed in that season (Jury, 1998). The South Coast and Zululand LSGs time series are closely correlated to the industry values, and these three tallied equally (79.0 ton/ha) in the1999/00 season.

The spatial differences in response and adaptation to climate impacts exist in the study area, since farmers in inland and irrigated regions adapt better to climate extremes than those in coastal and rain-fed agro-climatic regions.

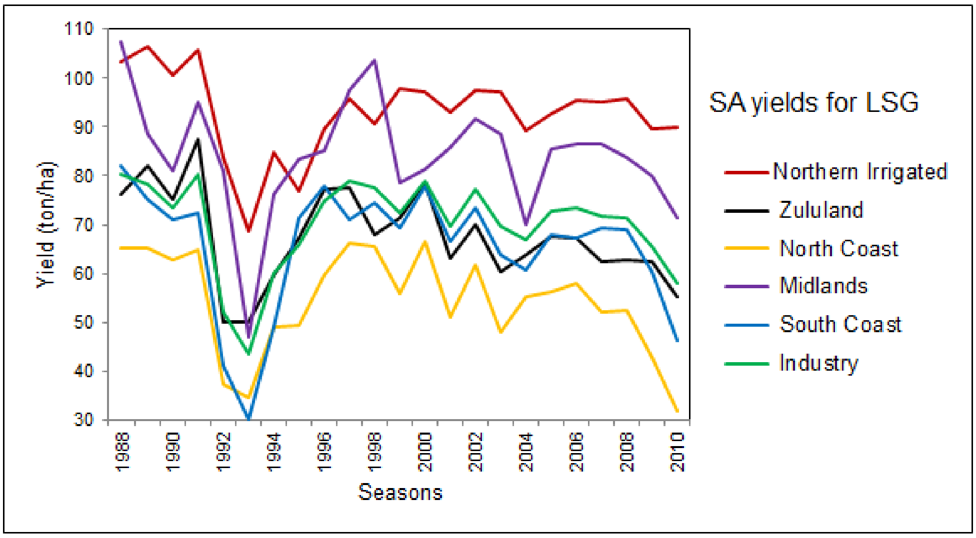

Figure 4.6: Historical sugarcane yields for large-scale growers over the South Africa (SA) sugar industry (Northern Irrigated, Zululand, North Coast, Midlands, and South Coast) for the period 1988-2010.

4.5.2 Small-scale growers (SSGs)

The Northern Irrigated region was observed to be doing well in both LSGs and SSGs in the SA sugar industry, but there is a remarkable dip in SSGs for the period 1988-2010 (Figure 4.7). The differences in magnitudes of actual sugarcane yield recorded for SSGs in different regions might not be solely the result of climate influences. Failure to adapt due to lack of resources might be a possible cause of small-scale growers and their yield decline.

Zululand region has the lowest SSGs time series, possibly due to pest. SSGs of sugarcane show understanding of sugarcane pests, but they lack knowledge of pest control management practices of pests and other damaging insects (Mulcahy, 2018). These growers mentioned *Eldana saccharina* as the main crisis in their production system. Midlands region has a good record of yield from small-scale growers, but in 1993/94-1995/96 staggeringly dropped almost below all the regions. The interventions and decisions for action employed thereafter resulted in a sharp increase in the time series. These could be infiltrated to other SSGs in order to stimulate their participation in sugarcane growing, thus maintaining viability of sugar production.

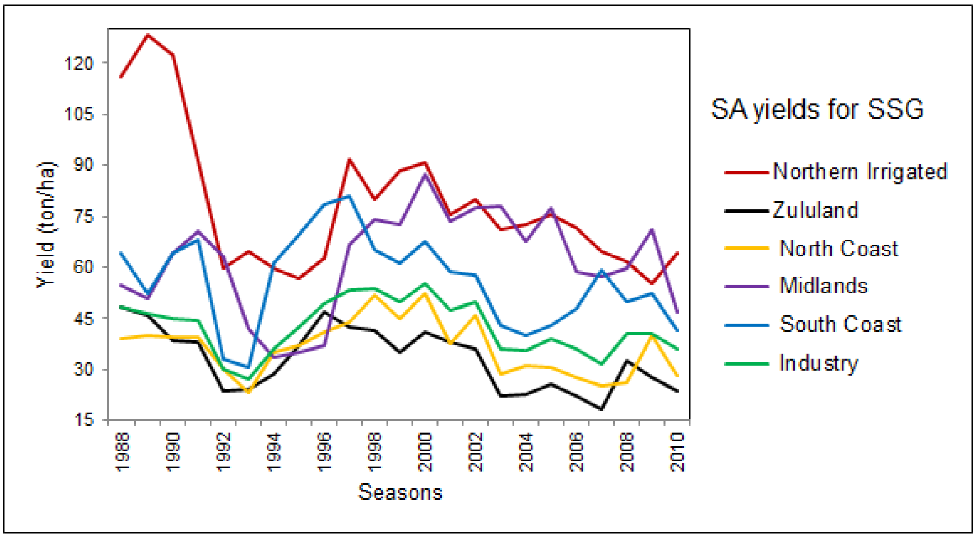

Figure 4.7: Representation of sugarcane yield time series from small-scale growers in the SA sugar industry from 1988-2010.

4.5.3 All-averaged sugarcane yield over SA growing areas

The majority of sugarcane in South Africa is rain-fed (Jones & Singels, 2015), hence rainfall has a steep gradient from South Coast (wet) to Northern Irrigated (dry), as illustrated in Figure A.1. The industry sugarcane yield values are computed from the five agro-climatic regions (Northern Irrigated, Zululand, Midlands, North Coast and South Coast). Figure 4.8 shows that - the South Coast region has a well-matched time series to that of the industry (all-averaged) yield values. It was clear from the time series analysis that - although SSGs are outnumbering the LSGs, their production output is less. This could be due to efficient use of additional crop management practices such as fertiliser application and use of improved variety.

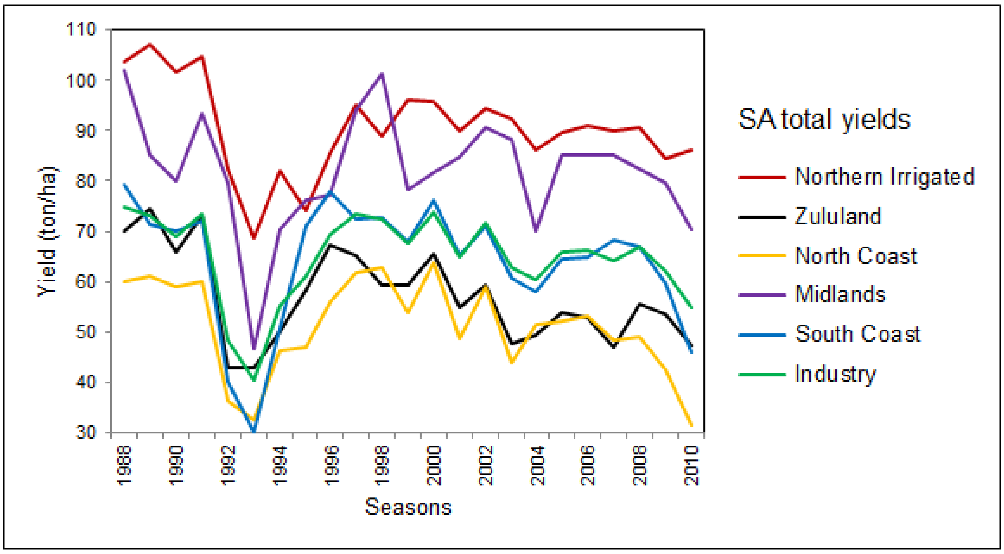

Figure 4.8: Inter-annual variability of all-averaged sugarcane yields produced in the SA sugar industry, as varying across the industry from 1988-2010.

4.5.4 Simulated sugarcane yield for SA industry

Sugarcane yield data presented below (Figure 4.9) was simulated using the *Canesim* model as described in previous studies (Singels, 2007; van den Berg & Singels, 2013). This data was obtained from van den Berg & Singels (2013). This model forecasts the potential yield, and it fairly detects the evolution of yield as varying from season-to-season timescale. However, this model overestimates sugarcane yield in almost all agro-climatic regions of the SA sugar industry (*see* Figure 4.9). This was also reported by Jones and Singels (2015).

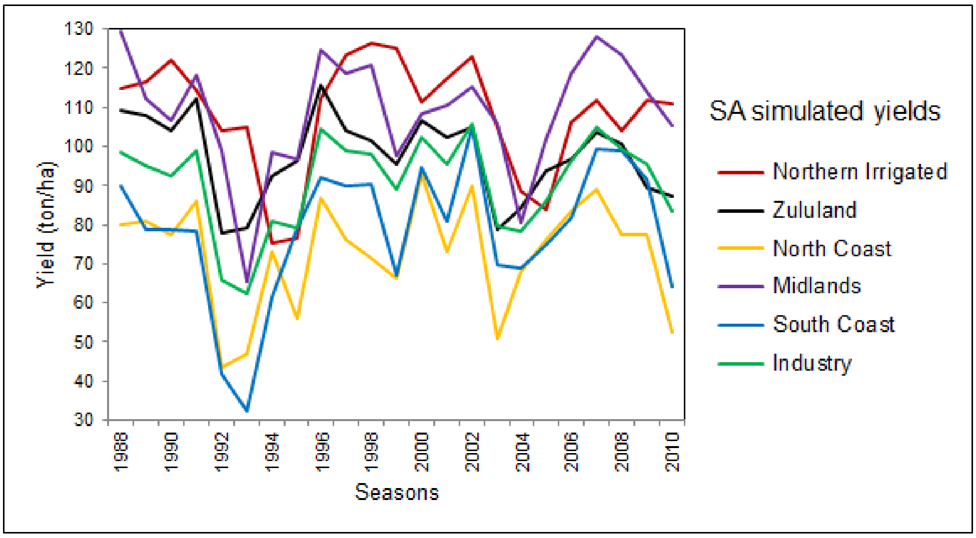

Figure 4.9: Simulated sugarcane yield trends, computed with Canesim model for agro-climatic regions of the SA sugar industry from 1988-2010.

High yield values (100-110 ton/ha in 1988) were observed in the Midlands and Northern Irrigated regions for LSGs. The Northern Irrigated is the only region that exhibited high sugarcane yields ($>$100 ton/ha) for the period from 1988-1990 for SSGs. The Midlands and Northern Irrigated regions documented total yield values $>$ 100 ton/ha in different growing levels from 1988-2010, but the model showed that all sugarcane growing regions has once recorded more 100 ton/ha, with the exception of the North Coast region, as illustrated in Figure 4.9.

4.6 Sugarcane yield trends

The Mann-Kendall test uses z-score and the p-values statistics to detect and evaluate trends and their significance. The significant trend must exhibit the absolute value of z of 1.96 with the $p \leq 0.05$. Table 4.1 presents a summary of the Mann-Kendall statistics for sugarcane yield from different regions of the South Africa sugar industry and Food and Agriculture Organisation (FAO) yields for SA and ESwatini. The trends were detected for LSGs, SSGs, total yield and simulated yields (SYs). Three agro-climate regions (Northern Irrigated, Zululand and South Coast) showed significant changes in linear trends in different growing scales at $p \leq 0.05$.

Table 4.1 reveals that South Africa exhibits a declining yield trend with z-score of -4.604 of p $-$value of 4.15×10^{-6}. ESwatini has z-transformation of -4.631 and $p-$ value of 3.63×10^{-6}. The Northern Irrigated region depicts a downward trend, which is indicated by a z-transiformation of -2.483 and p $-$value of 0.01 for SSGs. In the Zululand region the yield has been decreasing in all growing scales (LSGs and SSGs, which could be possibly due to drought conditions (Dubb, 2015).

Table 4.1: Mann-Kendall (MK) test statistics for sugarcane yield (ton/ha) trends over South African agro-climatic regions, bold z-score are significant at the 95% level.

Agro-climatic regions	**Statistics**	**LSG**	**SSG**	**Simulated**	**Total**
Northern Irrigated	z	-0.739	**-2.483**	-0.845	-1.215
Northern Irrigated	p-value	0.460	0.013	0.398	0.224
Northern Irrigated	Tau	-0.115	-0.375	-0.130	-0.186
Zululand	z	**-2.060**	**-2.905**	-1.532	**-2.641**
Zululand	p-value	0.039	0.004	0.126	0.008
Zululand	Tau	-0.312	-0.439	-0.233	-0.399
North Coast	z	-1.585	-1.268	0.211	-1.690
North Coast	p-value	0.113	0.205	0.833	0.091
North Coast	Tau	-0.241	-0.194	0.036	-0.257
Midlands	z	-0.739	1.215	0.211	-0.528
Midlands	p-value	0.460	0.224	0.833	0.597
Midlands	Tau	-0.115	0.186	0.036	-0.083
South Coast	z	**-1.954**	-1.690	1.321	-1.796
South Coast	p-value	0.051	0.091	0.187	0.073
South Coast	Tau	-0.296	-0.257	0.202	-0.273
Industry	z	**-1.954**	-1.690	1.321	-1.796
Industry	p-value	0.051	0.091	0.187	0.073
Industry	Tau	-0.296	-0.257	0.202	-0.273
		South Africa and ESwatini (FAO)			
SA_FAO	z	**-4.604**			
SA_FAO	p-value	4.15E-06			
SA_FAO	Tau	-0.465			
Swazi_FAO	z	**-4.631**			
Swazi_FAO	p-value	3.63E-06			
Swazi_FAO	Tau	-0.468			

There might be a possibility that other farmers have opted to participate in timber plantations (Kelbe, *et al*., 1991), and parts of the sugarcane area modified to become residential areas (rental houses). The industry LSGs yield depicted a significant downward trend and coincided with those of South Coast region LSGs, where z-transformation is -1.95 with p-value of 0.05. While the Mann-Kendall statistic test method is useful for investigating overall trend in the time series, It is always important to determine important parameters such as regions when the trends begin and how far do they go before they recover again. Therefore, a Sequential Mann-Kendall trend test method is useful for this purpose because it detects trends and their potential turning points (Chatterjee, *et al.,* 2014). Figure 4.10 shows the

Sequential Mann-Kendall trend test results for SA FAO (a) and SWAZI FAO (b). In this figure, the red solid line indicates the sequential statistic values of forward/progressive (Prog) and the solid black line represents the backwards/retrograde (Retr) Sequential Mann-Kendall statistic for yearly mean sugarcane yield data from SA (a) and ESwatini (b), respectively.

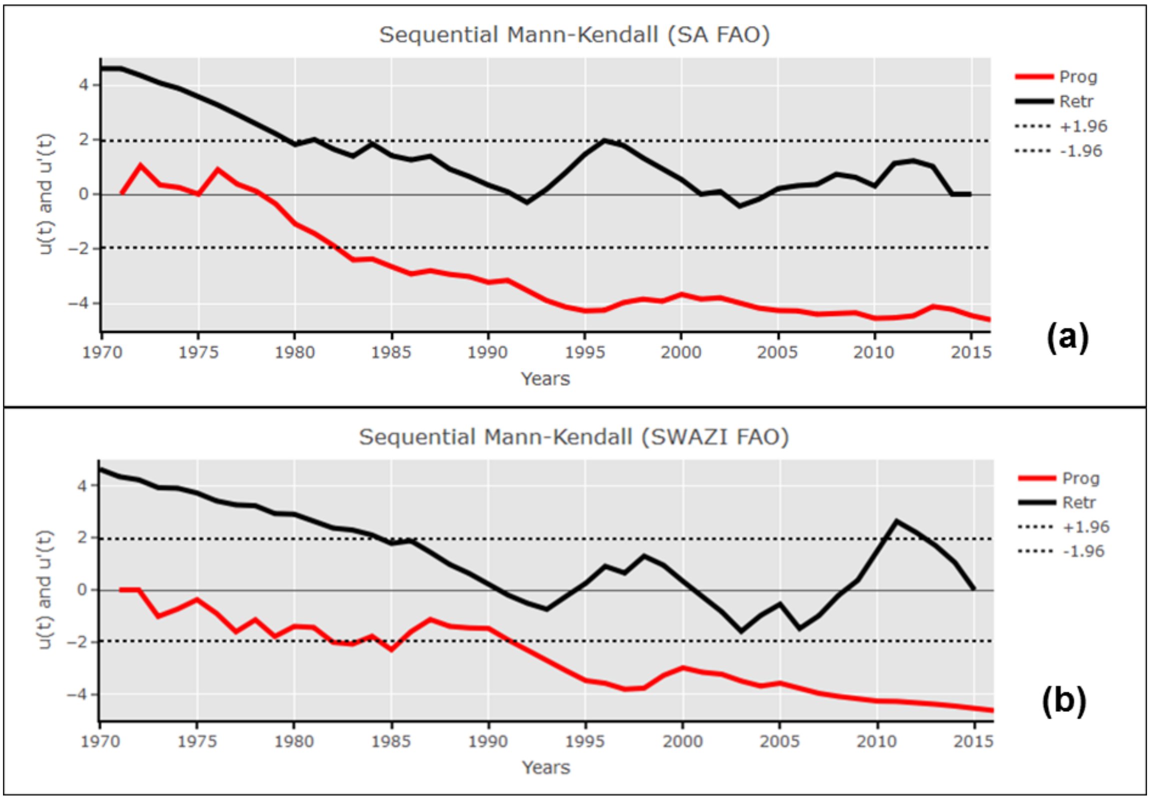

Figure 4.10: Trends in FAO sugarcane yield sequential version of Mann-Kendall test statistic, $u(t)$ forward sequential curve represented in solid-black line and $u'(t)$ backward sequential curve represented in solid-red line over a) South Africa and b) ESwatini.

The Mann-Kendall statistic test indicated that sugarcane yields have certainly been decreasing since 1980s. A huge decline of the yield was observed during the period from 2010-2016, where z-score values were observed to be below -4, which is an indication of a significant downward trend (*see* Figure 4.10). These results are consistent with observations by van den Berg and Singels, (2013) in their study of modelling and monitoring for strategic yield gap diagnosis. The trend is declining and additional influences in a form of non-climate have been reported (Dube & Jury, 2000; van den Berg & Singels, 2013), which makes the discrepancy complicated and requiring multidisciplinary action. The intersection of the curves $u(t)$ and $u'(t)$ located the approximate PTTPs, hence from FAO sugarcane yield time series no

PTTP was detected, but these were detected in different agro-climatic zones of the SA sugar industry, as illustrated in Figure C.1. All identified approximate trend turning points are significant at the 5% level, and these PTTPs tend to be located above ‘0’ point during the wet seasons and below ‘0’ point in dry periods (Figure C.1), resembling the oscillations of local and remote climate oscillations. Remarkably, all agro-climatic zones of the SA sugar industry revealed approximate PTTPs in the simulated yield, but other regions have no PTTPs (e.g Zululand region) in all production levels or scale (LSGs, SSGs and TOT). During the 2000-2004 seasons the curves $\mathrm{u(t)}$ and $\mathrm{u'(t)}$ are in phase, and this contrast between actual and potential yields requires further scrutiny.

4.7 *Canesim* relative performance

The *Canesim* crop forecasting system requires the *Canesim* sugarcane model and daily weather data from 33 weather stations in 48 homogenous climate zones. It is generally preferred over other, more complicated, models (e.g DSSAT-Canegro model) because it has been configured for operational use in South Africa, and less effort is needed for its implementation in crop forecasting studies in the country. The data input required for the Canegro model is not available at application scale for other studies. The model has been used and validated in previous studies (Singels, 2007b; van den Berg & Singels, 2013), and here, the performance is evaluated with the use of Taylor diagrams.These diagrams use the root-mean-square-difference (RMSD), correlation coeffient (*r*) and standard deviation (SD). If the correlation coeffient is high (i.e. closer to +1), the RMSD and SD are small, which indicates that the model outperformed the actual yield. In this study observation refers to simulated value of sugarcane, because there are three reference data/variables (e.g actual sugarcane yield from SG, LG and TOT).Figure 4.11 shows how potential sugarcane yield simulates or mimics the actual sugarcane yield in different agro-climatic regions of the SA sugar industry from 1988-2010. The statistical correlations revealed that the ‘*Canesim’* model simulates sugarcane yield better in rain-fed areas than its counterpart irrigated agro-climatic regions, as illustrated in Figures 4.11 and D.1, and these results are analogous to those of van den Berg and Singels (2013). There is a strong positive correlation between simulated (SY) and actual all-averaged (TOT) sugarcane yield ($r \geq +0.85$) in the South Coast region, while in the industry as a whole the value increased by 1% ($r \geq +0.86$).

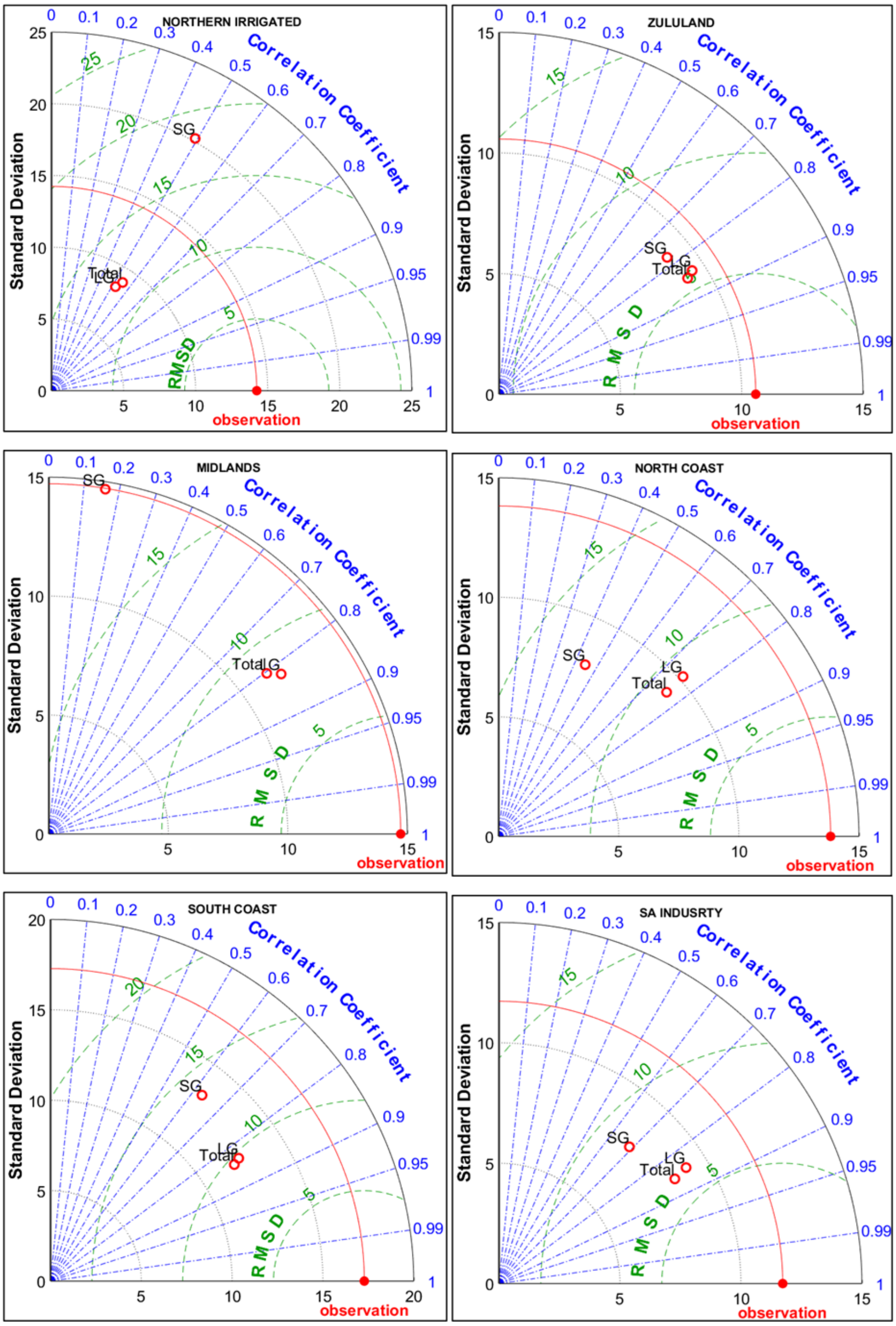

Figure 4.11: Taylor diagrams for inter-comparisons between simulated and actual sugarcane yields from different production scales (LSGs, SSGs and Total) over the SA sugar industry from 1988-2010.

However, moderate positive association ($r \geq +0.55$) between potential and actual yield was observed over the Northern Irrigated region, partially due to irrigation because even during the dry season storage dams provide a buffer. This reduces the fidelity of crop-climate models.

Nonetheless, these findings presented in Figure 4.11 are analogous to those reported in previous studies (Bezuidenhout & Singels, 2007b; van den Berg & Singels, 2013). The root-mean-square-difference (RMSD) and standard deviations (SD) were introduced to the diagrams to supplement r statistics. The RMSD was corrected for bias and expressed as a percentage (%). In the South Coast region there is low RMSD and SD (RMSD = 10% and SD = 6.5 units for LSG and SY). However, higher RMSD and SD (RMSD = 12.5% and SD = 6.5 units for LSG and SY) were observed in the Northern Irrigated region. Much smaller magnitudes were evident in the industry (RMSD = 6% and SD = 5 units for LSG and SY). The SSG yield poorly correlated with SY (e.g. $r = +0.45$), with the exception of the Zululand region where SSG and SY showed a strong positive statistical link ($r \geq +0.78$).

4.8 Statistical climate-sugarcane relationship

In this study, the Pearson correlation was important for exploring the relationship between sugarcane yields, climate parameters and indices in different sugarcane growing regions of South Africa, as illustrated in Figure D.1. Figure 4.12 shows the heatmaps of Pearson correlation coefficient statistics for data used here for the period from 1970-2016 (for FAO yield) and area-averaged meteorological data. These statistics were derived using R procedures over the subtropical sugar belt of SE Africa. However, the Pearson correlations for all agro-climatic zones are also done (*see* Figure D.1).

The model output from MLR algorithms shows the influence of rainfall, temperature, PDSI, SOI, SSTs, and Niño4 on sugarcane yield (Tables 4.3 and E.1). These climate variables and indices were chosen because of their interdependence and potential role in climate variability over the subcontinent.

A negative Pearson correlation (PCC = -0.68) between temperature and sugarcane yield was observed in South Africa (Figure 4.12a), and in ESwatini sugarcane is 100% irrigated but the statistical linear relationship (PCC = -0.48) between temperature and yield does exist, as illustrated in Figure 4.12b. Rainfall and yield have a statistical association of PCC = +0.5 and PCC = +0.45 for South Africa (a) and ESwatini (b), respectively.

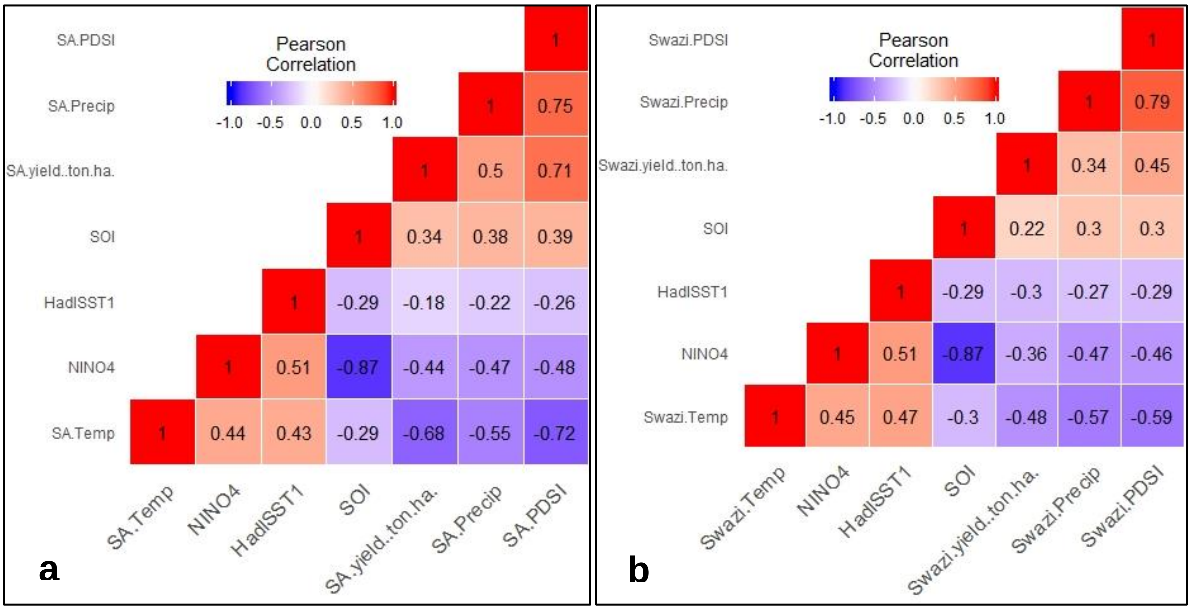

Figure 4.12: Heatmap of Pearson Correlation representing statistical degree of association and its extent between climatic factors and sugarcane yield from 1970-2016 in a) South Africa and b) ESwatini. PCC is defined as +1 for strong positive correlation, 0 indicates that there is no linear relationship, and -1 means strong anti-correlation. In some cases closer to 0 values result from the noise in the time series.

The abrupt temperature and potential evapotranspiration increase tends to reduce the amount of soil moisture which then suppress sugarcane yield. This implies that despite potential rainfall increasing or decreasing, temperature has the ability to deplete soil moisture and surface water through potential evapotranspiration. These interactions are incorporated in the PDSI, and the study affirms this drought index as a good proxy for sugarcane yield because these two are strongly correlated ($PCC > +0.7$) in South Africa. In ESwatini this index explains 50% of cane variation from season-to-season, as expected.

4.9 Rainfall, temperature and yields correlations

The annualised PDSI (precipitation minus potential evapotranspiration) has a strong positive correlation with sugarcane yield (*see* Figure 4.12), and as a result the 3-month lead time detrended correlations between monthly GPCC8 rainfall and CRU4 temperature with detrended sugarcane yield index (N =45), as illustrated in Table

4.2. These determined the relevant seasons to be studied. Sugarcane yield showed statistically significant correlations during Dec - May with rainfall and temperature, and also in September (for temperature). This demonstrates the influence of climatic conditions associated with temperature before and during the growing season. Surface air temperature and the yield display negative correlations ($r < -0.4$), which implies that: a hot preceding season is expected to cause a sugarcane yield decrease in the following season. Area-averaged rainfall has a positive statistical link ($r \geq +0.5$) with sugarcane yield. These correlations indicate that sufficient rainfall is imperative for soil moisture recharge and filling reservoir storage, thus sugarcane yield could increase, as demonstrated in Table 4.2. These correlations (Table 4.2) identify the important seasons to be investigated in this current study, and as a result most analyses were restricted to Dec-May. It should be noted that correlations less than 50% ($r \leq \pm 0.5$) could be ascribed to detrending and proximity of correlated variables. Too remote climate indices correlate weakly with yield over SE Africa, while local climate variables (PDSI, rainfall and temperature) show strong signals and influences on the yield.

Table 4.2: Correlation per month of 1970-2014 of sugarcane yield with detrended rain and temperature in the sugarcane growing area, with climate leading by 3 months. Numbers in bold indicate the significant correlations. Positive correlations indicate proportionality and negative correlations show inverse relationship.

Months	Rain	Temp
Jan	**0.496**	**-0.476**
Feb	**0.253**	**-0.288**
Mar	**0.270**	-0.145
Apr	**0.292**	**-0.295**
May	**0.424**	**-0.483**
Jun	0.110	-0.042
Jul	0.186	-0.207
Aug	-0.043	0.061
Sep	0.099	**-0.317**
Oct	-0.060	-0.125
Nov	**0.345**	0.033
Dec	**0.264**	-0.189

Sugarcane requires minimal rainfall during the harvest season, and this season spans from early winter to late spring. Excessive rainfall could favour the outbreak of sugarcane pests and other dangerous insects. The nodes may even re-germinate when it rains during harvest, thus reducing the amount of cane to be submitted for milling.

In Figure 4.12 strong associations between different climate variables and indices exist, wherein short and long-term effects of climate were detected. The comprehensive-holistic multiple linear regressions were derived using the R "trend" package, and this was useful for testing variable importance in climate variables that are expected to influence the inter-annual variability of sugarcane yield. The results are shown in Tables 4.2 and E.1.

Table 4.3: Model output from MLR for FAO sugarcane yields (dependant variables) and climatic variables and indices are independent variables for the period 1970-2016.

MLR for South Africa					
	Estimate	Std. Error	t-value	p-value	Signif. Codes
(Intercept)	4.851e+01	1.004e+02	0.483	0.6318	
SA_PDSI	5.842e-02	2.248e-02	2.599	0.0131	*
SA_Precip	-1.505e-04	2.009e-04	-0.749	0.4584	
SA_Temp	-1.260e-01	5.499e-02	-2.291	0.0274	*
HadISST1	1.486e-01	8.900e-02	1.670	0.1029	
HadSLP	-4.473e-02	9.905e-02	-0.452	0.6541	
Niño4	-6.986e-02	7.438e-02	-0.939	0.3534	
SOI	-2.863e-02	6.432e-02	-0.445	0.6586	
MLR for Eswatini					
	Estimate	Std. Error	t-value	p-value	Signif. Codes
(Intercept)	2.413e+01	5.086e+01	0.474	0.6378	
Swazi_Precip	-5.737e-05	8.396e-05	-0.683	0.4985	
Swazi_Temp	-4.073e-02	2.408e-02	-1.691	0.0987	.
Niño4	-4.310e-02	3.871e-02	-1.113	0.2724	
SOI	-3.193e-02	3.209e-02	-0.995	0.3260	
HadSLP	-1.843e-02	5.016e-02	-0.367	0.7153	
HadISST1	5.250e-03	4.446e-02	0.118	0.9066	
Swazi_PDSI	1.268e-02	9.581e-03	1.323	0.1935	

*Signif. codes: 0 '***' 0.001 '**' 0.01 '*' 0.05 '.' 0.1 ' ' 1 where these numbers from 0-1 are p-values and the order of significant is strongest at $p - value = 0$ and denoted with '***' while p-value = 1 means that the independent variable is not statistically significant.*

The analysis revealed a statistically significant relationship between potential sugarcane yield (simulated) and PDSI in Zululand, Midlands and South Coast regions at 0.1-1% levels, as illustrated in Table E.1. This confirms the high correlations observed between these two variables in Figures 4.11 and D.1. The influence of PDSI on yield was more enhanced for large-scale commercial growers, and reached the 0% level of significance, as shown in Figure E.1. This was also evident in large-scale commercial production in all agro-climatic zones of the SA sugar industry since the yield showed that PDSI is by far the most important indicator of sugarcane yield at the 1% level, which implies that LSGs farming operations and decision-making are informed by climate departures. There are many SSGs than LSGs but their contribution to total yield (TOT) over SA is marginalised, possible due to abrupt climate variability and lack of resources for adaptation. In addition to PDSI, these farmers are also affected by temperature increase and ENSO, as indicated by SOI and Niño4. Sugarcane yield over the South Coast region is expected to be driven by pressure systems such as the coastal low and Mascarenes High, which adds onto ENSO and evaporation influences, as illustrated in Table E.1. These pressure systems are explored in the spatial analysis (Chapter 5). The FAO sugarcane yield time series was analysed and the findings showed a strong relationship between PDSI, temperature and sugarcane yield at the 1% level in South Africa, while in ESwatini the yield is more suppressed by temperature at the 5% level. This decrease in climate influence in ESwatini was expected, due 100% irrigation but temperature tends to exacerbate evaporation during intense drought conditions (e.g. 2014-2016, as reported in Mbatha & Xulu, 2018), hence rivers dry up and sugarcane could be diminished.

4.10 Summary

Southeastern Africa's subtropical sugar belt receives ≥800 mm/yr of mean annual precipitation (MAP) (*see* Figure 4.2a), while DJF rainfall is above 100 mm/month (Figure 4.1). PDSI and sugarcane yield have a strong positive correlation for South Africa ($r \geq +0.7$) and ESwatini ($r \geq +0.5$), respectively. This is expected because climate is the main driver of rain-fed sugarcane yield over southern Africa. This also indicates differences in response to climate between rain-fed and irrigated. In general, PDSI seems to be a good indicator of sugarcane yield, and incorporating this index in crop models could increase performance skill and accuracy. Moreover, it was expected that the reduced MAP and increased surface air temperatures supress sugarcane yield.

Sugarcane yield depicted a downward trend (*cf*. Table 4.1 and Figures 4.10 and C.1) in both local and global sugarcane yield. This necessitates further scrutiny which will lead to the establishment of a climate service which will offset the impacts of climate variability and change. Pressure systems showed an influence in sugarcane yield in the South Coast region (Table E.1), and this will be interrogated further in Chapter 5 under spatial analysis. All statistical associations showed that climate and sugarcane yield is 50-80% related. This indicates that 20-50% of seasonal sugarcane yield variations could be defined and controlled by non-climatic factors, subject to farming operations and climate of the agro-climatic region.

It is also important to note that a new index for approximating soil moisture has been devised in this study (*cf*. Figure 4.5). This index integrates MERRA2 SHF and surface evaporation to formulate a distinct index, where high values indicate soil moisture loss and low values are linked to minimal soil moisture loss.

CHAPTER 5

LOCAL CLIMATE AND SUGARCANE YIELD

5.1 Introduction

Approximately 90% of agriculture in southern Africa is rain-fed (Rosegrant, *et al.,* 2002) and climate is a key factor that controls production. Strategies to mitigate or adapt to climate variability and change in southern Africa are needed to improve yields (Stringer, *et al*., 2009). This chapter presents the application of climate science to yields in the sugarcane growing region of southeastern Africa for the period 1970 to 2016; the period of data analysis was informed by data availability. The results presented in this study were produced using the research methodology outlined in Chapter 3, but this might differ when applying a different method.

5.2 Mean spatial patterns during Dec-May

In Table 4.2 sugarcane yield correlated positively with rain ($r \geq +0.5$) and negatively with temperature ($r \leq -0.4$) from Dec-May and Sep for surface air temperature. The South Coast region showed significant response to local climate systems, as illustrated in Table E.1. These correlations and MLRs revealed important seasons and weather systems to be studied, respectively. This current study found if useful to study Dec-May climatology of climate elements for the period from 1970-2016, subject to data availability. Climatology helps to analyse the spatial distribution of the climate elements during this important season, and identify key weather systems for sugarcane production over SE Africa. The results are presented next.

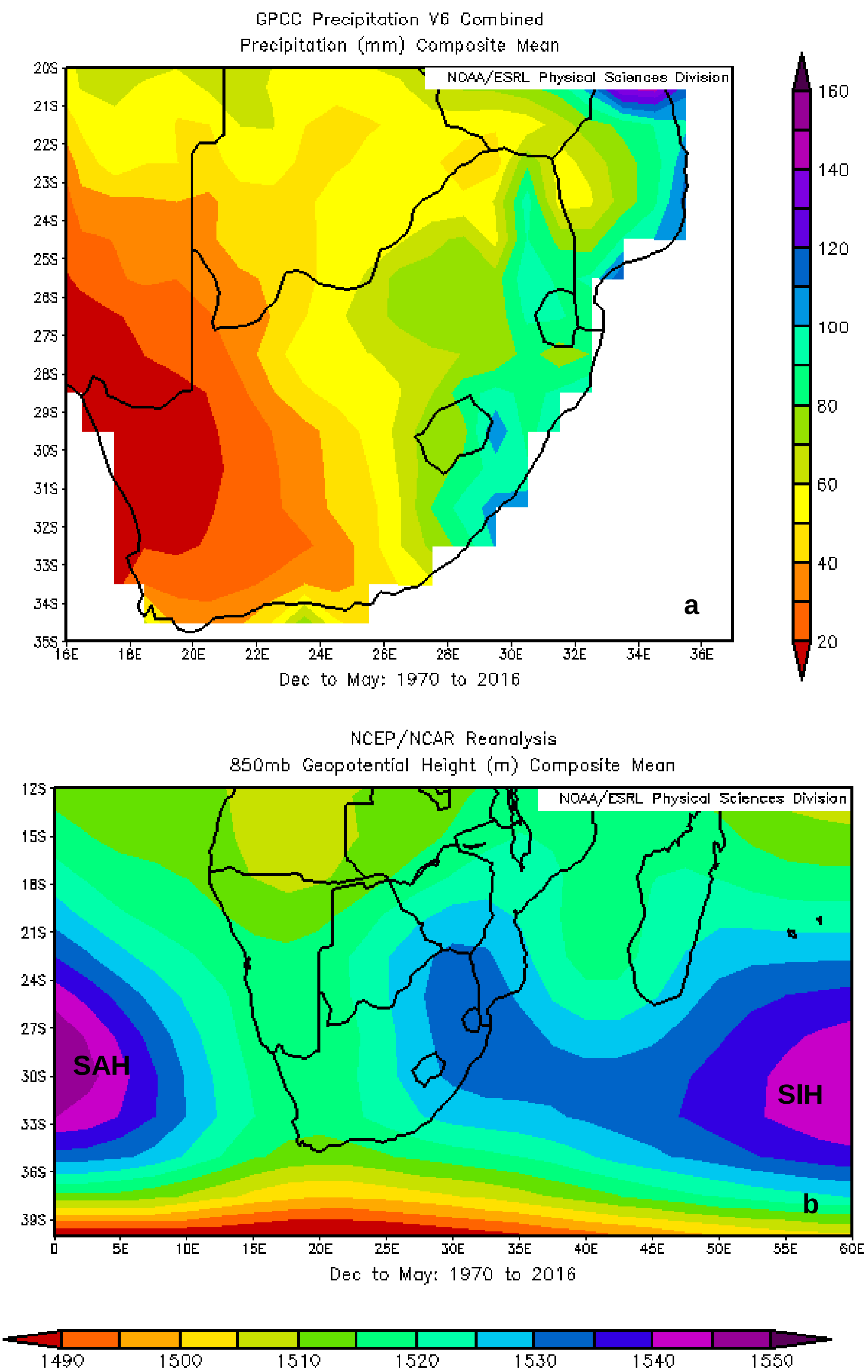

Figure 5.1: A climatology of Dec – May a) seasonal mean precipitation (mm/month) and b) geo-potential height (m) at 850 hPa from NCEP/NCAR reanalysis over southeastern Africa for the period 1970-2013.

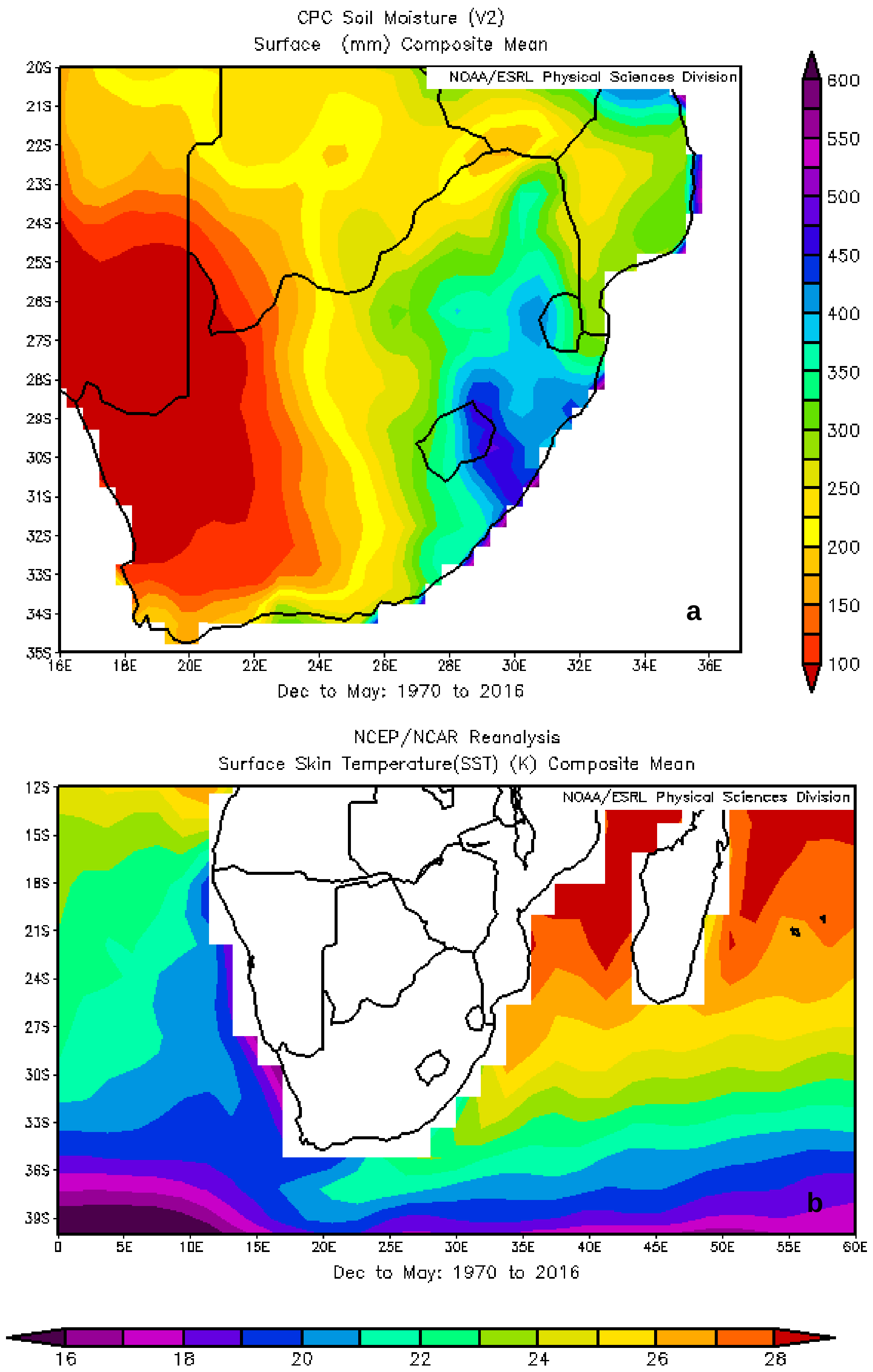

Figure 5.2: Spatial distribution of the mean: a) CPC surface V2 soil moisture (mm/month) and b) sea surface temperature patterns (°C) over southern Africa.

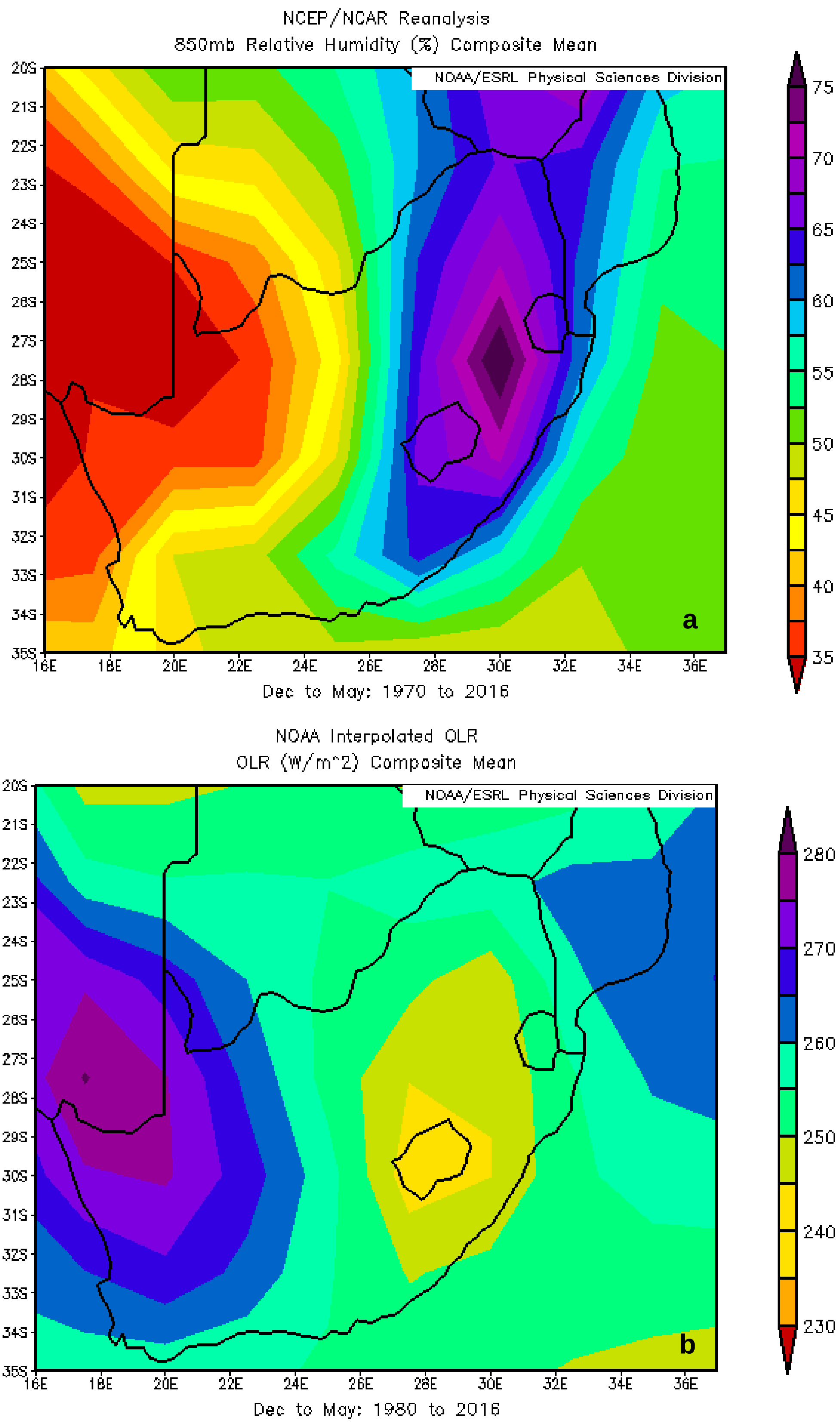

Figure 5.3: Spatial distribution of Dec-May mean a) NCEP reanalysis relative humidity (% at 850 hPa), and b) NOAA satellite interpolated Out-going Longwave Radiation (Watts per metre square) over southern Africa.

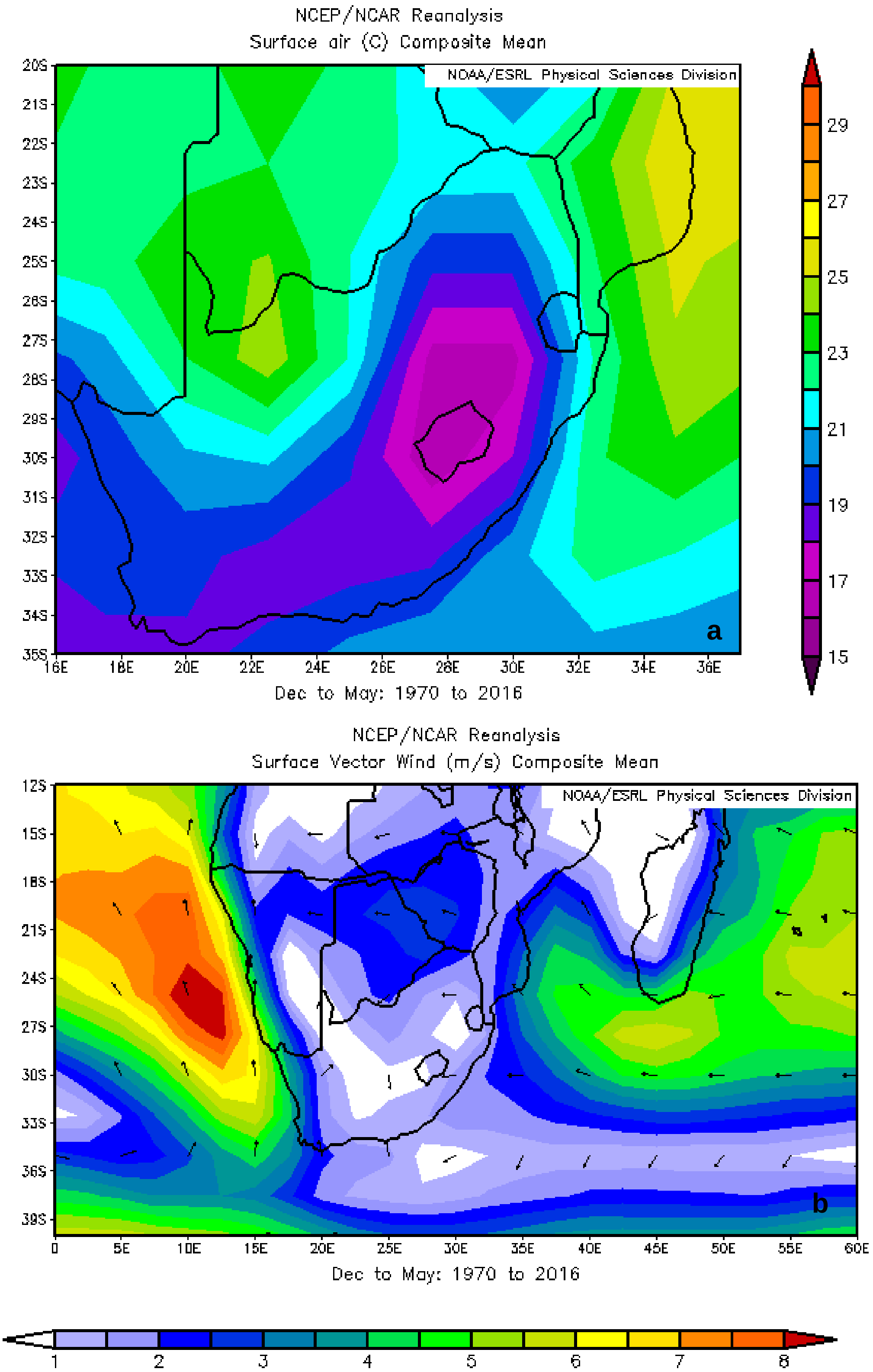

Figure 5.4: Spatial distribution of mean NCEP/NCAR reanalysis of a) surface air temperature (°C) and b) wind vector (m/s at 850 hPa) over southern Africa.

The climatology of the study area shows west to east gradients according to the elevation. Approximately 100-120 mm per month of precipitation is accumulated in the sugarcane area during Dec – May, while the western portion is dry (Figure 5.1a). The climate of southeastern Africa is characterised by surface air temperatures of >18 °C (Figure 5.4a) and marine anticyclones with high geo-potential height (Figure 5.1b). The Mascarene high is ridged towards the subcontinent and trade winds are found to be strong (Figure 5.4b) during Dec – May. This advects moisture from the Indian Ocean towards the sugarcane area during Dec – May, yielding a positive influence during this period (rainfall, Table 4.2). The terrestrial low pressure triggers summer rainfall and convection, which increases soil moisture a fraction (>400 mm during Dec – May) and the greening of crops and vegetation in KwaZulu-Natal Province, Mpumalanga Province and ESwatini. The humid conditions (RH ≥ 75%) near the east coast and its warm Agulhas Current help to retain soil moisture, even during the winter season (Figures 5.3a and b).

5.3 AVHRR satellite vegetation (NDVI)

The next results show spatial distribution and annual averaged NDVI over southeast Africa for the period 1981-2013, derived from the IRI Climate Library. The NDVI can also be used as a proxy for sugarcane yield but there is a lead time of about 1-2 months. The west is brown-dry and the east is green-wet. The dashed box shows the area averaged, which is characterised by dense vegetation fraction (*cf.* Figure 5.5a); and other crops such as maize and sorghum are also present in this grid box (31-23°S and 28-33°E).

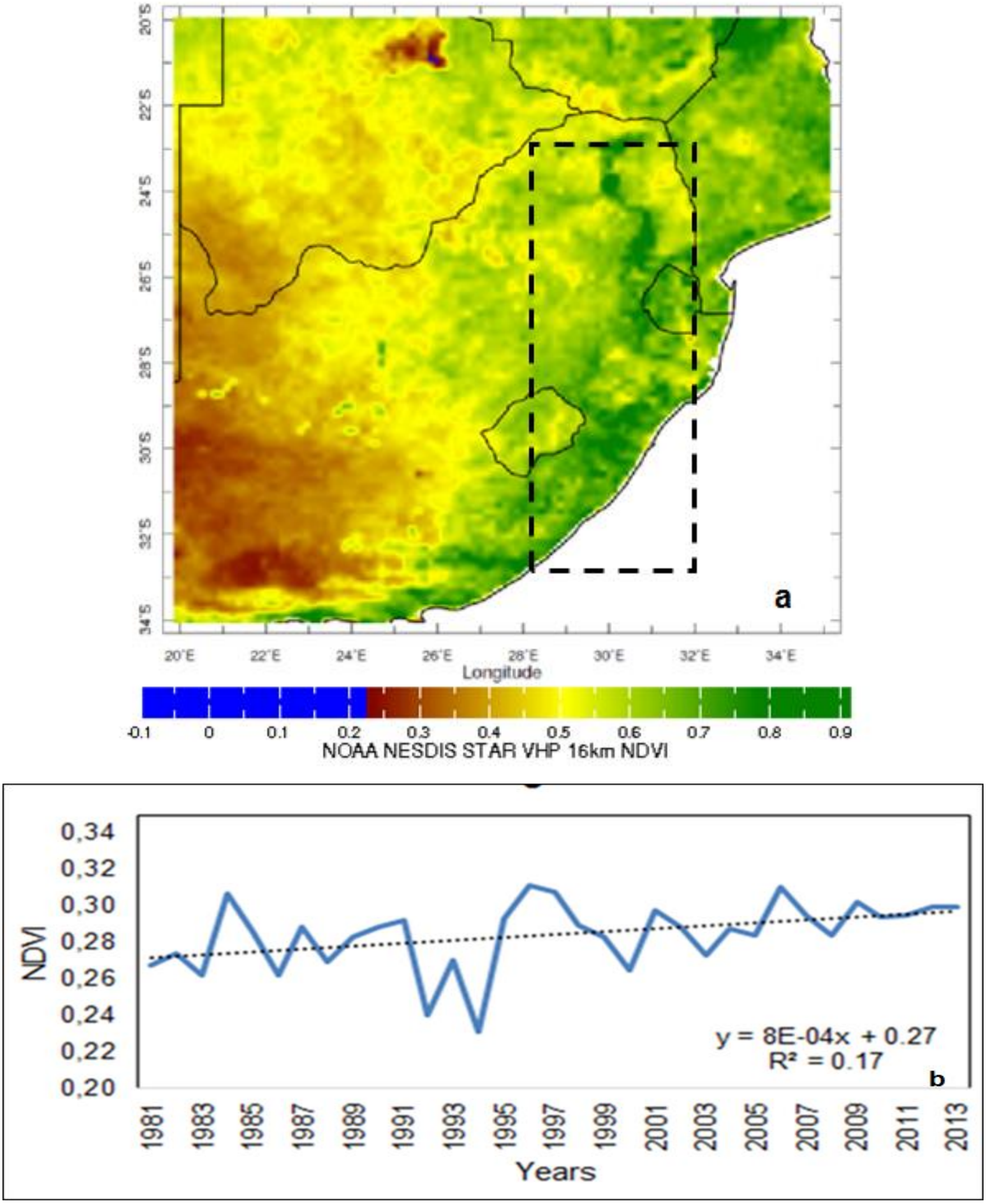

Figure 5.5: Normalized Difference Vegetation Index (NDVI) illustrating the vegetation conditions over southeastern Africa from 1981 to 2013 a) NDVI map where the black-dashed box marks the area-averaged and b) NDVI time-series showing variability and upward trend of satellite vegetation fraction in the study area. R-square value of 1 indicates that all data points in the time series are closer to each other, but here NDVI is unevenly distributed over time, and that is an indication of strong seasonal variability.

The sugarcane growing region (within the dashed box in Figure 5.5a) on the eastern seaboard of the subcontinent exhibits dense green vegetation. Vegetation canopy depends on climate variability, elevation and soil type. Regions of high rainfall (>1000 mm/yr), high elevation (Drakensberg), and fertile soil are characterised by dense vegetation canopy (Richard & Poccard, 1998). NDVI in areas under cane range from 0.2-0.8, but vegetation fraction >0.6 is predominant (*see* Figure 5.5a), and both vegetation and sugarcane benefit from sufficient rainfall and are suppressed by drought conditions.

5.4 Rainfall and sugarcane cycles

Rainfall over the area averaged shows strong seasonality and cycles. To determine those cycles, the CWT analysis was done in KNMI-CE, and the results are presented in Figures 5.6 and 5.7.

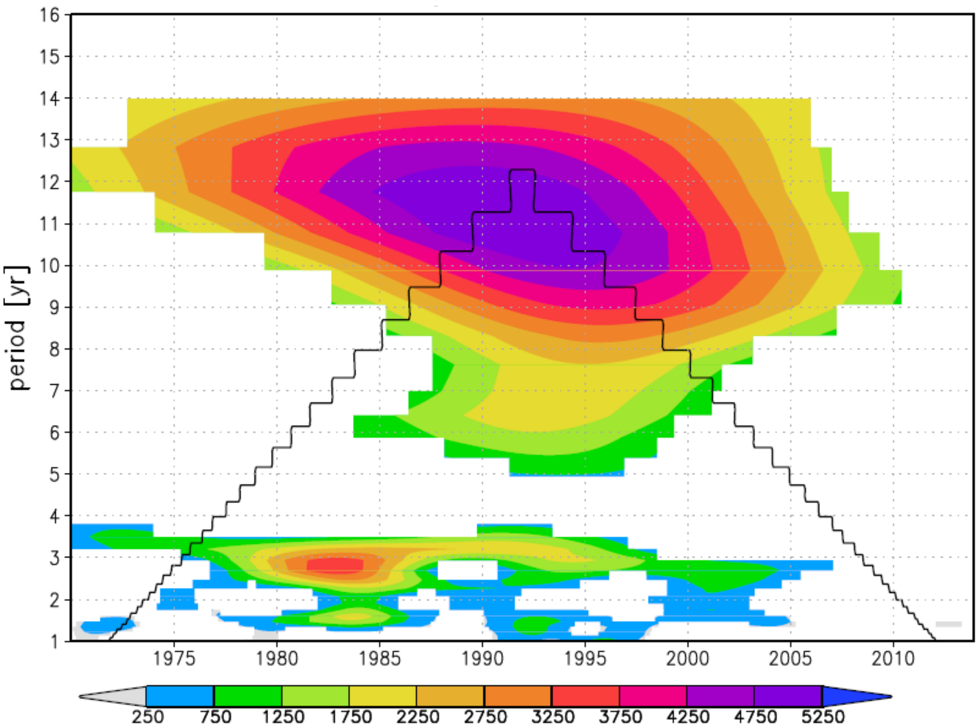

Figure 5.6: Wavelet spectral power of the sugarcane index 1970-2016 for 1-16 yr periods to determine sugarcane yield cycles. Values below 90% confidence are masked.

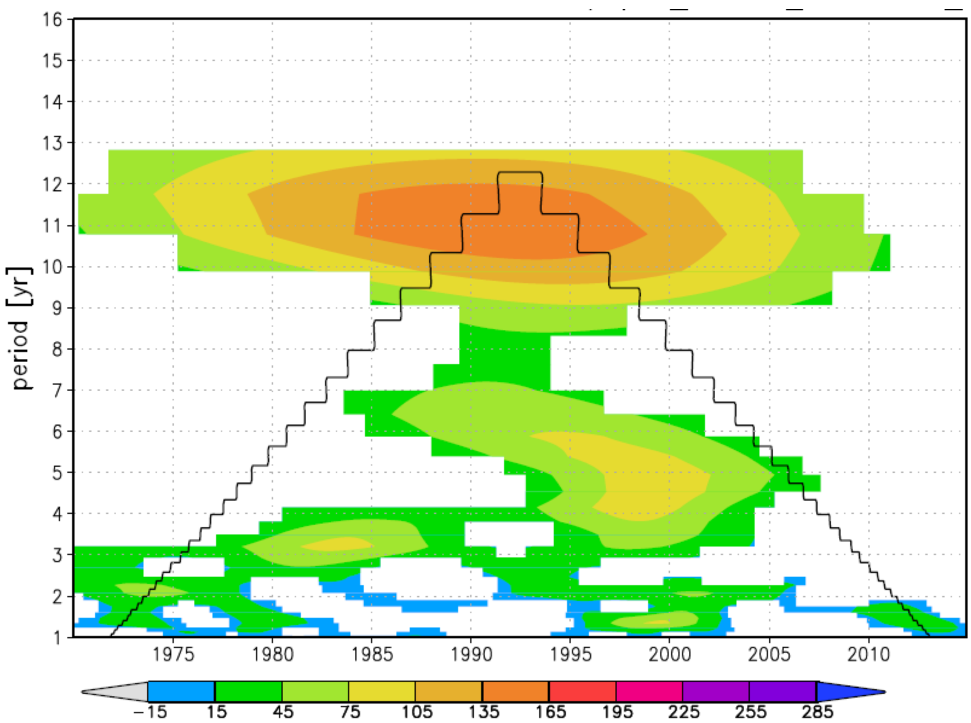

Figure 5.7: Wavelet spectral power of the Palmer Drought Severity Index from 1970 to 2016 averaged in the sugar-belt of southeast southern Africa. Values below 90% confidence are masked.

The UCAR Palmer Drought Severity Index (PDSI) was employed to signal the water budget via precipitation minus potential evaporation (Dai, *et al*., 2017). Both the combined yield index and the PDSI wavelet spectrum show cycles of 1-2 years during 1995-2000, 3-6 years during the 1980s and 10-12 years during 1980-2005 (see Figures 5.6 and 5.7). However, there is a strong cycle of 3+ years in sugarcane yield during 1983. The cycles imply that there is a strong seasonality in sugarcane yield, which is mainly due to drought conditions as a result of ENSO. These findings correspond to oscillations of the local climate (Mbatha & Xulu, 2018).

5.5 Seasonal NDVI correlation with sugarcane yield

In this study, the seasonal (DJF, MAM, JJA and SON) statistical detrended correlation between detrended sugarcane yield index (DSYI) and NDVI was also performed using the KNMI-CE. Mbatha and Xulu (2018) studied NDVI over eastern KwaZulu-Natal and the reported findings showed that NDVI response to climate is analogous to that of sugarcane. This section tests how good or fair NDVI behaves as a proxy for the yield.

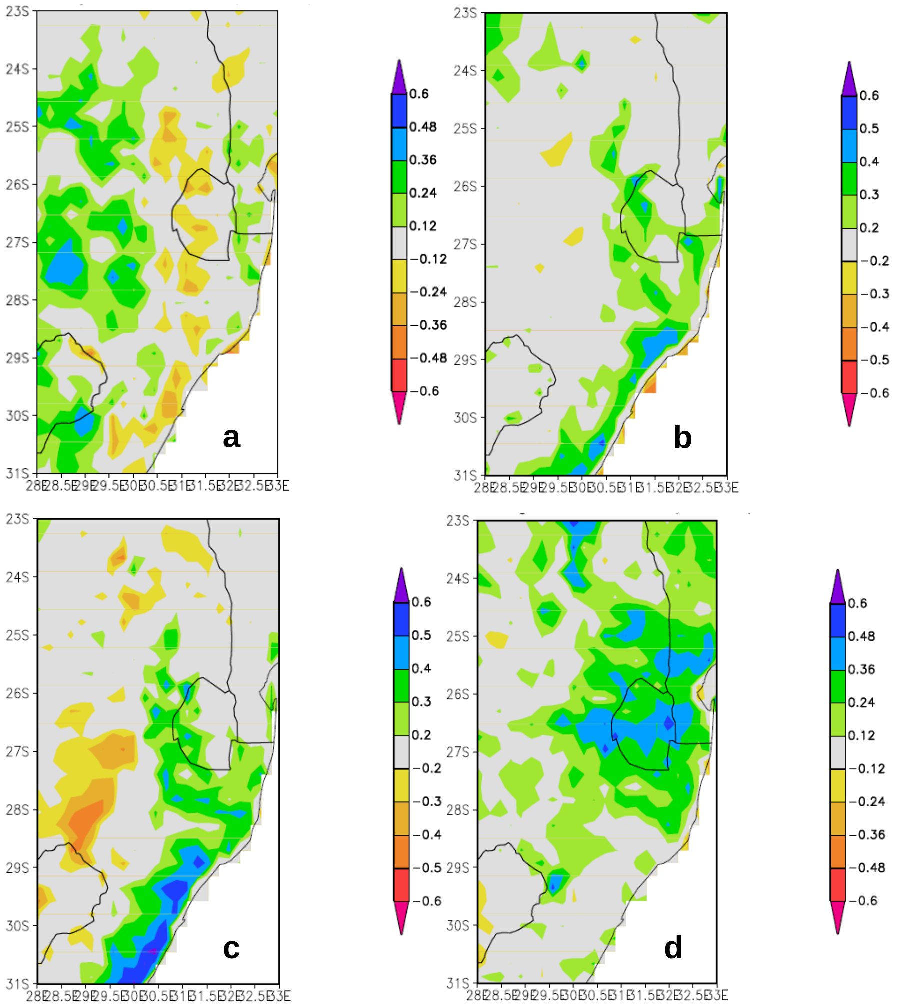

Figure 5.8: Correlation of detrended sugarcane yield index with seasonal NDVI over SE Africa (31-23°S and 28-33°E) a) Dec - Feb from 1981-2006 b) Mar – May from 1981-2006 c) Jun – Aug from 1981-2006 and d) Sep – Nov from 1981-2006.

The seasonal NDVI correlation shows the expected positive correlation ($r > +0.4$) that shifts around over the eastern zone. Correlations are strongest in southern KZN (i.e. $r > +0.5$ over South Coast region) in winter, possibly due to Agulhas retroflection, marine anticyclones and delayed onset of the monsoon. Over the Northern Irrigated region and ESwatini the correlation is stronger ($r \approx +0.4$) during spring, presumably because of irrigation. The negative relationship during DJF (rainy season) might be a result of too much rainfall in DJF relative to vegetation colour or high vegetative growth than crop growth and also to irrigation in parts of the sugarcane area.

5.6 December - May local climate correlations

In Table 4.2 the season Dec-May was identified as an important season for sugarcane development. In this section the local climate impacts on sugarcane yield was estimated with the use of rainfall and MERRA2 SHF. The results and analysis are presented below.

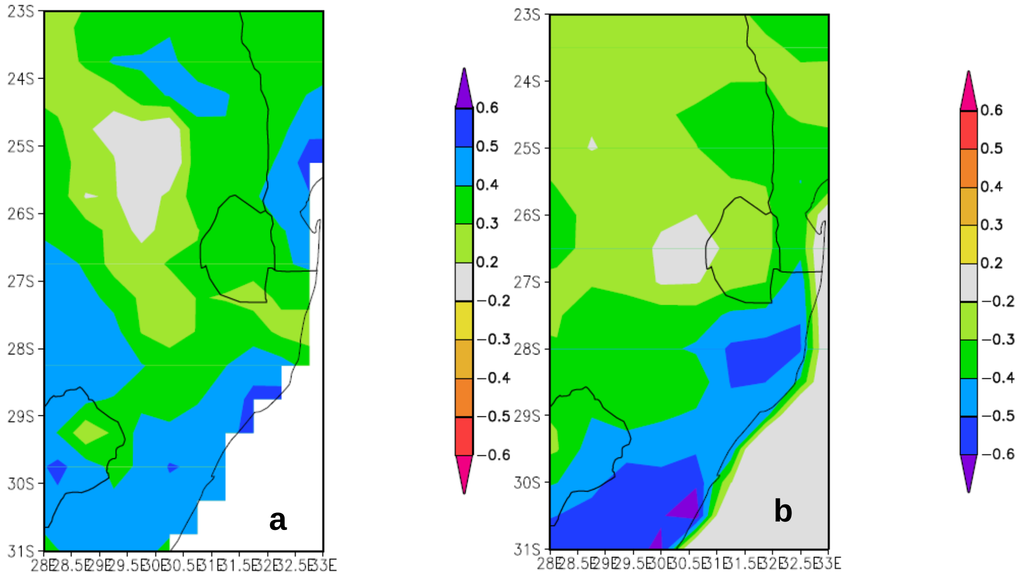

Figure 5.9: Detrended correlation of sugarcane yield index with a) GPCC8 rainfall 1970-2016, and b) MERRA sensible heat flux (SHF) 1980-2013 over southeastern Africa (31-23°S and 28-33°E). Blue indicates high rainfall and red is high SHF, since these two have different impacts on the yield.

The correlation of annual GPCC V8 0.5 degree rainfall and DSYI depicted a positive relationship ($r > +0.5$), as illustrated in Figure 5.9a. The correlation of preceding summer rainfall and sugarcane yield exceeds 0.5. Hence, seasons of high rainfall tend to be followed by increased sugarcane yields.

There is a strong negative correlation between sensible heat flux and sugarcane yield during Dec - May, as shown in Figure 5.9b. This shows that a decrease of potential evaporation has a positive effect on the annual sugarcane yield. Conversely, a high evaporation rate is harmful to crop yield and vegetation.

5.7 Correlation analysis during the dry season

Monthly correlations, based on main crop drivers (rainfall and temperature) in Table 4.2 determined Dec – May as an important season for consideration by the empirical-statistical models employed in this study.

Yet there are statistically significant correlations in the dry season (*cf*. Table 4.2) in spring-time with respect to temperature. The proxy for crops (NDVI) and yield showed high correlation values during late summer (Feb-Mar) and before the growing season (Sep-Oct), as illustrated in Figure 5.8 here, and elsewhere. Therefore, the results presented below show the statistical relationship between various climate elements and the sugarcane yield. They are distinct from those produced in Dec-May correlations in section 5.7 and Chapter 6 of this study, although their magnitudes may look similar.

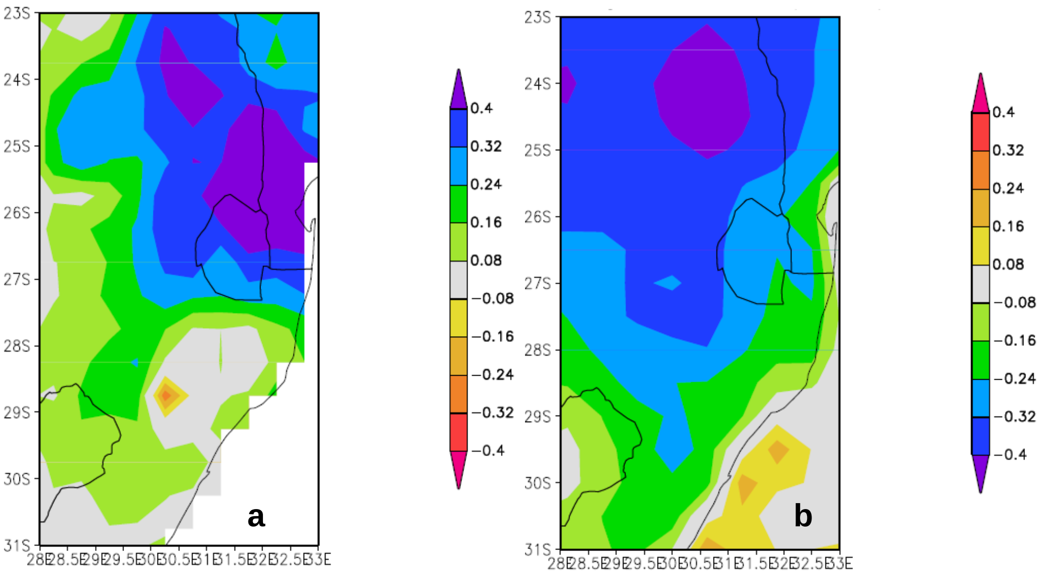

Figure 5.10: Detrended correlation of combined yield index with year-1 SON for: a) GPCC8 precipitation 1980-2013, and b) MERRA surface temperature. Blue indicates high rainfall and red indicates high air temperature according to the scale bar.

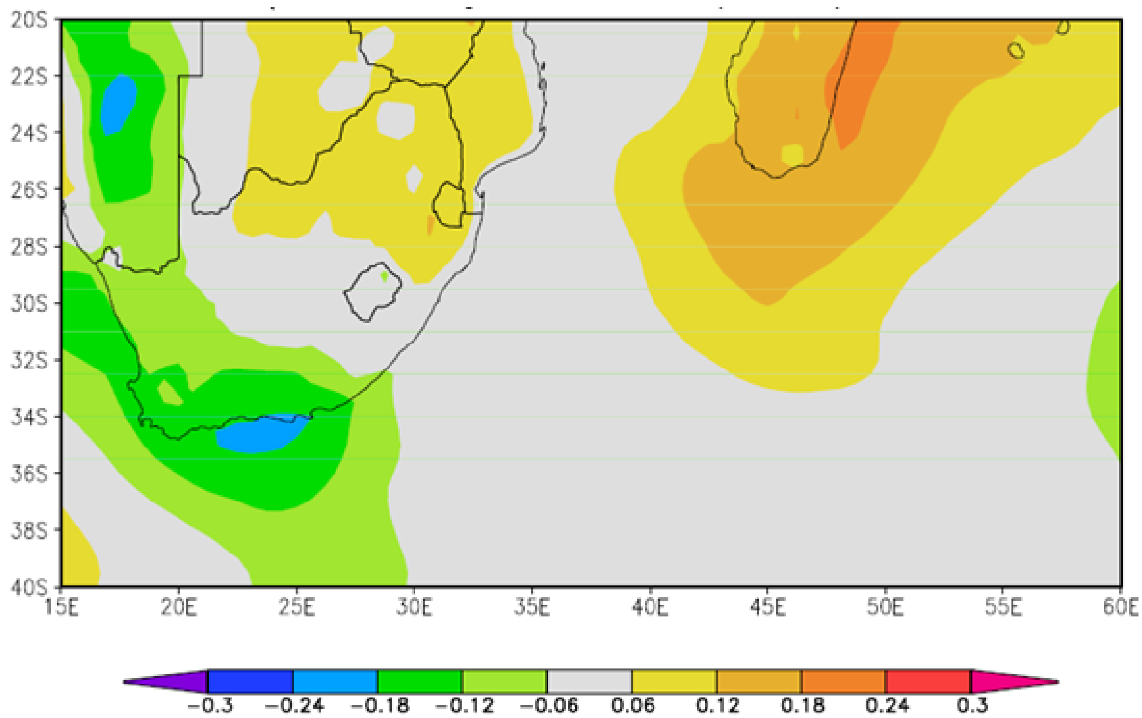

Figure 5.11: Detrended correlation of detrended sugarcane yield index with year-1 SON for MERRA sea level pressure (detrended) for the period 1979 to 2013.

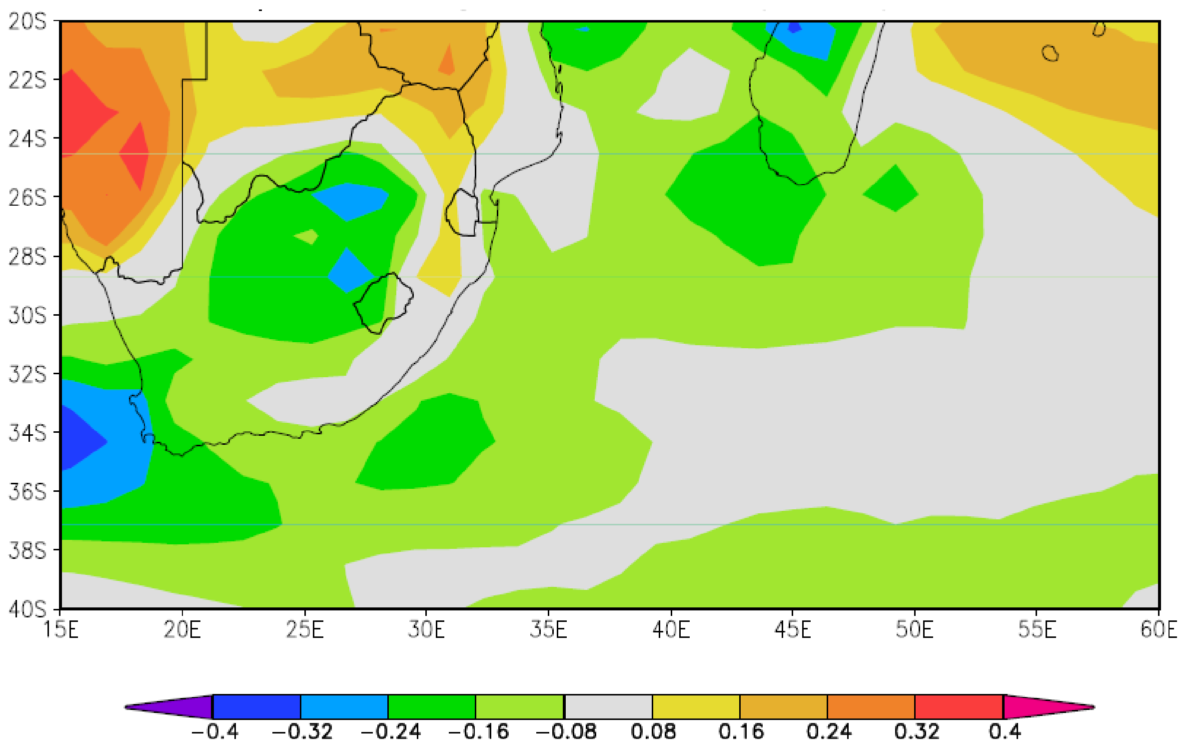

Figure 5.12: Detrended correlation of detrended sugarcane yield index (DSYI) with year-1 SON for ERA-int 850 hPa zonal wind 1979-2013.

During SON the sugarcane growing area is often dry, except the SE coast, and the yield shows a stronger correlation with rainfall in irrigated than rain-fed regions, as illustrated in Figure 5.10a. Elevated surface temperatures are likely to increase the rate of soil water loss, and sugarcane correlated negatively with MERRA air temperature ($r > -0.4$) as demonstrated in Figure 5.10b. Ridging of the SW Indian Anticyclone brings a favourable onshore flow, as seen in the negative west - positive east correlation pattern with sugarcane along the coast (Figure 5.11).

The 850 hPa zonal wind depicts a weak negative correlation with sugarcane yield in South Africa during SON (Figure 5.12), indicating that easterly flow from the South West Indian Ocean (SWIO) brings moisture and a climate favourable to sugarcane growth.

5.8 Composite circulation anomalies for Dec-Apr

The composites show that there is a deep anticyclone in the Mozambique Channel (Figures 5.13 and 5.14), which manifests itself as the main climatic feature affecting sugarcane growth over the study area. The anticyclonic flow brings warm moist air from the Mozambique Channel towards the east coast where sugarcane growing takes place.

The warm Agulhas Current and the anticyclonic circulation bring favourable weather conditions for sugarcane to flourish over SE southern Africa. The regional temperature difference map (Figure 5.15) shows that years of high growth are preceded by a cool land-warm ocean pattern. This also adds to the global ENSO influence.

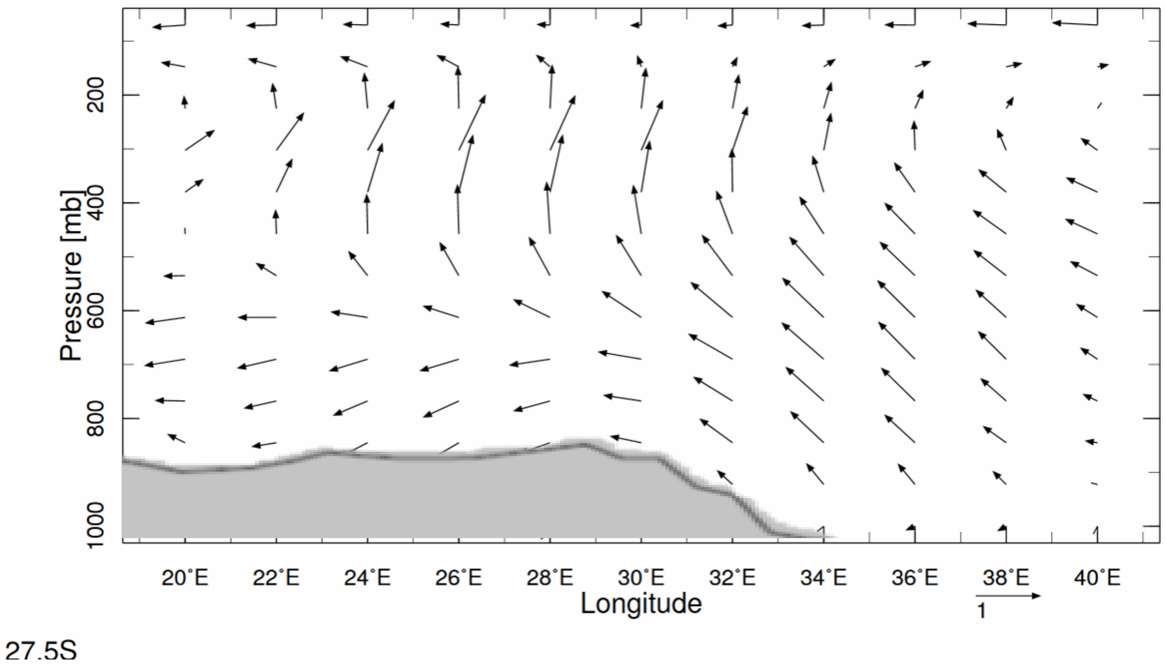

Figure 5.13: Composite difference of circulation during Dec-Apr season, years of high (1971, 1972, 1975, 1976, 1997, 1998, and 2000) minus years of low sugarcane yields (1980, 1983, 1992, 1993, 1994, 1995, and 2012). This vertical slice is on 27.5°S.

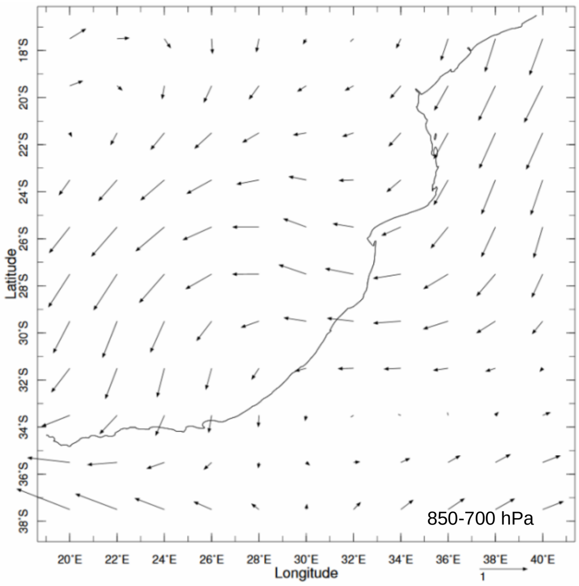

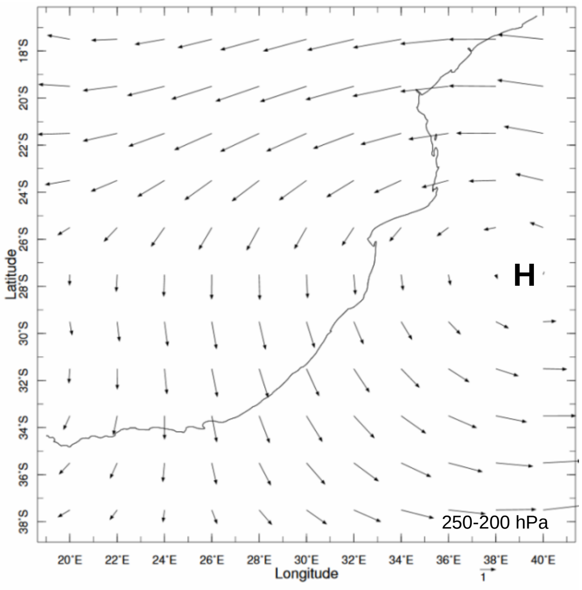

Figure 5.14: Structure of the difference composite circulation for Dec-Apr season for years of high minus low sugarcane yields at 850-700 hPa (top) and 250-200 hPa (bottom) over eastern southern Africa.

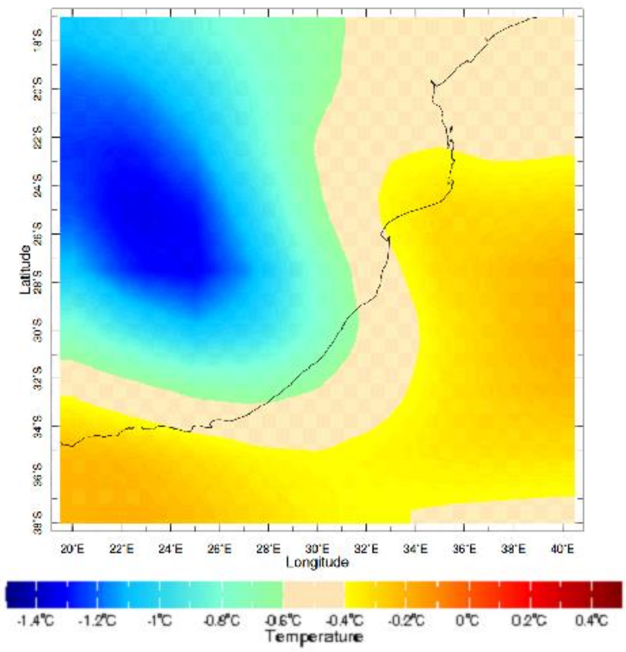

Figure 5.15: Differences in Dec-Apr temperature at 850-700 hPa over the eastern part of the subcontinent, between years with high and low sugarcane yields.

The winds blowing over the heated escarpment of SE Africa cause atmospheric instability and kinematic convergent fields, which induces uplift as a result of intense convective activity during the day. This accelerates sugarcane growth, as illustrated in Figure 5.13 here and these findings reaffirm the mesoscale considerations (Fig. 9.10 of Tyson & Preston-Whyte, 2000).

5.9 Scatterplots of climate elements and sugarcane index

The following scatterplots illustrate the impacts of local climate and Pacific ENSO on sugarcane yield. In this section local climate variables, climate indices and yield are expressed as the differences of observed values and long-term mean. Here, the correlation of determination (R^2) indicates the influences of each variable expressed as a percentage (*see* Figure 5.16 and Table 5.1). The positive slope shows positive correlation (*see* Figure 5.16 Rainfall vs yield anomalies) and negative slope indicates negative correlation (*see* Figure 5.16 Temperature vs yield anomalies).

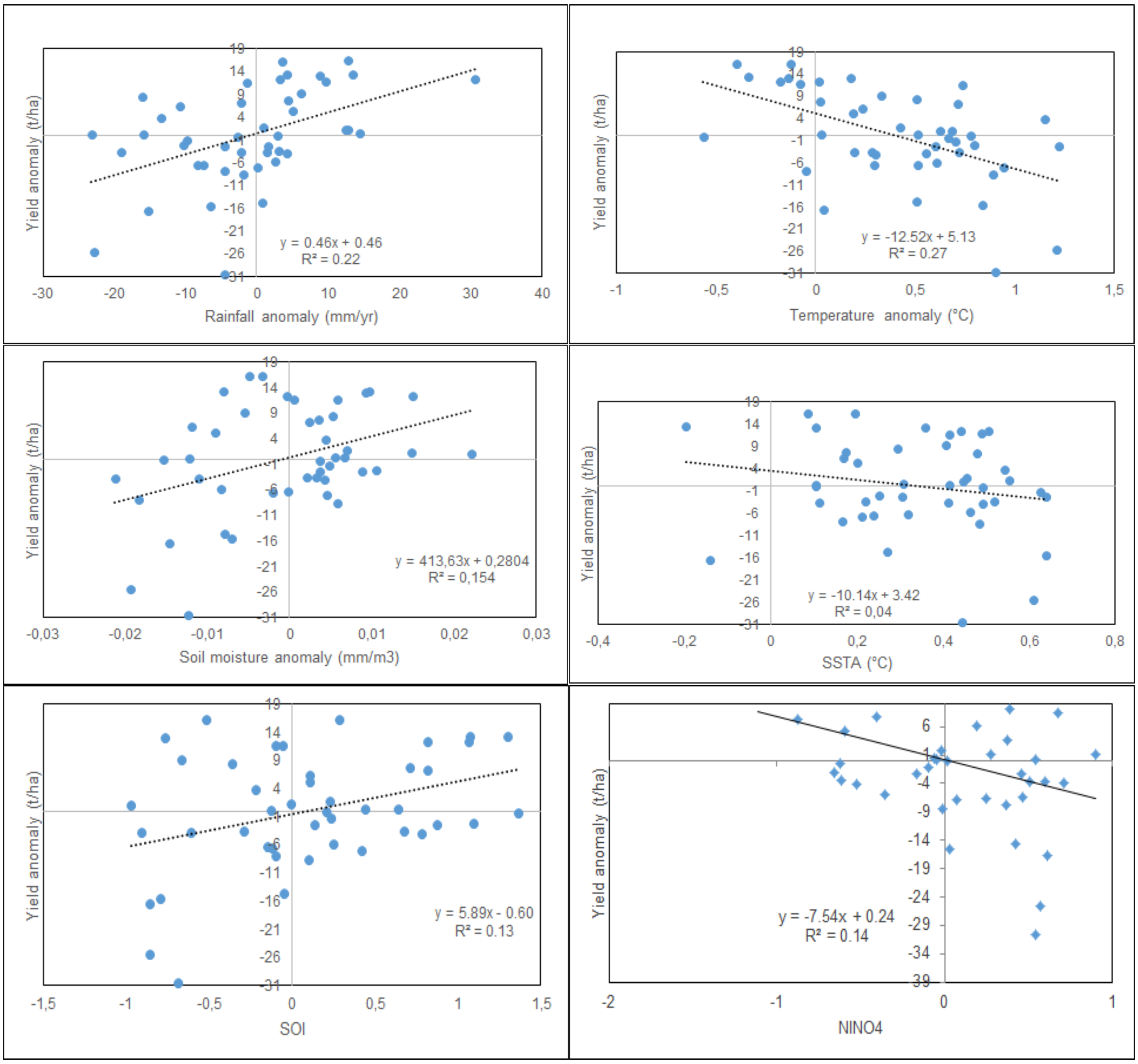

Figure 5.16: Scatterplots displaying the relationship between annual anomalies of local and global climate variables and sugarcane yield index for the period 1970 to 2013.

Table 5.1: Relationship between sugarcane yield and annual anomalies of climate and Pacific ENSO from 1970-2013.

Variables	R-sq (%)
Rainfall	22.42
Temp	27.20
Soil moisture	15.40
SOI	13.14
Niño4	13.98

Figure 5.16 is a catalogue of pair-wise scatterplots fitting sugarcane yield index and climate anomalies. The results depict highest sensitivity for increased temperature followed by reduced local rainfall. This adds to the evidence of local to global climate impacts on sugarcane yield at the inter-annual time-scale.

5.10 Summary

The analysis showed that Dec-May and Sep are important seasons for sugarcane production over SE Africa, as demonstrated in Table 4.2. The composite-mean analysis in section 5.3 showed that climate elements have steep gradients from west-dry and east-dry. This spatial variability stimulates greater sugarcane production over the eastern seaboard of southern Africa than its counterpart (western seaboard). The Mascarene high and onshore flow from the South West Indian Ocean are the main climatic features that benefit sugarcane growth in the study area.

According to Figure 5.5, NDVI shares similar characteristics with sugarcane, and its values in the sugar belt range between 0.2-0.8 fractions. In general, there is a noticeable positive relationship between NDVI and sugarcane yield (Figure 5.8).

In terms of wavelet analyses, both the rainfall and sugarcane yield have 1-2, 3-6 and 10-12 years cycles. This implies that high potential evaporation as a function of soil moisture content and temperature reduce sugarcane yield while good rainfall is linked to high sugarcane yields. These cycles provide an insight with reference to after how long (frequency of reoccurrence) below-normal and above-normal rainfall and sugarcane yield can be observed in the study area. This could help to mitigate the consequential effects on the yield and prevent the possibility of local economic stagnation.

The correlations between climatic parameters and the sugarcane yield show statistically significant relationships, where $|r| = 0.5$ for global yield and $r \geq \pm 0.7$ for local yield. Increased surface air temperature and high sensible heat flux reduce sugarcane yield (Figures 5.9b and 5.10b) because they deplete soil water, while soil moisture inputs such as rainfall show a significant positive correlation with the sugarcane index in the area-averaged, as illustrated in Figures 5.9a and 5.10a.

Statistical correlations between the yield and climate elements indicate that individual regional climate variables in Dec-May explain 40-60% of variations in the SE Africa sugarcane yield for the following season. The composites (Figures 5.13 and 5.14) show that conventional ENSO is more significant for sugarcane production over SE Africa than its counterpart (ENSO Modoki), because only one Walker cell was observed from the composite-different analysis. Climate information and forecasts can help farmers and the sugar industry to mitigate the impacts of varying sugarcane yield related to Pacific ENSO, as discussed in the following chapter.

CHAPTER 6

GLOBAL AND ENSO INFLUENCES ON SUGARCANE YIELD

6.1 Introduction

The previous chapter assessed the influence of local crop-drivers (rainfall, temperature and evaporation) on sugarcane yield, the degree of association and the extent to which the two are related. This chapter will consider global and remote influences such as the influence of Pacific El Niño Southern Oscillation (ENSO) on sugarcane yield in the eastern part of South Africa and ESwatini.

ENSO is one cause of inter-annual climate variability (Bannayan, *et al*., 2011) which affects the global sugarcane yield. ENSO events (La Niña and El Niño) can be determined using various indices or parameters but in this dissertation the Southern Oscillation Index (SOI) is used. SOI refers to the standardised sea level pressure difference between Tahiti and Darwin, Australia, as related to gradients of SST (Huang, *et al*., 2015). The Dipole Mode Index (DMI) of the Indian Ocean SST (Behera, *et al*., 2005; Cai, *et al*., 2011), and the Niño4 of the central Pacific region were also used to investigate the influence of ENSO and IOD on sugarcane yield.

In this chapter, ENSO and IOD influences on sugarcane yield are documented, whereby high and low sugarcane yields are linked to ENSO and non-ENSO years. Thereafter, the statistical correlations per month and year-wise between SSTs, SLP, wind fields and detrended sugarcane yield index were done in KNMI-CE.

6.2 Inter-annual variability of ENSO

The inter-annual variability of ENSO and IOD influences on sugarcane yield are documented next, whereby high and low sugarcane yields are linked to ENSO and non-ENSO years, as shown in Tables 6.1. The results presented here revealed that the number of El Niño years (warm phase-dry conditions) is outnumbering the occurrence of La Niña years (cold phase-wet conditions), and a slight decline in SOI trend has been detected (Figure 6.1). This adds on the evidence of global warming and the predominance of intense drought conditions over the southeast (SE) part of Africa (Mbatha & Xulu, 2018). Yet most drought events relate to warm phases of ENSO and suppressed sugarcane production.

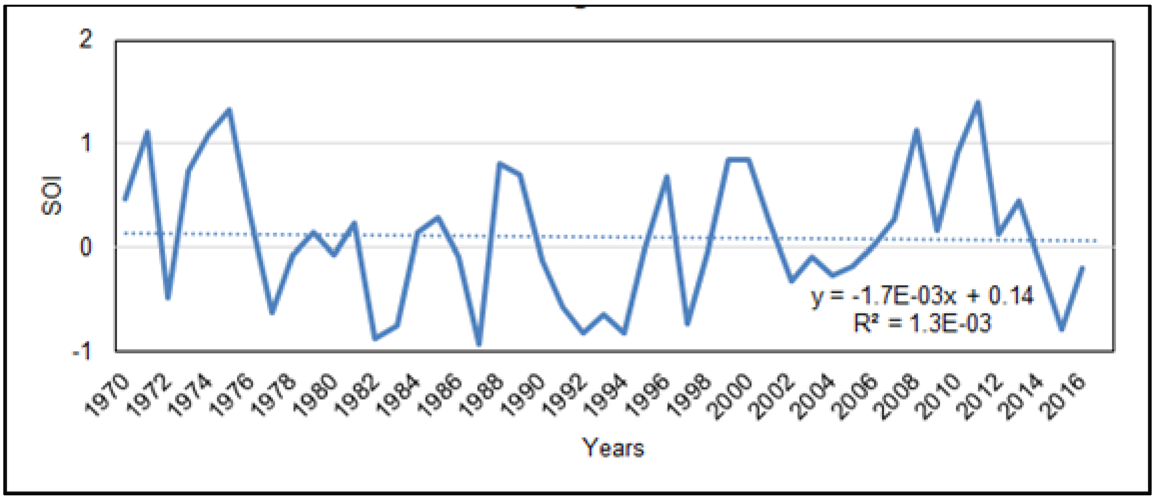

Figure 6.1: Southern Oscillation Index for the period 1970-2016, values above and below ±0.5 signal El Niño and La Niña episodes. The negative gradient indicates a declining trend and regression fit (R^2) too less than 1 show that data points are very scattered.

The La Niña condition of +SOI and – Niño4 favours increased sugarcane yield 6 months later, as illustrated in Figure 5.1 and Table 6.1. In addition, a positive Indian Ocean Dipole promotes yield as depicted in Table 6.2. Eighty-six percent (86%) of the seven numerically selected years of highest sugarcane yields correspond to the preceding years of weak, moderate and strong La Niña events (Figure 6.1 and Table 6.1). The highest yield (97 ton/ha) of 1976 corresponds to the preceding year characterised by La Niña of 1975/76 as illustrated in Figure 6.1 above and Table 6.1 below.

Table 6.1: Comparison of top 7 high and low South Africa and ESwatini sugarcane yields (combined index) and preceding annual SOI and Niño4 phases (La Niña and El Niño- weak, moderate and strong) leading by 6-12 months.

Years of high yield	Yield (ton/ha)	Mean SOI	Mean Niño4	Years of low yield	Yield (ton/ha)	Mean SOI	Mean Niño4
1971	93.9	0.5	-0.1	1980	72.8	-0.3	0.2
1972	96.9	1.1	-0.7	1983	65.2	-1.5	0.5
1975	93.9	0.9	-0.9	1992	55.2	-1.0	0.7
1976	97.1	1.3	-1.1	1993	50.1	-1.2	0.6
1997	93.7	0.6	-0.1	1994	64.1	-1.1	0.5
1998	92.3	-1.3	0.7	1995	65.9	-1.4	0.6
2000	92.9	0.8	-0.9	2012	72.1	1.4	-0.6

The main discrepancy is 1997/98, wherein the El Niño-La Niño change was so sudden that yield responses were inverted. Most years of low yields are preceded by El Niño events. Some neutral years (e.g. 1992-1994) were followed by low sugarcane yields (50.1 ton/ha in 1993), suggesting the need for customised statistical models in addition to pre-existing climate indices.

Table 6.2: Correlation per month 1970-2016 of sugarcane yield with detrended climate indices, all leading by 6 months. Bold numbers indicate significant correlations.

Months	SOI	Niño4	DMI
Jan	**0.389**	**-0.348**	**0.203**
Feb	**0.335**	**-0.340**	**0.204**
Mar	**0.378**	**-0.359**	**0.428**
Apr	**0.394**	**-0.334**	**0.403**
May	-0.046	**-0.357**	0.084
Jun	0.178	**-0.355**	**0.291**
Jul	**0.234**	**-0.413**	-0.042
Aug	**0.287**	**-0.402**	-0.032
Sep	**0.382**	**-0.384**	-0.139
Oct	**0.509**	**-0.363**	-0.185
Nov	**0.383**	**-0.336**	-0.056
Dec	**0.386**	**-0.367**	0.089

6.3 Correlations of DSYI with SST, SLP and wind fields

After monthly correlations (Chapter 5), the seasonal correlations between yield and SST, SLP and wind fields leading by 6-12 months were performed and the results are presented below, followed by interpretation and analysis.

A negative correlation is observed in the equatorial Pacific Ocean between year-1 SST and sugarcane yield (Figure 6.2), while SLP is correlated positively with the yield (Figure 6.3). Such a hydrostatic relationship was expected, because when SST is cooler and Sea Level Pressure is higher in the Pacific Ocean, the upcoming season will have increased sugarcane yield (Table 6.1; Figures 6.2 and 6.3). This condition is connected with low-level circulation, whereby the easterlies of the Pacific and west Indian Ocean extend towards southeast Africa (Figure 6.4), bringing moisture to the sugarcane growing region.

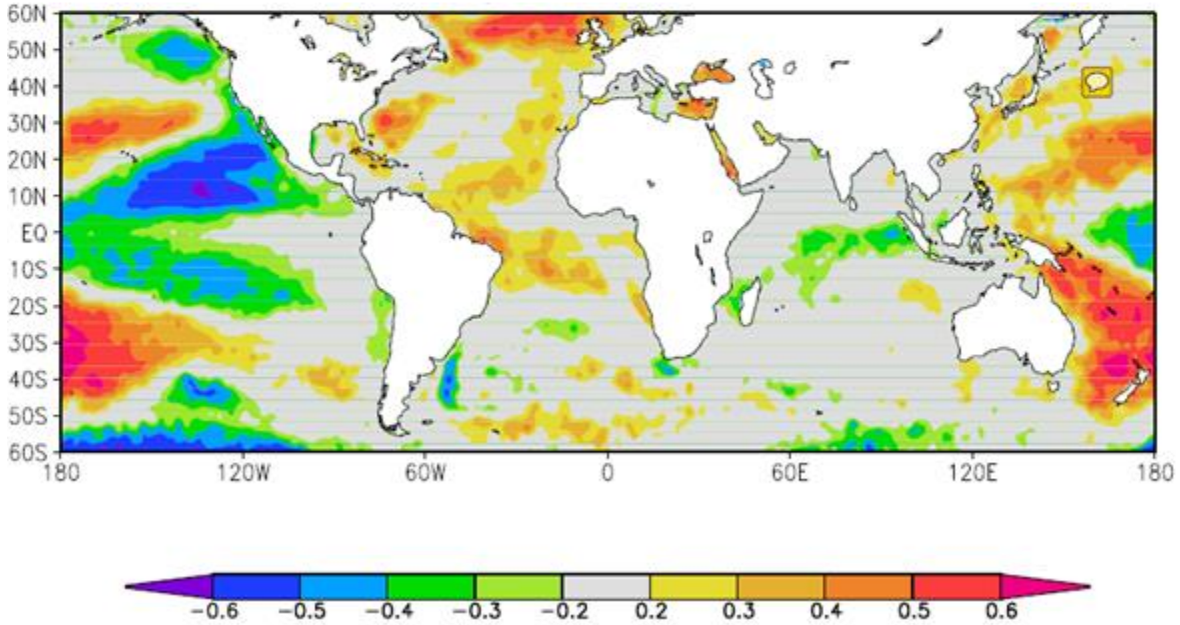

Figure 6.2: Detrended annual correlation between the sugarcane yield index (DSYI) and year-1 HadISST1 sea surface temperature (SST) 1970-2016.

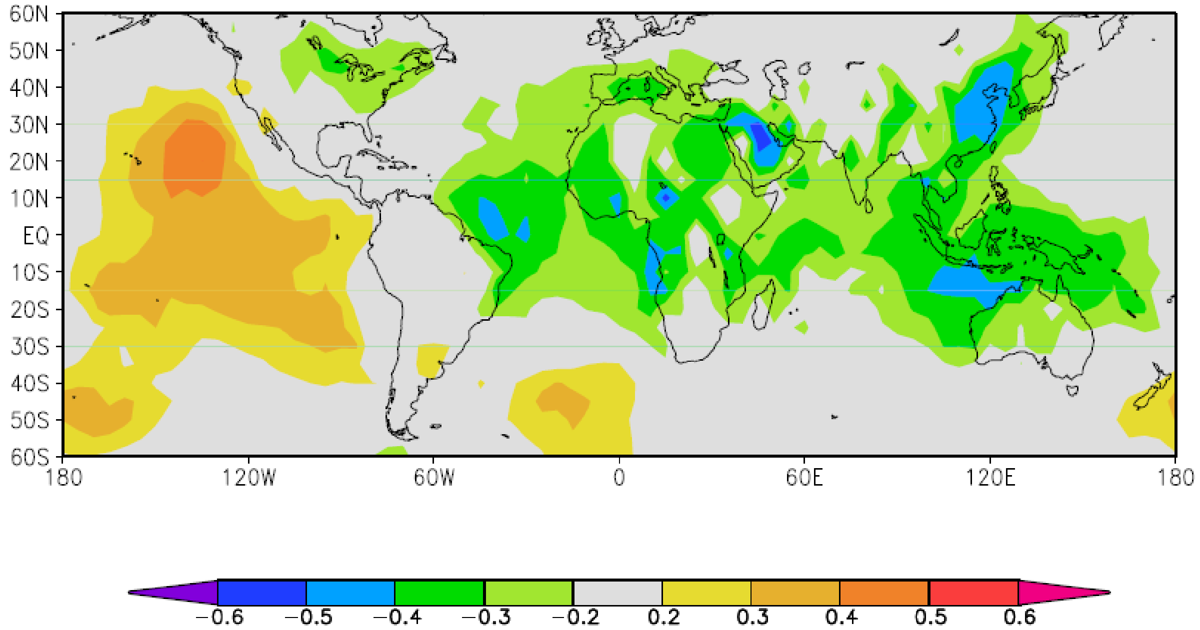

Figure 6.3: Statistical correlation between the sugarcane yield index and year-1 HadSLP2 sea level pressure for the period of 1970-2016.

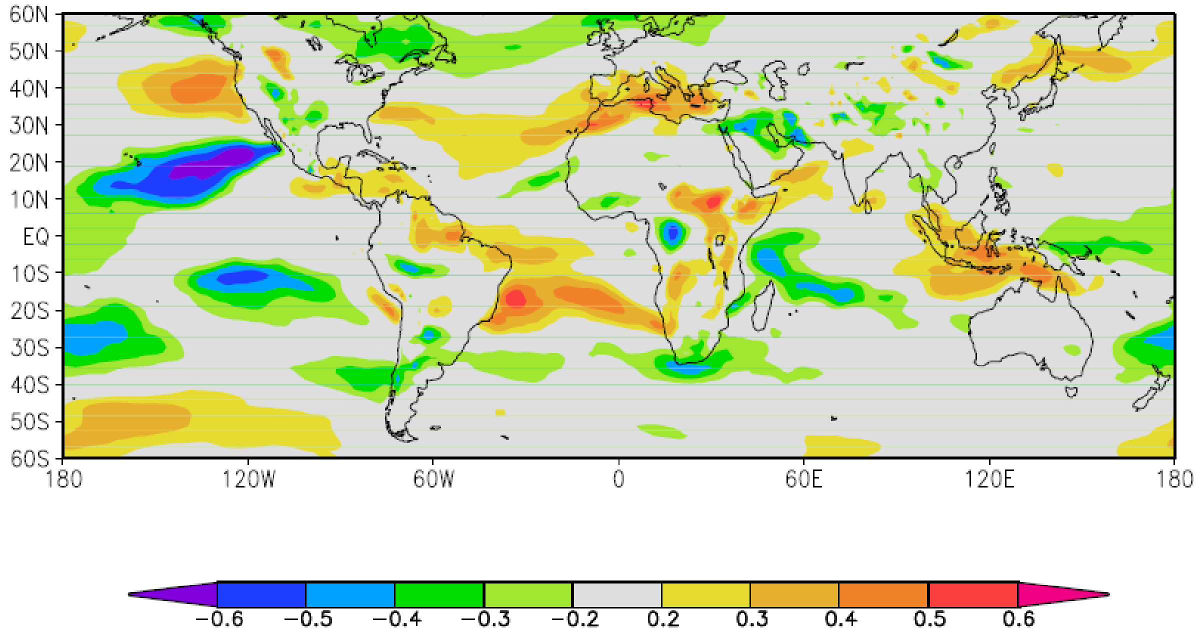

Figure 6.4: Correlation between DSYI and year-1 ERA-int 850 hPa zonal wind 1979 to 2016.

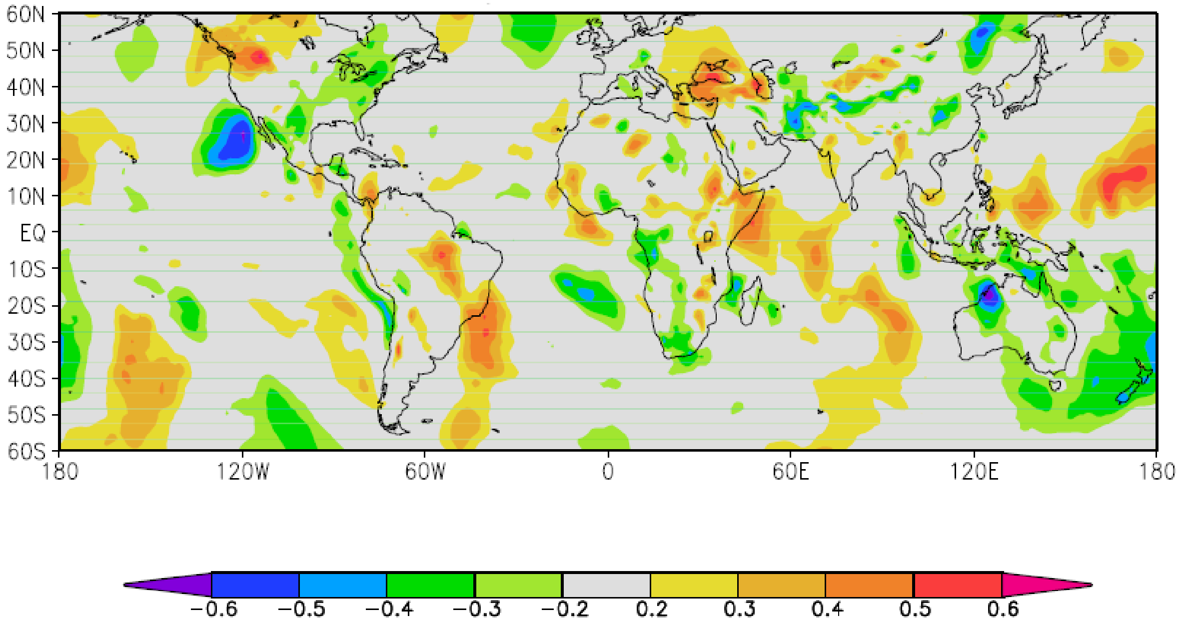

Figure 6.5: Correlation between sugarcane yield index and year-1 ERA-int meridional wind (at 850 hPa) for the period 1979 to 2016.

The SST correlation map (Figure 6.2) shows that sugarcane yield is reduced when increased SSTs in the equatorial Atlantic and decreased SSTs in the equatorial Indian Ocean were observed. Hence, in addition to ENSO signals, there are regional influences that alter the atmospheric circulation. Warming of the Pacific Ocean causes the Botswana Upper High to intensify while the Angola Low weakens

(Chikoore, 2017), causing dry conditions over the subcontinent and diminished sugarcane growth.

6.4 Sugarcane yield prediction using the MLR model

Chapters 4 and 5 revealed that there is a general consensus that sugarcane yield is declining. This study developed a statistical model which foretells sugarcane yield using large-scale climate drivers and sugarcane proxy (PDSI). This is different from the MLR results presented in Chapter 4 in the sense that - in this section it is used to develop sugarcane yield model, while in the former it was used for testing the importance of variables.

This Aug-Nov forecasts will help farmers make informed decisions on farming operations such as when to commence growing, and adjusting farming schedules accordingly. This could reduce loss of profit and improve sugarcane yield. It was evident from the MLR that - PDSI gives by far the best explanation of sugarcane yield variability in the entire sugar industry of South Africa, but variable importance suggests that other regions are affected by ENSO (*see* Table E.1). This includes the Zululand and South Coast regions where SOI, Niño4, and SLP manifested themselves as important predictors of the yield. Over North Coast, Midlands and ESwatini surface air temperature also plays an important role in determining the average sugarcane yield. This is because temperature has the ability to offset the benefits of good rain (e.g sufficient soil water for sugarcane development) through enhancing the potential evapotranspiration and reducing soil moisture. This condition relates to reduced sugarcane yield, and a forecast tool that will incorporates local climate variables (crop-drivers) and large-scale climate drivers (e.g ENSO) is desirable.

6.4.1 Exploration of PDSI predictors

Having noted the negative temperature and positive rain correlation (Table 4.2), the PDSI which is the P-E (precipitation minus potential evaporation) becomes a useful proxy of sugarcane yield for evaluation of Dec-Mar variations as a function of prior Aug-Nov predictors. Ideally, sugarcane yield should be used in the model but since it has a longer cycle (12-24 months) and depends on various predictors other than climate, it could be misrepresentative of the intended outcomes.

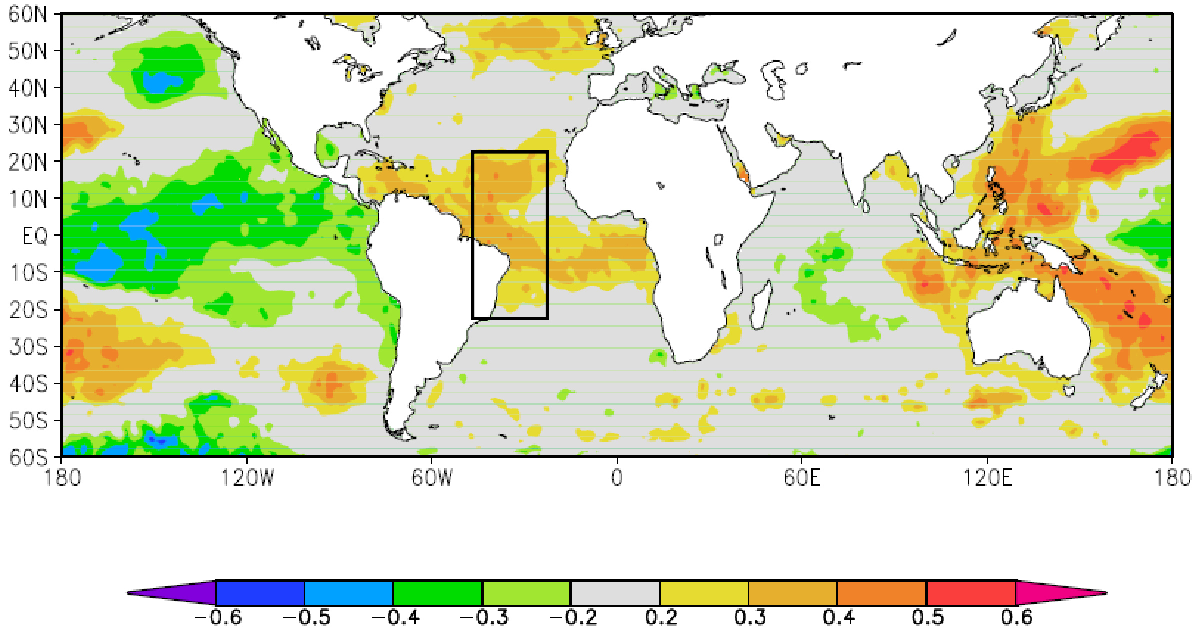

Figure 6.6: Aug-Nov year-1 SST correlated with Dec-Mar PDSI covering the adjacent oceans for the period 1980-2014. Predictors selected are shown by boxes.

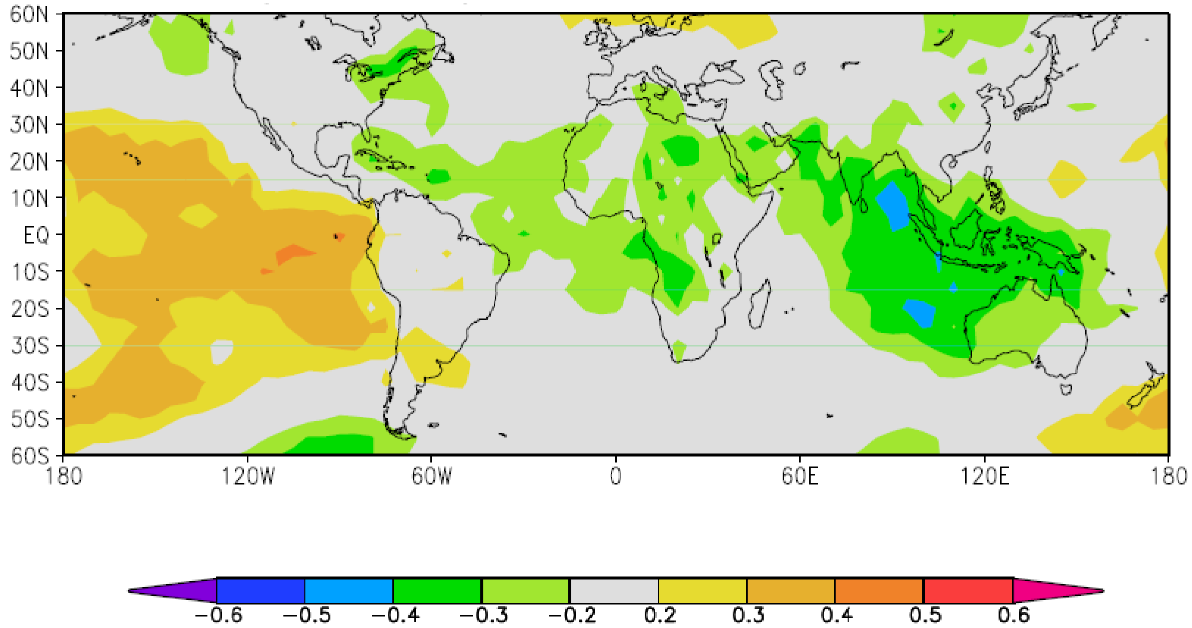

Figure 6.7: This is the same as Figure 6.6 but for SLP and sugarcane PDSI.

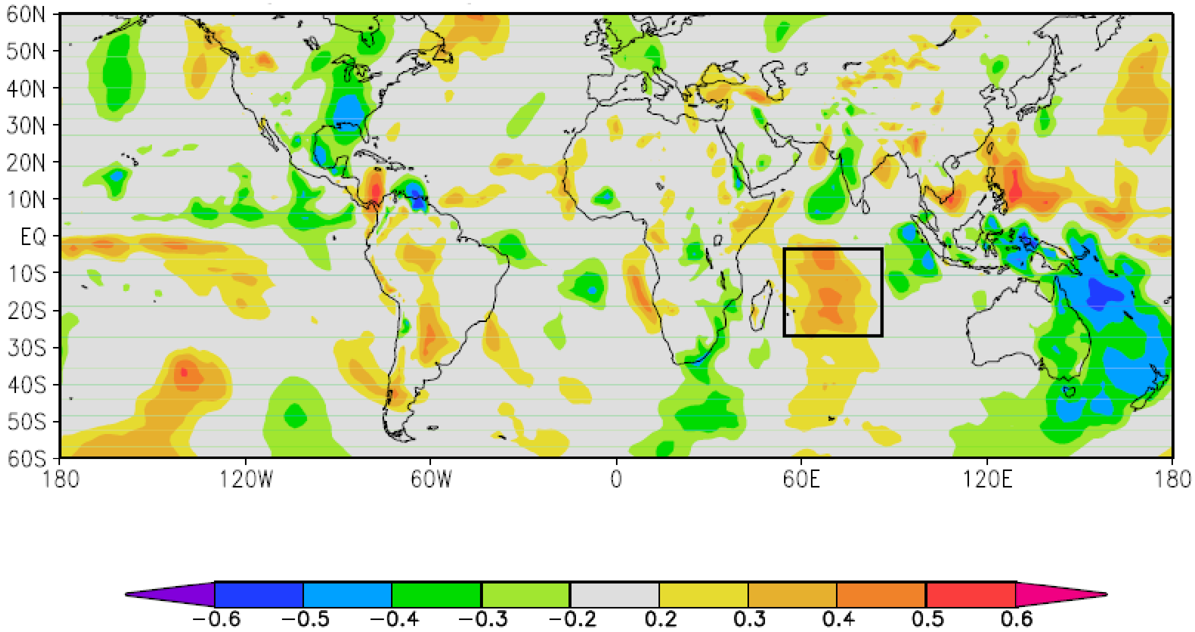

Figure 6.8: This is the same as Figure 6.6 but for meridional wind (V 850 hPa) and sugarcane PDSI. Box shows the predictor selected.

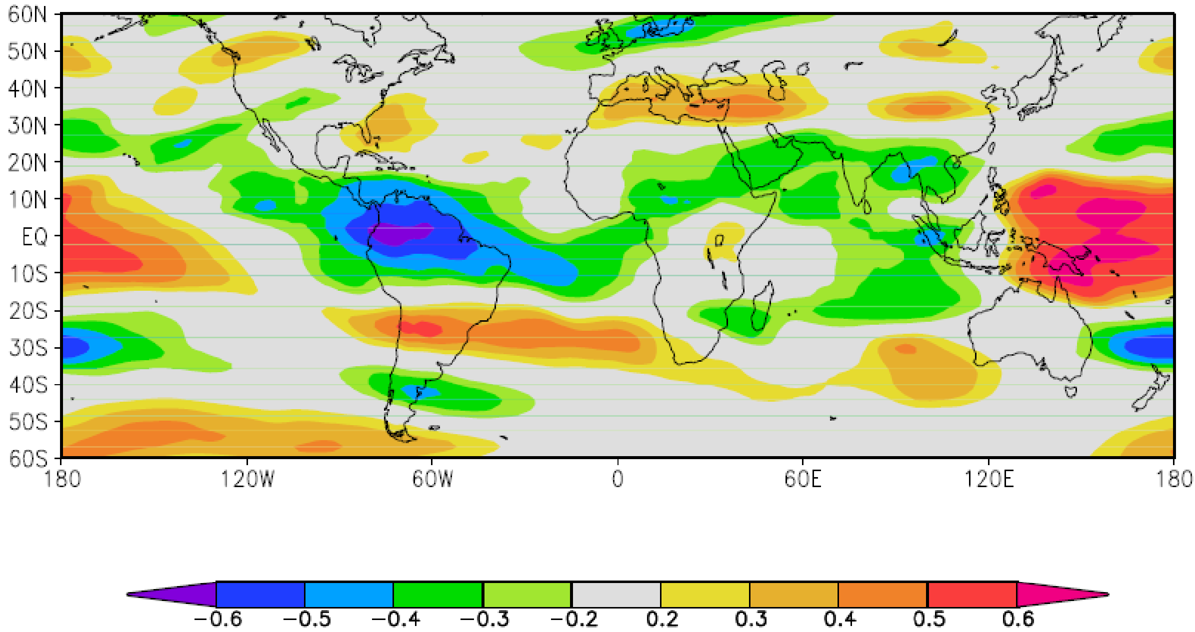

Figure 6.9: This is the same as Figure 6.6 but for Zonal wind (U 200 hPa) sugarcane PDSI.

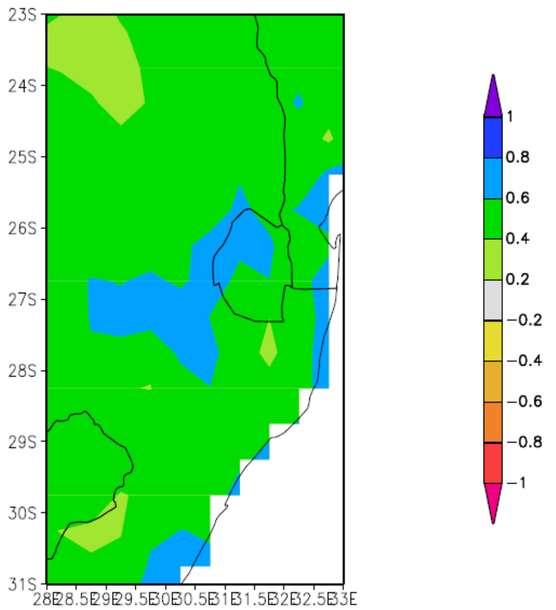

Figure 6.10: Correlation of Dec-May PDSI and detrended sugarcane yield index in southeastern Africa (31-23°S and 28-33°E) for the period 1970-2016, showing a strong positive correlation $(r \geq +0.6)$.

Table 6.3: Definitions and locations of prior Aug-Nov predictor-candidates for SE Africa Dec-Mar PDSI (31-23°S and 28-33°E).

Predictor	**Parameter**	**Area-averaged**	**Boundaries (lat; long)**
SST1	sea surface temperature	East Pacific Ocean	15°S-15°N; 120-80°W
SST2	sea surface temperature	West Atlantic Ocean	20°S-20°N; 45-60°W
SST3	sea surface temperature	Indonesia	5°N-20°S; 80-120°E
SST4	sea surface temperature	SW Indian Ocean	15-30°S; 60-70°E
SLP1	sea level pressure	West Indian Ocean	30°S-5°N; 60-90°E
SLP2	sea level pressure	East Pacific Ocean	30°S-5°N; 120-80°W
V1	meridional wind (850 hPa)	West Indian Ocean	0°Eq-25°S; 50-80°E
V2	meridional wind (850 hPa)	Southern Ocean	35-60°S; 50-40°E
V3	meridional wind (850 hPa)	East Australia	10-25°S; 140-160°E
U1	zonal wind (200 hPa)	Amazon	15°S-15°N; 50-100°W
U2	zonal wind (200 hPa)	West Pacific Ocean	15°S-15°N; 180-120°W
U3	zonal wind (200 hPa)	Northern Australia	10°S-20°N; 120-180°E

6.4.2 Pair-wise correlation

Table 6.4 below shows the pair-wise correlation between PDSI predictors. This helped to remove predictors with colinearity and in ensuring that only those with similar signs (positive or negative) with PDSI and in the multi-variate regression model coefficients are used to develop the model. From the predictor search map correlations in section 6.4.1, 12 predictor candidates time series were extracted but, essentially due to a screening process, only two were finally employed in the development of the model.

*Table 6.4**:** Cross-correlation between PDSI and predictor candidates and bold-black indicates high correlations.*

	SST1	*SST2*	*SST3*	*SST4*	*SLP1*	*SLP2*	*V1*	*V2*	*V3*	*U1*	*U2*	*U3*
SST1												
SST2	**0.89**											
SST3	**0.49**	0.12										
SST4	0.21	0.24	0.04									
SLP1	0.09	**0.40**	**-0.53**	-0.15								
SLP2	0.24	0.29	-0.18	0.12	**0.51**							
V1	-0.11	-0.31	**0.54**	-0.39	-0.27	-0.24						
V2	-0.11	-0.18	0.18	**0.40**	-0.24	-0.02	-0.09					
V3	0.04	0.36	**-0.57**	0.30	**0.53**	0.34	**-0.63**	0				
U1	0.09	0.38	**-0.63**	0.02	**0.59**	0.18	**-0.65**	-0.18	**0.52**			
U2	-0.18	0.10	**-0.56**	-0.14	**0.50**	-0.07	-0.24	-0.20	0.20	**0.76**		
U3	0.16	-0.26	**0.72**	-0.14	-0.64	-0.12	**0.51**	-0.02	**-0.79**	**-0.63**	**-0.52**	
PDSI	-0.15	-0.37	**0.51**	-0.03	-0.33	-0.25	**0.66**	0.22	**-0.57**	**-0.61**	-0.25	**0.46**

6.4.3 Multi-variate regression summary output

Table 6.5 below shows the model output wherein the model was evaluated for significance, using multi-variate regression for predictors with p-values <0.15. These were further screened to ensure that the sign of multi-variate regression and pair-wise correlation matches.

Table 6.5: Model output from a backward-step-wise linear regression where sugarcane-PDSI is the dependant variable predicted using the large-scale climate drivers.

Regression Statistics	
Multiple R	0.69
R Square	0.47
Adj R Square	0.44
Standard Error	0.73
Observations	34.

ANOVA

	Df	*SS*	*MS*	*F*
Regression	2.00	14.81	7.40	13.91
Residual	31.00	16.49	0.53	
Total	33.00	31.30		

	Coefficients	*Standard Error*	*t Stat*	*P-value*
Intercept	0	0.13	-7.40	2.50E-08
SST2	-0.18	0.13	-1.37	1.80E-01
V1	0.58	0.13	4.43	1.10E-04

Therefore, the multi-variate regression equation is given by: Dec-Mar sugarcane-PDSI = -0.18(SST2) $+0.58$(V1) using Aug-Nov predictors. The model validation is presented below. The model was validated through inter-comparison between observed (solid-black) and predicted (dashed-red) PDSI (Figure 6.11) and Figure 6.12.

6.4.4 Model validation

The model was validated through plotting the observed and model- predicted PDSI, and a statistical significant linear relationship was envisaged between observed and predicted PDSI (Figure 6.11). Thereafter, the observed and predicted values correlate positively with $r \geq +0.5$) signalling that the model is statistically significant, and the model has an $R^2 = 0.47$ and $p - value$ =1.10E$-$0.4, as illustrated in Table 6.5.

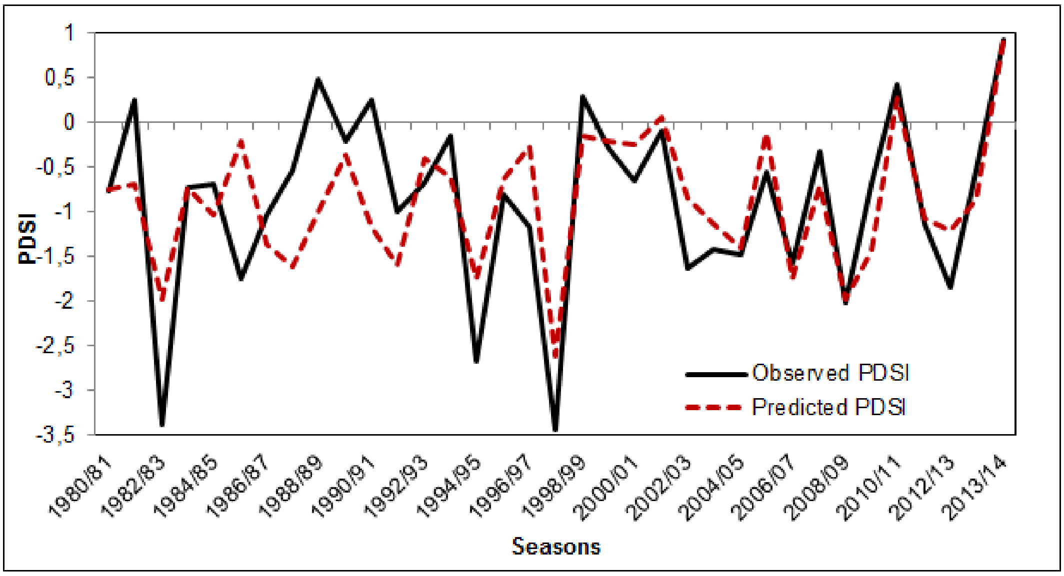

Figure 6.11: Observed PDSI (solid-black) vs predicted PDSI (dashed-red).

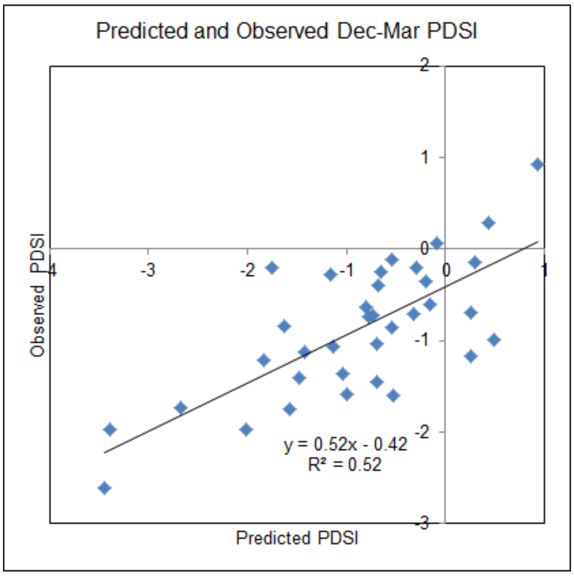

Figure 6.12: Scatterplot of predicted Dec-Mar sugarcane-PDSI (predicted PDSI) and observed PDSI over SE southern Africa for the seasons 1980/81 to 2013/14.

The following year sugarcane yield correlates positively ($r > +0.6$) with the Palmer Drought Severity Index (PDSI) in the preceding Dec-Mar season. A multi-variate linear regression was developed to predict sugar-PDSI, using a combination of both oceanic and atmospheric precursor conditions. The predictors have the teleconnections SST2 -0.18 and V1 $+0.58$, which serve as the underlying reason for predicted sugar-PDSI accounting for 47% of the variance for the observed PDSI.

6.5 Summary

Previous studies reported ENSO Modoki influence in climate variability over southern Africa and elsewhere (Ashok, *et al*., 2001; Ratnam, *et al*., 2014; Chikoore, 2017). During ENSO Modoki two cells are observed in the central Pacific Ocean contrary to its counterpart, the conventional ENSO which is characterised by a single cell. During an El Niño Modoki event, low pressure is located in the central Pacific Ocean which results in cloud formation and rainfall over the ocean rather than land. La Niña Modoki is characterised by upper-level convergence and lower-level divergence in the central Pacific Ocean, which allows rainfall occurrence in both west and east Pacific Ocean. In this study only the conventional ENSO impacts were detected from sugarcane yield. ENSO Modoki influences were not detected in sugarcane yield over the study area (*see* Figures 5.13 and 5.14).

Pacific ENSO helps to drive changes in the SW Indian Ocean (Hermes & Reason, 2009). A deeper thermocline, as part of the Indian Ocean Dipole (IOD), has been linked to a shift in DJF rainfall from SE Africa to the West Indian Ocean (WIO), with negative impacts on the sugarcane yield. When both ENSO (as indicated by Niño4 and SOI) and IOD (as indicated by DMI) coincide, there is a larger change in sugarcane yields (Table 6.3).

The Indonesian SST anticipates how the Pacific ENSO and IOD interact, and is important given that SST anomalies tend to move westward (Wang, *et al*., 2016). The seasons of positive V wind coincide with those of positive phase of ENSO, and the former is inversely related ($r \leq -0.6$) to the West Indian Ocean (WIO) SST patterns during Aug-Nov. This indicates that - the WIO must be cool and the Tibetan High weakens to produce southerly meridional flow, and that accelerates sugarcane growth which relates to high sugarcane yield over the SE Africa. From the model output, V1 wind revealed a strong connection with sugarcane-PDSI. Its teleconnections and features will be discussed further in Chapter 7.

CHAPTER 7

CLIMATE CHANGE AND LONG-TERM TREND

7.1 Introduction

Chapter 7 presents the findings on climate change and long-term climate trends over SE Africa. The main features and teleconnections of the meridional wind (V1) are also explored in this chapter. Long-term climate trends were analysed using observed (historical) and projected (future) data from the KNMI-CE website. While earlier chapters used de-trended datasets, this chapter considers trends without detrending, but datasets have been locally smoothened. The area-averaged is over the subtropical sugar belt of SE Africa for the period from 1970-2016 observed and 1970-2050 simulated.

7.2 Southerly meridional flow

A climatic excursion with reference to climate processes, interactions and features of the meridional wind (V1 component) has been made to explore the importance of V1 wind over SE Africa. The V1 wind indicates southerlies when positive, while negative V1 wind signals northerlies. The forecast model discussed in section 6.4 of the previous chapter in this study showed that there is a positive correlation ($r \geq +0.5$) between meridional wind at 850 hPa and PDSI over the western Indian Ocean (Figure 6.8). Figure 7.1 below shows the variability of mean meridional wind averaged over the western Indian Ocean (0°Eq-25°S; 50-80°E) from 1980-2016.

Figure 7.1 shows that seasons which are characterised by strong negative V1 wind anomalies are linked to the warm phases of ENSO, and the wind is northerly, which relate to low sugarcane yield. The cases include: 1982, 1991, and 1994, but the cold phases of ENSO are associated with positive V1 wind anomalies and increased yields (e.g. 1998), as illustrated in Table 6.1 and Figure 7.1.

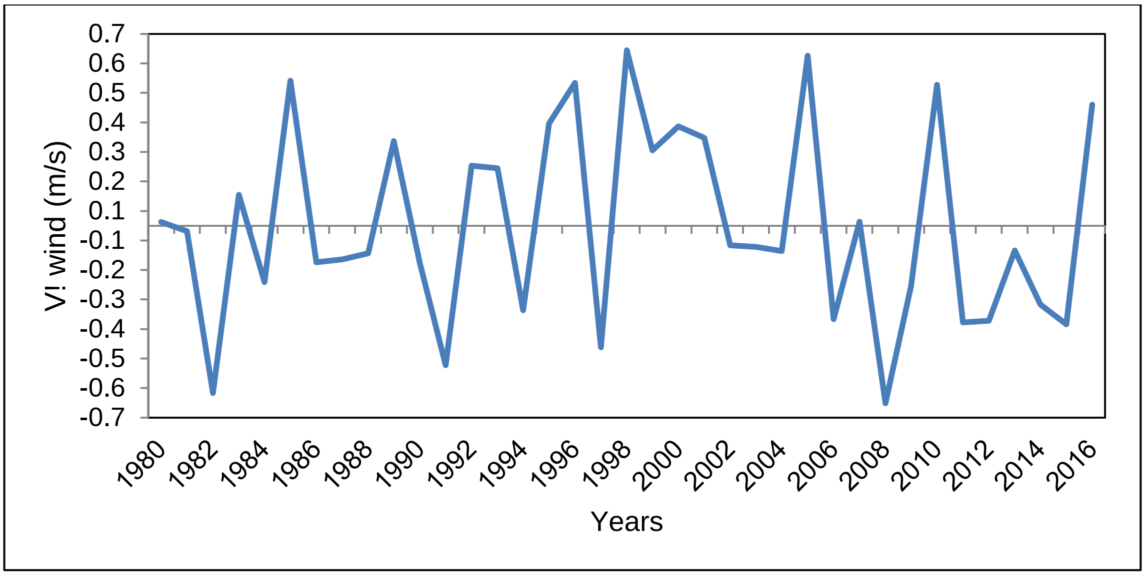

Figure 7.1: Time series of annualised-anomalies of Aug-Nov meridional wind (V component from ERA-int) at 850 hPa over western Indian Ocean (0°Eq-25°S; 50-80°E) from 1980-2016.

Nairobi (1979), reported that rainfall maxima are experienced during the weakest monsoon seasons, hence the early cessation of the dry monsoon season is beneficial for rainfall in the sugar belt of SE Africa. The southerly meridional wind anomaly at 850 hPa during Aug-Nov causes strong seasonal concentration of rainfall. The V wind is linked to a westerly wave where the SWIO is characterised by upper-level divergence and surface convergence ahead of the Equatorial trough (Mulenga, *et al., 2003*). This causes a vertical motion and cyclonic curvature at 850 hPa which enhances convection, hence rainfall is sustained over coastal regions and the Lowveld of eastern South Africa (Tyson & Preston-Whyte, 2000).

In the Inter-tropical Convergence Zone (ITCZ) the column of moisture convergence mainly results from the meridional wind convergence over the waterbody, while in other convergence zones such as the South Indian Convergence Zone (SICZ) this is largely a function of zonal wind convergence (Cook, 2000).

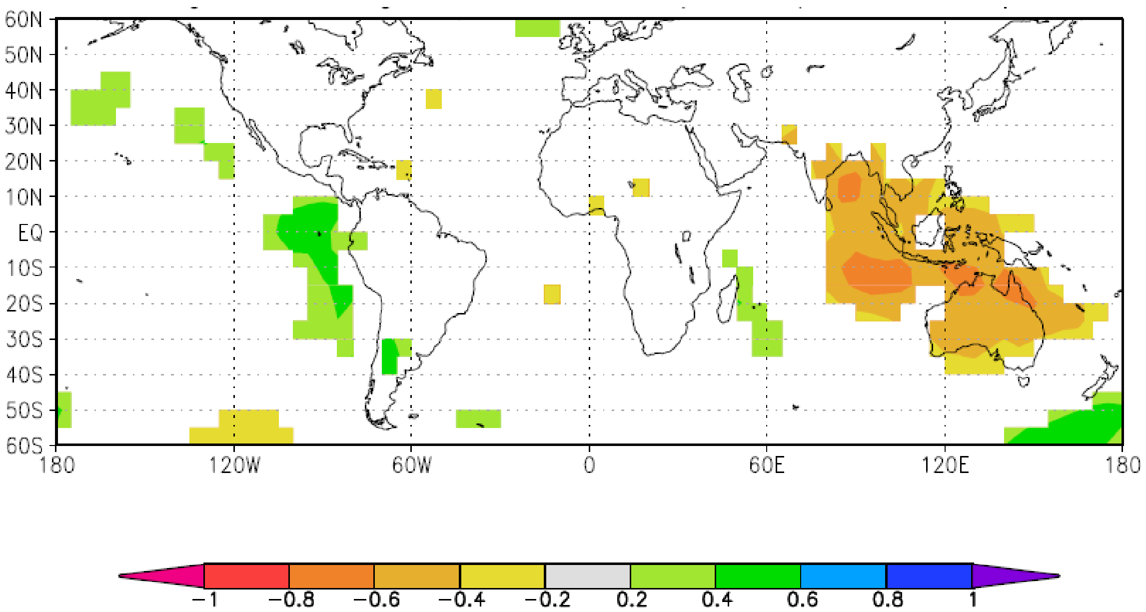

Figure 7.2: Aug-Nov correlation for HadSLP2r SLP and MERRA2 Western Indian Ocean meridional wind (V1) for the period 1980-2016.

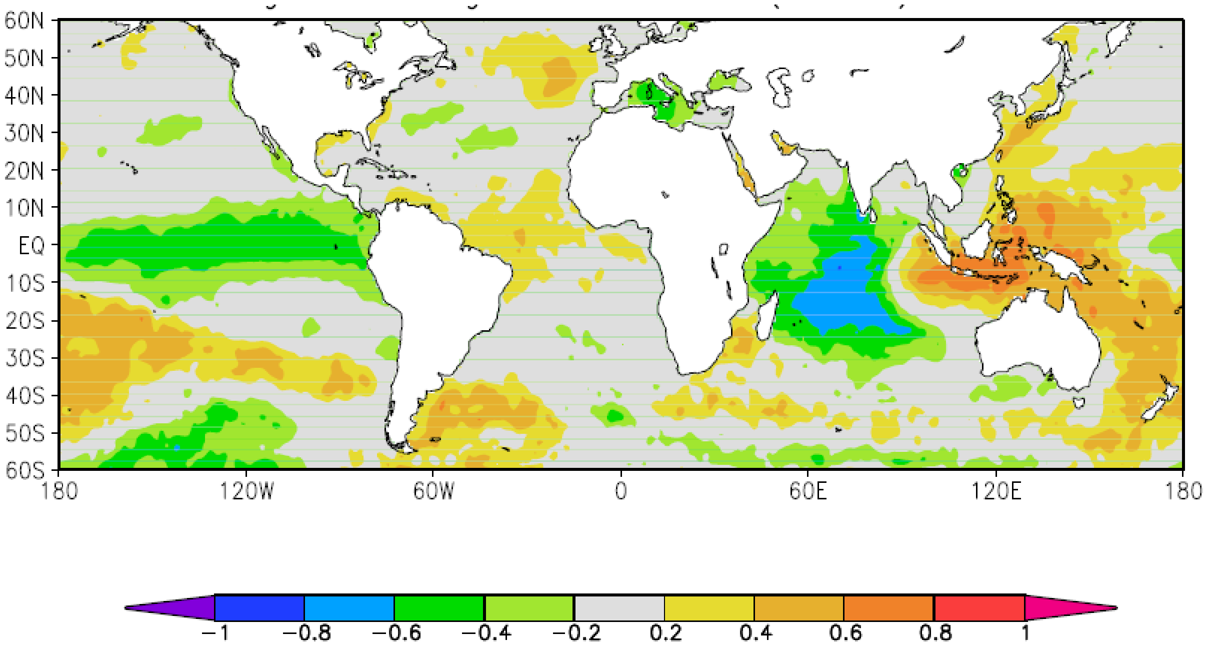

Figure 7.3: Aug-Nov statistical correlation between global HadISST1 SST patterns and MERRA2 WIO meridional wind (V1) for the period 1980-2016.

Philippon, *et al.* (2012) reported that La Niña events are characterised by stronger than normal southerly winds, which trigger the occurrence of rainfall in southern Africa. Tyson and Preston-Whyte (2000) mentioned that the ITCZ moves from the southern hemisphere to the northern hemisphere between January and July, which implies that during Aug-Nov the Hadley cell has not shifted southward to produce the expected northerly wind and uplift then. This occurs when the Tibetan and Southeast

Asia highs are weak (Figure 7.2), and the tropical SW Indian and equatorial Pacific Oceans are cool (Figure 7.3). The Aug-Nov mean Hadley circulation and circulation differences of years of high minus low PDSI are analysed in vectors as illustrated below (*see* Figure 7.4).

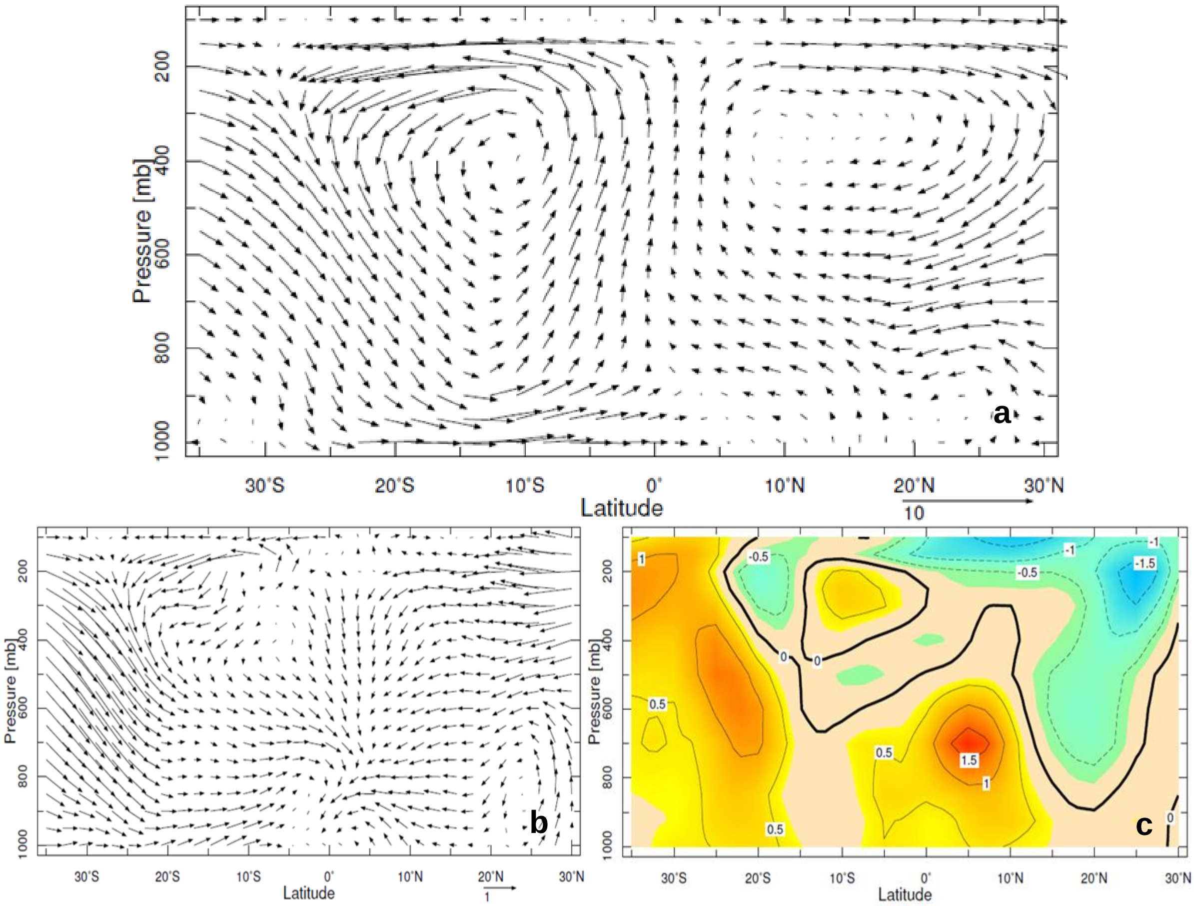

Figure 7.4: Aug-Nov circulation difference for years of high (1987, 1988, 1995, 1996, 1997, 1999, 2000 and 2001) minus years of low PDSI (1982, 1991, 1992, 1993, 1994, 2003, 2004 and 2015) for the period from 1980-2016 averaged over Indian Ocean (60-80°E) where a) mean Hadley cell b) Vertical wind (meridional) circulation differences and c) Horizontal wind (zonal) circulation differences.

From the analysis it is clear that the southern Hadley cell is accelerated prior to the years of good sugarcane yield (high PDSI) and that this is related to an acceleration of the upper level southern subtropical jet stream and to a lesser extent to a westerly wind difference over the equatorial zone (*see* orange shading in Figure 7.4c). This may be related to IOD and ENSO, as indicated by SST pattern anomalies and the mean sea level pressure.

7.3 Observed climate trends

The two time-series below (Figures 7.5 and 7.6a and b) are for observed soil moisture and SST patterns to evaluate the trends without de-trending and maintaining variance. Soil moisture and SSTs are used in weather forecasting as initial boundary conditions because they are conservative in nature. The negative slope of −0.3 for soil moisture trend indicates a declining trend over SE Africa (Figure 7.5), which resembles the downward trend in regional and local sugarcane yield (Figures 4.10 and C.1 and Table 4.1). This inference could be linked to regional warming, as illustrated in Figure 7.6a and b below.

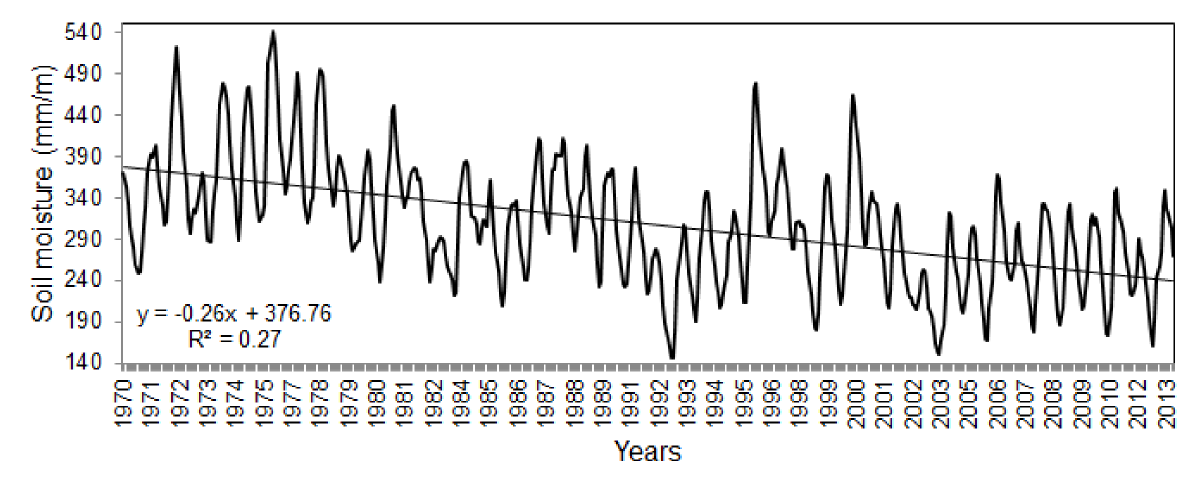

Figure 7.5: Monthly Climate Prediction Centre (CPC) soil moisture from IRI Climate Library over SE Africa (31-23°S and 28-33°E) for the period 1970-2013. R-squared (R^2) shows how data points are distributed in the time series and trend equation quantifies if the trend is inclining-positive slope or declining-negative slope.

Figure 7.5 below indicates that there is a slight declining trend in surface soil moisture over SE Africa and these results accord with Figure 6.2 of Chikoore (2017), where soil moisture decline was reported and ascribed to reduced rainfall and increased evaporation over southern Africa. Moreover, SST patterns over SWIO depicted an increasing trend (*cf*. Figure 7.6a and b), which was expected given the diminishing sugarcane yield observed in this study.

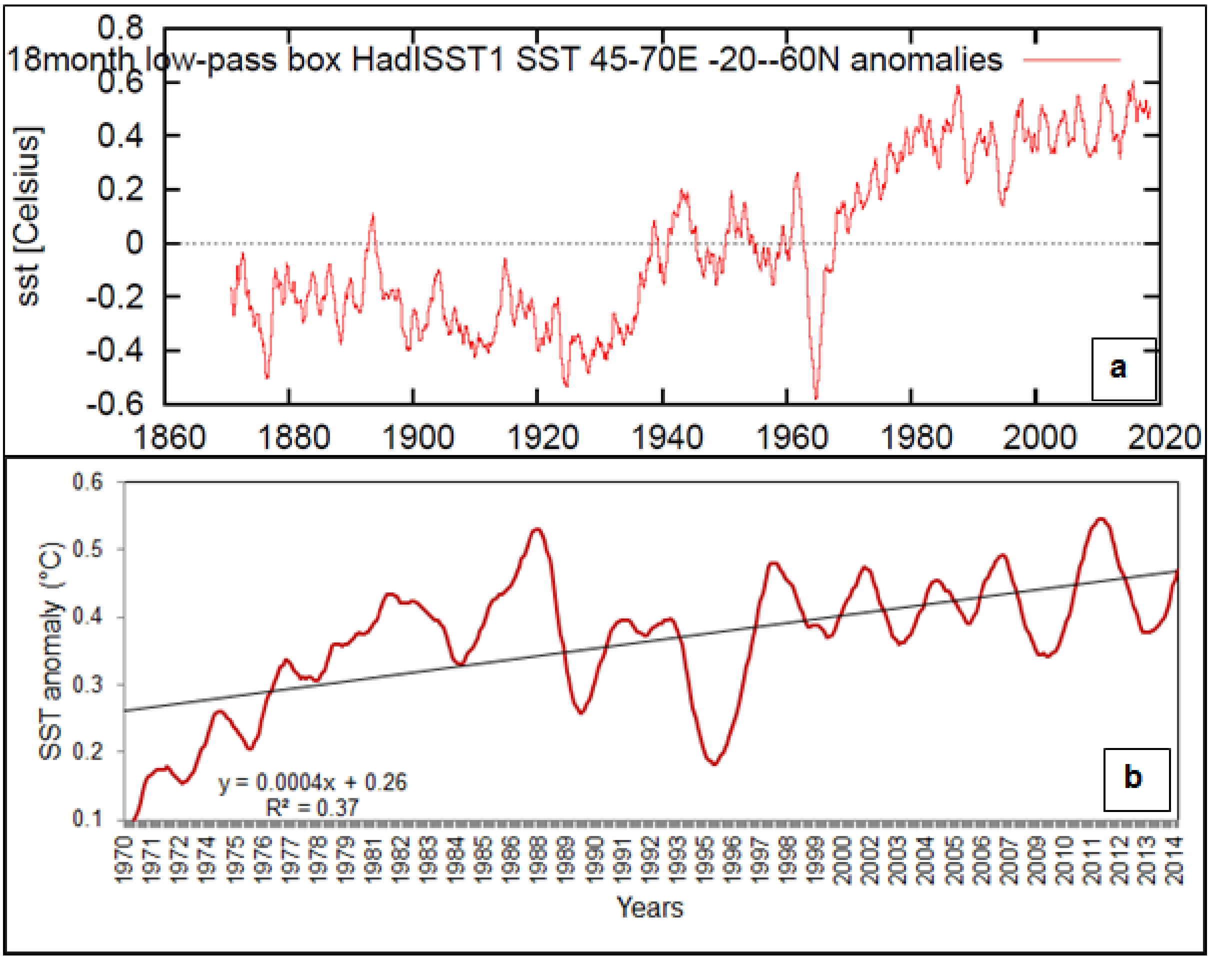

Figure 7.6: Anomalies of Sea Surface Temperature patterns over SW Indian Ocean for the period (a) 1860-2019 and (b) 1970-2014. The area-averaged is SWIO (20-60°S; 45-70°E). Trend equation and R-squared are displayed in the chart.

Ideally, the western Indian Ocean must be cool to promote rainfall and sugarcane yield. Increased SSTs over SWIO strengthen drought persistence over the subcontinent, as described in previous studies (Tadross, *et al.,* 2011; Chikoore, 2017), where the rate of soil water loss (evaporation) exceeds the rate of replenishment (precipitation).

7.4 Long-term climate trends

The trends results presented below (Figures 7.7- 7.9) inform the scientific community about future evolution of climate over SE Africa and the need for mitigation or adaptation measures. Figure 7.8 is the comparison between drought indices (PDSI and P-E datasets) to evaluate their usefulness and reliability. Soil moisture data is very scarce and its analyses are limited to the satellite era (from 1979) and most studies depend on the reanalysis fields. Soil moisture projections for the future are not available in CMIP5, but P-E incorporates soil moisture content, hence it could be used as an indicator of the latter owing to the former.

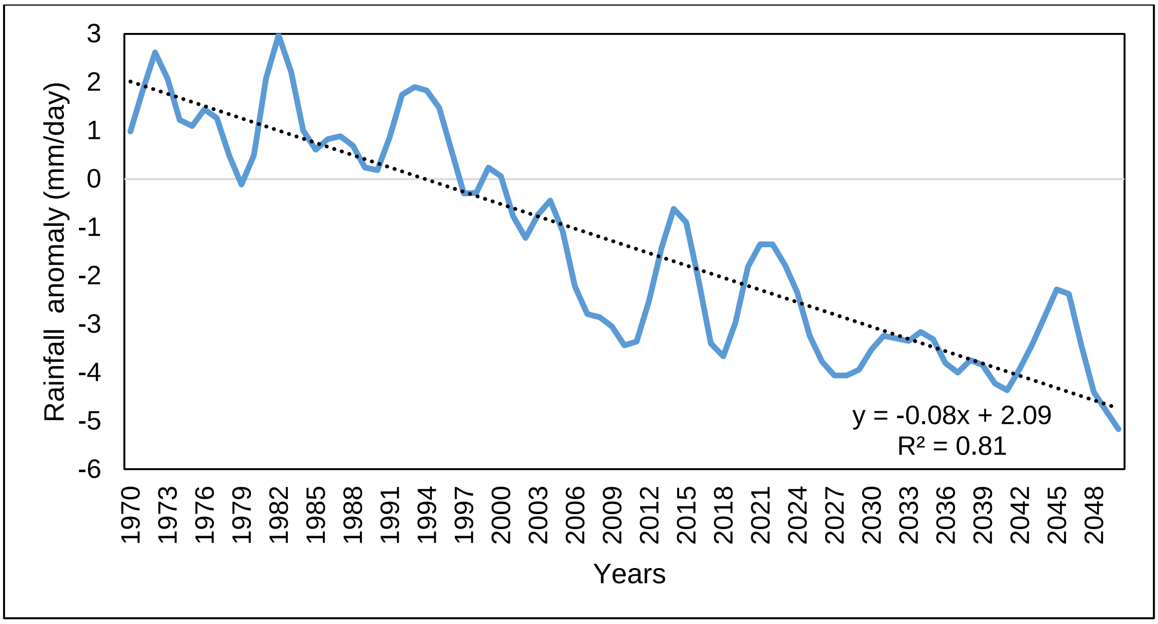

Figure 7.7: CMIP5 simulated under representative concentration pathway (RCP4.5) scenario for rainfall anomalies over the sugarcane growing area of SE Africa for the period 1970-2050 with 2-year filter.

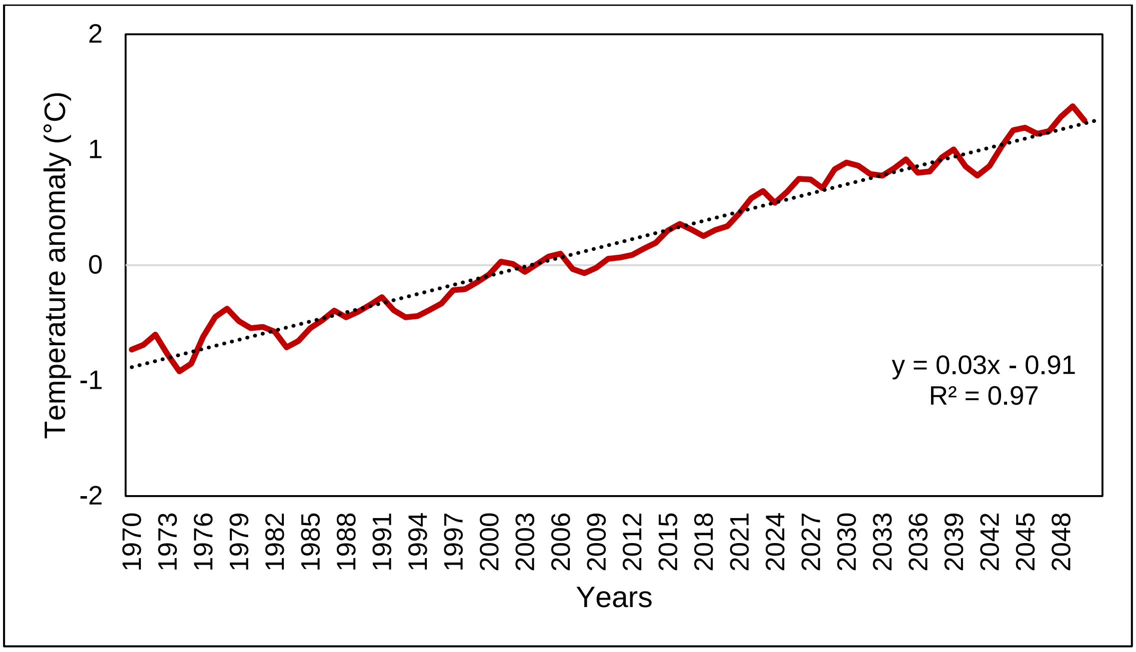

Figure 7.8: CMIP5 simulated under representative concentration pathway (RCP4.5) temperature anomalies over the sugar-growing area of SE Africa for the period 1970-2050 with 2-year filter.

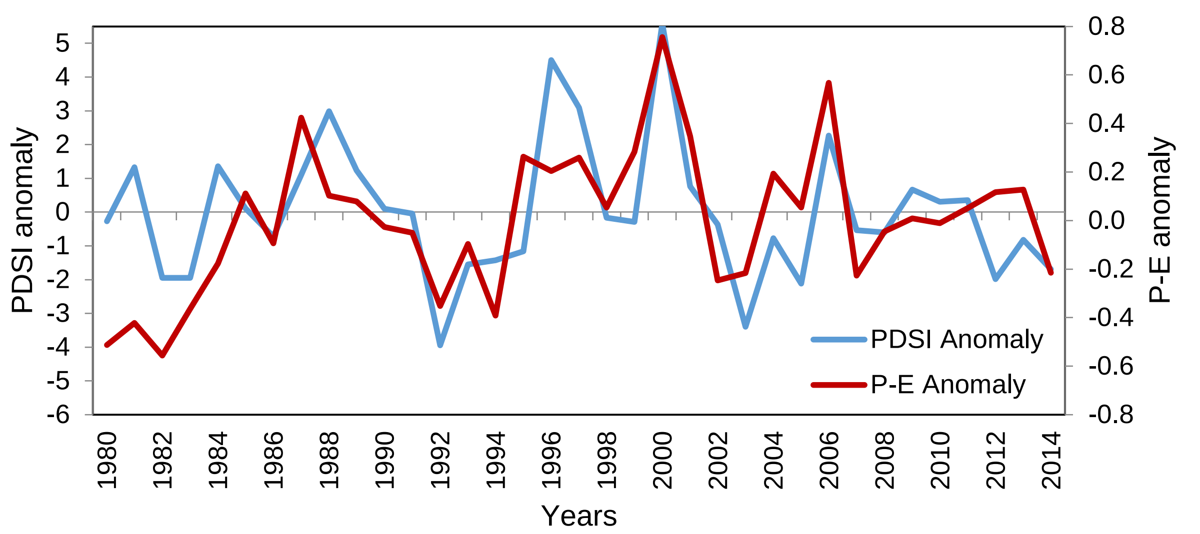

Figure 7.9: Inter-comparison between Palmer Drought Severity Index (PDSI) and MERRA2 Precipitation minus Potential Evaporation (P-E) anomalies to determine drought events over the sugar-area of SE Africa for the period 1980-2014.

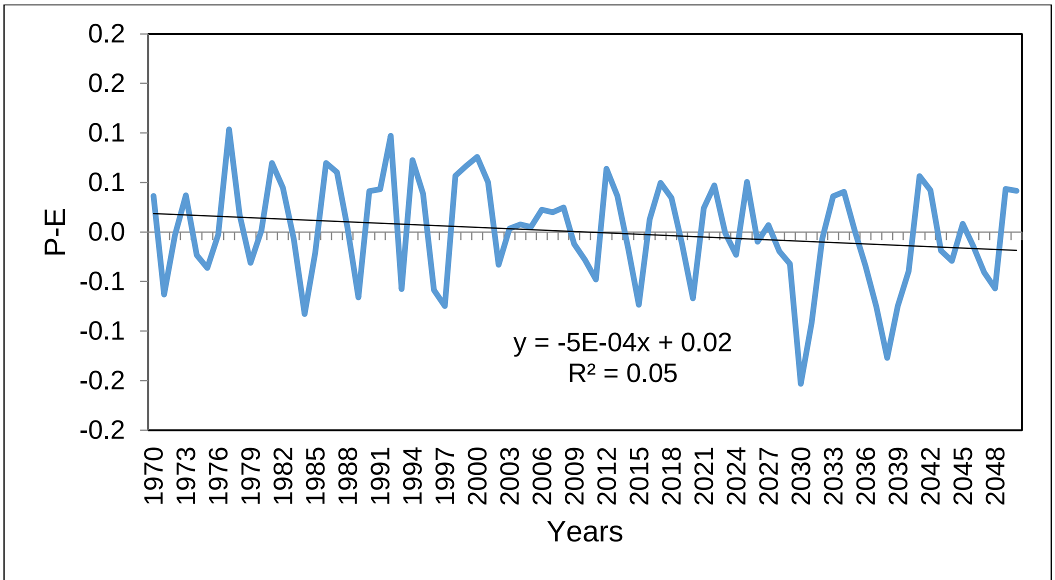

Figure 7.10: Inter-annual variability of Precipitation minus Evapotranspiration (P-E) from CMIP5, which is available in KNMI-CE, and averaged over SE Africa for the period 1970-2050.

Long-term trend analysis suggests that soil moisture has a slight downtrend from 1970-2013 (Figure 7.7), and in the same period the observed rainfall has decreased by a small amount of –0.02 mm.day^{-1} per year (*cf*. Figure 4.2a). Sea surface temperature patterns suggest an increased moisture advection from the Indian Ocean as illustrated in Figure 7.6a and b, but surface air temperatures show a clear upward trend of +0.03 °C per year over the sugarcane-area, both in historical observations and future simulations. The decrease of soil moisture relates to increased surface air temperature (Figures 4.3a and 7.8), whereby on-shore wind flow brings humid air to coastal areas. Simulations from CMIP5 ensemble models show a reduction in rainfall and increase in temperature in future using the RCP4.5 scenario (Figures 7.7-7.8 and 7.10). Temperatures are expected to rise 2 °C, causing faster soil water loss by potential evaporation, as illustrated in Figure 7.10. Sugarcane yield may therefore decrease unless farmers seek technological solutions. The negative impacts may be compensated by benefits of rising CO_2, as suggested by the rising trends of vegetation in this present study (Figure 5.5b) and elsewhere (Lobell & Field, 2007).

Annual mean of actual evapotranspiration is the input of water content to the atmosphere. The CMIP5 simulations depicted a dip in a long-tern trend of drought index (P-E) which suggests more drought conditions in future 2019-2050 (Figure 7.10), and these findings are consistent with the literature (Dube, 1998; Rouault & Richard, 2005; Chikoore, 2017), and this is related with low sugarcane yield (Table 6.1 and Figures 7.1-7.4).

7.5 Summary

Surface air temperatures show an upward trend, as illustrated in Figure 7.8, while rainfall is projected to decrease in future, as displayed in Figure 7.7. This may detrimentally affect agricultural outputs. Sugarcane farmers (both small-scale and large-scale) should rely on predicted impacts of the preceding year's climate (Aug-Nov forecasts are early enough for farmers to take the necessary action) and these could help growers plan for negative impacts that climate might cause to the sugar industry in the upcoming season. The model developed in Chapter 6 could inform farmers' decision-making for short-term climate effects.

The CMIP5 models have a low resolution, which may not resolve the coastal plains where sugarcane is grown, and the model overestimates rainfall over SE Africa. Yet there is agreement that surface air temperatures will increase by 2 °C by the mid-21st century, causing increased evaporation and reduced rainfall (*cf.* Figure 7.10). The temperature signal provides a warning of the need for adaptation and mitigation in agricultural practices. It should be noted that this could be used for long-term proactive measusres, but these trends need to be continosly calibrated for precise decision-making and policy formulation.

CHAPTER 8

CONCLUSIONS AND RECOMMENDATIONS

8.1 Introduction

This dissertation has investigated the degree of correlation between temporal and spatial climatic patterns and sugarcane yield in southeastern Africa. The research focused on local climate impacts and global climate forcing of sugarcane yield. Therefore, a statistical model to predict sugarcane yield was developed. Observed and projected climate trends relevant to sugarcane production were evaluated using CMIP5 models of the IPCC. The summary of results, recommendations for further research and overall conclusions of this study are presented in this chapter. The results summarised in this chapter were obtained using the methodology described in Chapter 3, and it should be noted that different methods and datasets could produce different results.

8.2 Summary of key findings

The area-averaged time series revealed an evidence of local climate influence on sugarcane yield (Figures 4.2a-4.4b). The latter, showed that there is a strong linear relationship between rainfall and PDSI and sugarcane yield over southeastern Africa. Both South Africa and ESwatini have a z-score of less than negative 4 at 95% level (Table 4.1 and Figures 4.10 and C.1), and the Mann-Kendall and Sequential Mann-Kendall (Seq.MK) tests statistics indicated that sugarcane yield has a significant downward or negative trend as indicated with $z \approx -4$ and p-value of 0.05. These trends could be largely attributed to rainfall reduction and temperature increase over SE Africa.

The study used averaged MERRA2 model-derived sensible heat flux (SHF) and pan evaporation datasets to formulate a 'distinct index' for estimating soil water loss (Figure 4.5). Abrupt positive magnitudes of this index indicate high evaporation and SHF, hence this is related to soil water deficit. Soil moisture is essential for sugarcane growth and development. Hence, soil moisture data scarcity, which is limited to the satellite-era (1979-present) and other regions do not afford satellite soil moisture products. These limitations hinder the historical analysis and prevents comprehensive analysis of climate, thus this index could be used to overcome the abovementioned limitations.

The positive statistical link between PDSI, satellite NDVI and sugarcane yield (Tables 4.3 and E.1 and Figure 5.8a-d), verified the use of NDVI as a proxy of sugarcane yield. The inclining trend of the satellite vegetation (Figure 5.5b) is counter-intuitive to the declining trend in sugarcane yield (Table 4.1; Figures 4.10a and b). This also suggests other factors which define the seasonal sugarcane yield variations and high vegetative growth than crop growth over the study area.

The main findings of this study are that the correlations of key local climate parameters (i.e. rainfall and temperature) with sugarcane yield are strong, especially for the time period from December to May before harvest. This indicates that Dec – May is an important season for sugarcane production over SE Africa. This further implies that sugarcane requires sufficient rainfall and reasonable potential evaporation (as a function of temperature, soil moisture and SHF) for a period of six months in order to mature and develop, but this is subject to elevation and spatio-temporal distribution of meteorological patterns.

The study revealed that the preceding year climate accounts for about 40-70% of sugarcane yield variability from season-to-season (Figures 4.12 and 5.9), which suggests the influence of non-climatic influences. However, the weak correlation values of $r \approx \pm 0.5$ between ENSO indicators and sugarcane yield show that sugarcane production is less sensitive to global and remote climate influences than are shorter cycle crops such as maize.

The inter-comparison between the annualised Southern Oscillation Index (SOI) of the previous year and sugarcane yield revealed that $>$75% of strong Pacific El Niño events are followed by low sugarcane yield (Figure 6.1 and Table 6.1).

The CCWT spectral analysis showed that there are cycles of 1-2 years, 3-6 years and 10-12 years (*see* Figures 5.6 and 5.7). These cycles show that drought and sugarcane yield have the frequency of reoccurrence according to these cycles, which means drought and low sugarcane yields could be, or were once expected, after 1-2 years, or 3-6 years. The latter seems to be shorter cycles and there is a longer cycle of 10-12 years over SE Africa from 1970-2010. This strong seasonality may be related to fast oscillations imposed by the Indian Ocean (e.g. shorter cycles), while the longer cycle relates to the slower Pacific ENSO.

The surface air temperature has increased by 1 °C in the sugar belt of SE Africa and is projected by CMIP5 models to continue to rise another 1 °C up to 2050 (Figure 7.8), accompanied by reduced rainfall (*see* Figure 7.7). The increased temperature of 2 °C was projected globally by Tyson & Preston-Whyte (2000) using CSIRO coupled models and Hadley Centre model simulations. The downward trend of rainfall (Figure 7.7) was reported in the study of Jury (2013), where various rainfall datasets from different parts of southern Africa were analysed and trends were calculated. Rainfall reduction can also be ascribed to enhanced surface air temperatures and potential evapotranspiration (Figures 7.8 and 7.10), which will increase the rate of water loss, while reducing the rate of replenishment.

There is evidence of heatwave conditions occurring over the eastern part of southern Africa. This also reduces the precipitation rate (Lyon, 2009; Kruger & Sekele, 2013), and the former is expected even in future (Russo, *et al*., 2016). Projected long-term climate trends (2020-2050) revealed that sugarcane growing will occur under warmer and dry climate conditions, as illustrated in Figures 7.7 and 7.8 in this study. Therefore, the question is what can be done to help the sugar industry cope with this projected climate change? The use of weather and climate information in sugarcane production could provide additional profits and stimulate interest and participation on the part of sugarcane growers.

8.3 Development of seasonal forecasts

The study provided insights on the climate-sugarcane relationship which may be applied in crop modelling and forecasting and in the quest for mitigation and adaptation strategies. With accurate and timely seasonal crop-climate forecasts the productivity of sugarcane could be improved for both small and large scale growers. These forecasts could help to inform their decisions on farming operations, and should reach end-users (growers) by early December of the preceding year.

The multi-variate/multiple linear regression (MLR) algorithms used in this study gave a statistical fit of 47% of sugarcane-PDSI (predicted PDSI) variability in Dec-Mar according to the 2 Aug-Nov predictors used, as illustrated in Table 6.5. This forecast system could be used to predict sugarcane yield during the proceeding season. It was revealed from the model output that a decrease of Aug-Nov SST in the west Atlantic Ocean by (−0.18 °C) and positive or increase of meridional wind (V wind at 850 hPa) over the West Indian Ocean by (+0.58 m/s) anticipates increased PDSI and therefore sugarcane yield. Decrease of Aug-Nov SLP over the East Indian Ocean and increase over the East Pacific Ocean (*cf*. Figure 6.7) contribute to a shift of rainfall from ocean to land, hence increasing sugarcane yield over SE Africa.

8.4 Overall conclusion

The results on trend analyses revealed that sugarcane yield in South Africa and ESwatini have a significant declining trend (i.e. z-score less than -4) for the period from 1970-2016. It should be noted that there was no significant trend detected from the simulated yield from all growing scales over the SA sugar industry. A declining trend, as indicated by z-score equal to -1.954 and p-value of 0.05, was observed at an industry level and over the South Coast region. Moreover, a downward trend of sugarcane yield was detected in the Zululand region for all growing scales (LSGs, SSGs and in the TOT), where the z-score was found to be -2.060 for LSGs, -2.905 for SSGs and -2.641 for total (TOT) at 95% level. The Northern Irrigated region has recorded much higher values of sugarcane yield (e.g 100 ton/ha for SSGs) but there is a clear and significant downward trend, as indicated by a z-score of -2.483 for SSGs at 95% level of confidence.

It was expected that the simulated yield would correlate more strongly with local climate parameters (rainfall and temperature) in rain-fed regions (South Coast) than irrigated regions (Northern Irrigated). However, low correlations were observed between sugarcane yield and ENSO indicators (i.e. $r = +0.28$ and -0.29 for SOI and Niño4, respectively) over the Northern Irrigated region. The PDSI seems to provide more explanation ($r = +0.45$ over the same region) of sugarcane variations than individual climate parameters. These statistical associations are much higher in rain-fed regions than in irrigated agro-climatic zones. For example, simulated yield correlated strongly with PDSI and rainfall ($r > +0.7$) over the South Coast region.

Climate influence on sugarcane is statistically estimated at 40-70%, which gives a greater explanation about sugarcane yield variability. However, $r < +0.8$ in all statistical tests implies that there are other significant sugarcane predictors which could be indirectly induced by climate or be completely non-climatic. Indirect factors include the outbreak of pests and diseases (e.g. *Eldana saccharina, Ustilago scitaminea and Fulmekiola serrata*) under certain weather conditions.

The climatology shows steep gradients from west-dry to east-wet, but drought recurrences are frequent over the sugarcane-belt of SE Africa. This is related to the phases of ENSO (El Niño and La Niña). The spatial gradients give insights to the scientific community about the location of southeastern sugar belt based on crop, climate and water requirements of sugarcane production.

Sugarcane growers can use the forecast system outlined in Chapter 5 of this dissertation to predict the yield by proxy, and search for mitigation and adaptation strategies and implement economic budget planning. In addition, farm extension services can spread the information and provide alternative resources. Southerly meridional flow over the Western Indian Ocean and anticyclonic activity in the Mozambique Channel are key climatic features for sugarcane production. All drought events and heatwave conditions are linked to anticyclonic conditions (Tyson & Preston-Whyte, 2000; Lyon, 2009; Russo, *et al*., 2016; Chikoore, 2017) This reinforces the need to incorporate PDSI and meridional wind in sugarcane forecasting in order to improve the accuracy and reliability of these forecasts.

The CMIP5 model simulations revealed that sugarcane growing will take place under warmer and drier climate conditions in future, but some of the negative impacts of increased temperatures due to global warming could be offset by increased uptake of carbon dioxide by vegetation since NDVI depicted an inclining trend over time, as illustrated in Figure 5.5b. Scientific and technological solutions can be used to maintain the viability of sugarcane production.

In addition, a paradigm shift from rain-fed to irrigated sugarcane could yield positive benefits for the sugar industry across SE Africa. Irrigation is expected to increase the sugarcane yield in future (2070-2100) (Jones, *et al.,* 2015). The methods of implementing irrigation, related constraints and arising benefits are detailed in sugarcane and climate change studies (Laclau & Laclau, 2009; Jones, *et al*., 2015; Amjath-Babu, *et al*., 2016). It should be noted that surface water resources are not sufficient for irrigation, and that other alternatives such as groundwater utilisation could help to supplement the available water resources.

REFERENCES

Abraha, M.G. and Savage, M.J., 2006. Potential impacts of climate change on the grain yield of maize for the midlands of KwaZulu-Natal, South Africa. Agriculture, Ecosystems & Environment, 115(1), pp.150-160.

Adams, M.J. and Carstens, E.B., 2012. Ratification vote on taxonomic proposals to the International Committee on Taxonomy of Viruses (2012), Archives of Virology, 157(7), pp.1411–1422.

Agrawala, S., Broad, K. and Guston, D.H., 2001. Integrating climate forecasts and societal decision making: challenges to an emergent boundary organization. Science, Technology, & Human Values, 26(4), pp.454-477.

Alderfasi, A.A. and Nielsen, D.C., 2001. Use of crop water stress index for monitoring water status and scheduling irrigation in wheat. Agricultural water management, 47(1), pp.69-75.

Allan, R. and Ansell, T., 2006. A new globally complete monthly historical gridded mean sea level pressure dataset (HadSLP2): 1850–2004. Journal of Climate, 19(22), pp.5816-5842.

Amjath-Babu, T.S., Krupnik, T.J., Kaechele, H., Aravindakshan, S. and Sietz, D., 2016. Transitioning to groundwater irrigated intensified agriculture in Sub-Saharan Africa: An indicator based assessment. Agricultural Water Management, 168, pp.125-135.

Ashok, K., Behera, S.K., Rao, S.A., Weng, H. and Yamagata, T., 2007. El Niño Modoki and its possible teleconnection. Journal of Geophysical Research: Oceans, 112(C11).

Atkinson, P.R. and Nuss, K.J., 1989. Associations between host-plant nitrogen and infestations of the sugarcane borer, Eldana saccharina Walker (Lepidoptera: Pyralidae). Bulletin of Entomological Research, 79(3), pp.489-506.

Bannayan, M., Lotfabadi, S., Sanjani, S., Mohammadian, A. and Agaalikhani, M., 2011b. Effects of precipitation and temperature on cereal yield variability in northeast of Iran. International Journal of Biometeorology, 55(3), pp.387–401.

Barnston, A.G., Van den Dool, H.M., Zebiak, S.E., Barnett, T.P., Ji, M., Rodenhuis, D.R., Cane, M.A., Leetmaa, A., Graham, N.E., Ropelewski, C.R. and Kousky, V.E., 1994. Long-lead seasonal forecasts—where do we stand?. Bulletin of the American Meteorological Society, 75(11), pp.2097-2114.

Behera, S.K., Luo, J.J., Masson, S., Delecluse, P., Gualdi, S., Navarra, A. and Yamagata, T., 2005. Paramount impact of the Indian Ocean dipole on the East African short rains: A CGCM study. Journal of Climate, 18(21), pp.4514-4530.

Bezuidenhout, C.N. and Schulze, R.E., 2006. Application of seasonal climate outlooks to forecast sugarcane production in South Africa. Climate Research, 30(3), pp.239-246.

Bezuidenhout, C.N. and Singels, A., 2007. Operational forecasting of South African sugarcane production: Part 2–System evaluation. Agricultural Systems, 92(1-3), pp.39-51.

Bosilovich, M.G., Lucchesi, R. and Suarez, M., 2015. MERRA-2: File specification.

Bradshaw-Rouse and Judith, J., 2015. SOIL degradation (ed*.),* Encyclopedia of Science, Salem Press, January*,* p.3.

Brookfield, C.P. and Parsons, H., 2005. Agrodiversity. Learning from Farmers Across the World. Geographical Research, 43(3), pp.329-336.

Cai, W., Van Rensch, P., Cowan, T. and Hendon, H.H., 2011. Teleconnection pathways of ENSO and the IOD and the mechanisms for impacts on Australian rainfall. Journal of Climate, 24(15), pp.3910-3923.

Caloiero, T., Veltri, S., Caloiero, P. and Frustaci, F., 2018. Drought Analysis in Europe and in the Mediterranean Basin Using the Standardized Precipitation Index. Water, 10(8), pp.1043-1050.

Carslaw, D.C., 2015. The openair manual — open-source tools for analysing air pollution data. Manual for version 1.1-4, King's College London.

Chandiposha, M., 2013. Potential impact of climate change in sugarcane and mitigation strategies in Zimbabwe. African Journal of Agricultural Research, 8, pp.2814–2818.

Chatterjee, S., Bisai, D. and Khan, A., 2014. Detection of approximate potential trend turning points in temperature time series (1941–2010) for Asansol Weather Observation Station, West Bengal, India. India. Atmospheric and Climate Sciences, 4, pp.64-69.

Cheavegatti-Gianotto, A., de Abreu, H.M.C., Arruda, P., Bespalhok-Filho, J.C., Burnquist, W.L., Creste, S., di Ciero, L., Ferro, J.A., Figueira, A.V.O., Filgueiras, T.S., Grossi-de-Sá, M.F., Guzzo, E.C., Hoffmann, H.P., Landell, M.G.A., Macedo, N., Matsuoka, S., Reinach, F.C., Romano, E., da Silva, W.J., Silva-Filho, M.C. and Ulian, E.C., 2011. Sugarcane (Saccharum X officinarum): a reference study for the regulation of genetically modified cultivars in Brazil. Tropical Plant Biology, 4, pp.62–89.

Chikoore, H., 2005. Vegetation feedback on the boundary layer climate of Southern Africa. MSc. dissertation, Department of Geography and Environmental Studies, University of Zululand.

Chikoore, H., 2017. Drought in Southern Africa: structure, characteristics and impacts. PhD thesis, Department of Geography and Environmental Studies, University of Zululand.

Cirino, P.H., Féres, J.G., Braga, M.J. and Reis, E., 2015. Assessing the Impacts of ENSO-related Weather Effects on the Brazilian Agriculture. In International Conference on Applied Economics (ICOAE), 2-4 July 2015, Kazan, Russia, Procedia Economics and Finance, 24, pp.146-155.

Cline, W.R., 1996. The impact of global warming of agriculture: comment. The American Economic Review, 86(5), pp.1309-1311.

Costa, A.C. and Soares, A., 2009. Trends in extreme precipitation indices derived from a daily rainfall database for the South of Portugal. International Journal of Climatology, 29(13), pp.1956-1975.

Dai, A. and National Center for Atmospheric Research Staff (Eds). Last modified 12 July 2017. "The Climate Data Guide: Palmer Drought Severity Index (PDSI)." Retrieved from https://climatedataguide.ucar.edu/climate-data/palmer-drought-severity-index-pdsi.

Dai, A., Trenberth, K.E. and Qian, T., 2004. A global dataset of Palmer Drought Severity Index for 1870–2002: Relationship with soil moisture and effects of surface warming. Journal of Hydrometeorology, 5(6), pp.1117-1130.

Darwin, R., 1999. The impact of global warming on agriculture: A Ricardian analysis: Comment. American Economic Review, 89(4), pp.1049-1052.

Daubechies, I., 1990. The wavelet transform, time-frequency localization and signal analysis. IEEE transactions on information theory, 36(5), pp.961-1005.

Dee, D.P., Uppala, S.M., Simmons, A.J., Berrisford, P., Poli, P., Kobayashi, S., Andrae, U., Balmaseda, M.A., Balsamo, G., Bauer, P. and Bechtold, P., 2011. The ERA-Interim reanalysis: Configuration and performance of the data assimilation system. Quarterly Journal of the Royal Meteorological Society, 137(656), pp.553-597.

Deressa, T., Hassan, R. and Poonyth, D., 2005. Measuring the impact of climate change on South African agriculture: The case of sugarcane growing regions. Agrekon, 44(4), pp.524-542.

De la Casa, A., Ovando, G. and Nasello, O., 2018. Changes in the Intensity and Variability of Precipitation in the Central Region of Argentina between 1960 and 2012. Climate, 6(3), pp.66-88.

Dubb, A., 2015. Dynamics of decline in small-scale sugarcane production in South Africa: evidence from two 'rural' wards in the Umfolozi region. Land Use Policy, 48, pp.362-376.

Dube, L.T., 1998. Causes, structure and impacts of the 1992/93 drought in KwaZulu/Natal. PhD thesis, Department of Geography and Environmental Studies, University of Zululand.

Dube, L.T. and Jury, M.R., 2000. The nature of climate variability and impacts of drought over KwaZulu-Natal, South Africa. South African Geographical Journal, 82(2), pp.44-53.

Egoume-Bossogo, P., 2003. Guyana: Experience with Macroeconomic Stabilization, Structural Adjustment, and Poverty Reduction. International Monetary Fund, Washington, DC.

Everingham, Y.L., Muchow, R.C., Stone, R.C. and Coomans, D.H., 2003. Using Southern Oscillation Index phases to forecast sugarcane yields: a case study for northeastern Australia. International Journal of Climatology: A Journal of the Royal Meteorological Society, 23(10), pp.1211-1218.

Everingham, Y.L., Muchow, R.C., Stone, R.C., Inman-Bamber, N.G., Singels, A. and Bezuidenhout, C.N., 2002. Enhanced risk management and decision-making capability across the sugarcane industry value chain based on seasonal climate forecasts. Agricultural Systems, 74(3), pp.459-477.

FAO (Food and Agriculture Organisation), 2015. El Niño Southern Oscillation (ENSO) possible impact on agricultural production during the second half of 2015, available on http://www.fao.org/3/a-i4713e (accessed 04 January 2016).

Field, C.B. ed., 2012. Managing the risks of extreme events and disasters to advance climate change adaptation: special report of the Intergovernmental Panel on Climate Change. Cambridge University Press.

Foufoula-Georgiou, E. and Krajewski, W., 1995. Recent advances in rainfall modelling, estimation, and forecasting. Reviews of Geophysics, 33(S2), pp.1125-1137.

Franzke, C.L., 2014. Warming trends: nonlinear climate change. Nature Climate Change, 4(6), pp.423-424.

Fraser, A.I., Harrod, T.R. and Haygarth, P.M., 1999. The effect of rainfall intensity on soil erosion and particulate phosphorus transfer from arable soils. Water Science and Technology, 39(12), pp.41-45.

Funke, T., 2013. Impact of Proposed Electricity Tariffs on Sugarcane Growers in KZN. Online at http://www.sasa.org.za (retrieved on 13 March 2015).

Gbetibouo, G.A. and Hassan, R.M., 2005. Measuring the economic impact of climate change on major South African field crops: a Ricardian approach. Global and Planetary Change, 47(2-4), pp.143-152.

Gilbert, R.O., 1987. Statistical methods for environmental pollution monitoring. John Wiley & Sons. 322pp.

Gleckler, P.J., Taylor, K.E. and Doutriaux, C., 2008. Performance metrics for climate models. Journal of Geophysical Research: Atmospheres, 113(D6).

Goodman, S.J., Buechler, D.E., Knupp, K., Driscoll, K. and McCaul, E.W., 2000. The 1997–98 El Niño event and related wintertime lightning variations in the southeastern United States. Geophysical Research Letters, 27(4), pp.541-544.

Guzzetti, F. and Tonelli, G., 2004. Information system on hydrological and geomorphological catastrophes in Italy (SICI): a tool for managing landslide and flood hazards. Natural Hazards and Earth System Science, 4(2), pp.213-232.

Halpert, M.S., Bell, G.D., Kousky, V.E. and Ropelewski, C.F., 1996. Climate assessment for 1995. Bulletin of the American Meteorological Society, 77(5), pp.S1-S44.

Hansen, J.W., Irmak, A., and Jones, J.W., 1998. El Niño-Southern Oscillation influences on Florida crop yields. Soil and Crop Science Society of Florida Proceedings 57, pp.12–15.

Harris, I.P.D.J., Jones, P.D., Osborn, T.J. and Lister, D.H., 2014. Updated high-resolution grids of monthly climatic observations–the CRU TS3. 10 Dataset. International Journal of Climatology, 34(3), pp.623-642.

Hastenrath, S. and Heller, L., 1977. Dynamics of climatic hazards in northeast Brazil. Quarterly Journal of the Royal Meteorological Society, 103(435), pp.77-92.

Heddinghaus, T. R. and Sabol, P., 1991: A review of the Palmer Drought Severity Index and where do we go from here? Seventh Conf. on Applied Climatology, Salt Lake City, UT, American Meteorological Society, pp.242–246.

Hermes, J.C. and Reason, C.J., 2009. The sensitivity of the Seychelles–Chagos thermocline ridge to large-scale wind anomalies. ICES Journal of Marine Science, 66(7), pp.1455-1466.

Huang, B., Banzon, V.F., Freeman, E., Lawrimore, J., Liu, W., Peterson, T.C., Smith, T.M., Thorne, P.W., Woodruff, S.D. and Zhang, H.M., 2015. Extended reconstructed sea surface temperature version 4 (ERSST. v4). Part I: Upgrades and intercomparisons. Journal of Climate, 28(3), pp.911-930.

Inman-Bamber, N.G., 1995. Climate and water as constraints to production in the South African sugar industry. Proceedings of the South African Sugar Technologists' Association, 69, pp.55-59.

James, M.E. and Kalluri, S.N., 1994. The Pathfinder AVHRR land data set: An improved coarse resolution data set for terrestrial monitoring. International Journal of Remote Sensing, 15(17), pp.3347-3363.

Jones, M.R. and Singels, A., 2015. Analysing yield trends in the South African sugar industry. Agricultural Systems, 141, pp.24-35.

Jones, M.R., Singels, A. and Ruane, A.C., 2015. Simulated impacts of climate change on water use and yield of irrigated sugarcane in South Africa. Agricultural Systems, 139, pp.260-270.

Jones, P.G. and Thornton, P.K., 2003. The potential impacts of climate change on maize production in Africa and Latin America in 2055. Global Environmental Change, 13(1), pp.51-59.

Jury, M.R., 2002. Economic impacts of climate variability in South Africa and development of resource prediction models. Journal of Applied Meteorology, 41(1), pp.46-55.

Jury, M.R. and Melice, J.L., 2000. Analysis of Durban rainfall and Nile river flow 1871–1999. Theoretical and Applied Climatology, 67(3-4), pp.161-169.

Jury, M.R. and Pathack, B.M.R., 1993. Composite climatic patterns associated with extreme modes of summer rainfall over southern Africa: 1975–1984. Theoretical and Applied Climatology, 47(3), pp.137-145.

Jury, M.R., 1998. Statistical analysis and prediction of KwaZulu-Natal climate. Theoretical and Applied Climatology, 60(1-4), pp.1-10.

Jury, M.R., 2013. Climate trends in southern Africa. South African Journal of Science, 109(1-2), pp.1-11.

Kanamitsu, M., Ebisuzaki, W., Woollen, J., Yang, S.K., Hnilo, J.J., Fiorino, M. and Potter, G.L., 2002. Ncep–doe amip-ii reanalysis (r-2). Bulletin of the American Meteorological Society, 83(11), pp.1631-1643.

Keating, B.A., Carberry, P.S., Hammer, G.L., Probert, M.E., Robertson, M.J., Holzworth, D., Huth, N.I., Hargreaves, J.N., Meinke, H., Hochman, Z. and McLean, G., 2003. An overview of APSIM, a model designed for farming systems simulation. European Journal of Agronomy, 18(3-4), pp.267-288.

Keeping, M.G. and Meyer, J.H., 2006. Silicon-mediated resistance of sugarcane to Eldana saccharina Walker (Lepidoptera: Pyralidae): effects of silicon source and cultivar. Journal of Applied Entomology, 130(8), pp.410-420.

Kelbe, B.E., Bodenstein, B. and Mulder, G.J., 1991. Investigation of the hydrological response to informal settlements on small catchments in South Africa. International Association of Hydrological Sciences (IAHS) Publication, pp.219-27.

Kendall, M.G., 1975. Rank correlation methods. 2nd impression. Charles Griffin and Company Ltd. London and High Wycombe.

Kew.org, 2015. Saccharum officinarum (sugar cane). Plants and Fungi at Kew. Available online at: http://www.kew.org/science-conservation/plants fungi/ *saccharum-officinarum*-sugar-cane (Accessed 01 March 2015).

Knox, J.W., Díaz, J.R., Nixon, D.J. and Mkhwanazi, M., 2010. A preliminary assessment of climate change impacts on sugarcane in Swaziland. Agricultural Systems, 103(2), pp.63-72.

Kruger, A.C. and Sekele, S.S., 2013. Trends in extreme temperature indices in South Africa: 1962–2009. International Journal of Climatology, 33(3), pp.661-676.

Kuhnel, I., 1993. Impacts of extreme climatic conditions on sugar cane production in northeastern Australia. IAHS PUBLICATION, pp.157-157.

Kumar, A. and Sharma, P., 2014a. Climate Change and Sugarcane Productivity in India: An Econometric Analysis. Journal of Social and Development Sciences, 5(2), pp.111-122.

Laclau, P.B. and Laclau, J.P., 2009. Growth of the whole root system for a plant crop of sugarcane under rainfed and irrigated environments in Brazil. Field Crops Research, 114(3), pp.351-360.

Lanzante, J.R., 1996. Resistant, robust and non-parametric techniques for the analysis of climate data: Theory and examples, including applications to historical radiosonde station data. International Journal of Climatology: A Journal of the Royal Meteorological Society, 16(11), pp.1197-1226.

Lázaro, R., Rodrigo, F.S., Gutiérrez, L., Domingo, F. and Puigdefábregas, J., 2001. Analysis of a 30-year rainfall record (1967–1997) in semi–arid SE Spain for implications on vegetation. Journal of Arid Environments, 48(3), pp.373-395.

Levey, K.M. and Jury, M.R., 1996. Composite intraseasonal oscillations of convection over southern Africa. Journal of Climate, 9(8), pp.1910-1920.

Levey, K.M., 1993. Intra-seasonal oscillations of convection over southern Africa. Unpublished MSc. thesis, Oceanography Department, University of Cape Town, 236 pp.

Liebmann, B. and Smith, C.A., 1996. Description of a complete (interpolated) outgoing longwave radiation dataset. Bulletin of the American Meteorological Society, 77(6), pp.1275-1277.

Lobell, D.B. and Field, C.B., 2007. Global scale climate–crop yield relationships and the impacts of recent warming. Environmental Research Letters, 2(1), p.014002.

Lyon, B., 2009. Southern Africa summer drought and heat waves: observations and coupled model behavior. Journal of Climate, *22*(22), pp.6033-6046.

Maidment, R.I., Allan, R.P. and Black, E., 2015. Recent observed and simulated changes in precipitation over Africa. Geophysical Research Letters, 42(19), pp.8155-8164.

Mann, H.B., 1945. Nonparametric tests against trend. Econometrica: Journal of the Econometric Society, 13(3), pp.245-259.

Manuel, T.A., 2008. Budget Speech 2008 obtained at www.treasury.gov.za (accessed 02 April 2015).

Maponya, P. and Mpandeli, S., 2012. Climate Change and Agricultural Production in South Africa: Impacts and Adaptation Options. Journal of Agricultural Science, 4(10), pp.48-60.

Martin, J.P., Wismer, C.A. and Ryan, C.C., 1989. Red stripe. Diseases of Sugarcane. Major Diseases, pp.81-95.

Mason, S.J. and Joubert, A.M., 1997. Simulated changes in extreme rainfall over southern Africa. International Journal of Climatology: A Journal of the Royal Meteorological Society, 17(3), pp.291-301.

Masson, S., Terray, P., Madec, G., Luo, J.J., Yamagata, T. and Takahashi, K., 2012. Impact of intra-daily SST variability on ENSO characteristics in a coupled model. Climate Dynamics, 39(3-4), pp.681-707.

Matsuno, T., 1982. A quasi one-dimensional model of the middle atmosphere circulation interacting with internal gravity waves. Journal of the Meteorological Society of Japan. Ser. II, 60(1), pp.215-226.

Matthieson, L., 2007. Climate change and the Australian Sugarcane Industry: impacts, adaptation and R&D opportunities, SRDC Technical Report, Sugar Research and Development, Brisbane, Australia.

Mayosi, B.M., Lawn, J.E., van Niekerk, A., Bradshaw, D., Karim, S.S.A., Coovadia, H.M. and Lancet South Africa team, 2012. Health in South Africa: changes and challenges since 2009. The Lancet, 380(9858), pp.2029-2043.

Mbatha, N. and Xulu, S., 2018. Time Series Analysis of MODIS-Derived NDVI for the Hluhluwe-IMfolozi Park, South Africa: Impact of Recent Intense Drought. Climate, 6(4), pp.95-118.

McCown, R.L., Hammer, G.L., Hargreaves, J.N.G., Holzworth, D.P. and Freebairn, D.M., 1996. APSIM: a novel software system for model development, model testing and simulation in agricultural systems research. Agricultural Systems, 50(3), pp.255-271.

McGregor, S., Ramesh, N., Spence, P., England, M.H., McPhaden, M.J. and Santoso, A., 2013. Meridional movement of wind anomalies during ENSO events and their role in event termination. Geophysical Research Letters, 40(4), pp.749-754.

Mendelsohn, R., Dinar, A. and Williams, L., 2006. The distributional impact of climate change on rich and poor countries. Environment and Development Economics, 11(2), pp.159-178.

Meyers, S.D., Kelly, B.G. and O'Brien, J.J., 1993. An introduction to wavelet analysis in oceanography and meteorology: With application to the dispersion of Yanai waves. Monthly Weather Review, 121(10), pp.2858-2866.

Mkhabela, M.S., Mkhabela, M.S. and Mashinini, N.N., 2005. Early maize yield forecasting in the four agro-ecological regions of Swaziland using NDVI data derived from NOAA's-AVHRR. Agricultural and Forest Meteorology, 129(1), pp.1-9.

Morlet, J., 1983. Issues in acoustic signal/image processing and recognition. Sampling theory and wave propagation. NATO ASI Series, Springer-Verlag, Heidelberg, pp.233-261.

Mulcahy, M.M., 2018. The implementation of a push-pull programme for the control of Eldana Saccharina (Lepidoptera: Pyralidae) in sugarcane in the coastal regions of KwaZulu-Natal, South Africa. MSc. thesis, Agriculture Department, Rhodes University, 187pp.

Mulenga, H.M., Rouault, M. and Reason, C.J.C., 2003. Dry summers over northeastern South Africa and associated circulation anomalies. Climate Research, 25(1), pp.29-41.

Nasri, M. and Modarres, R., 2009. Dry spell trend analysis of Isfahan Province, Iran. International Journal of Climatology: A Journal of the Royal Meteorological Society, 29(10), pp.1430-1438.

Nairobi, N.S., 1979. The East African monsoons and their effects on agriculture. GeoJournal, 3, pp.193-200.

Nape, K.M., 2011. Using Seasonal Rainfall with APSIM to Improve Maize Production in the Modder River Catchment. Soil, Crop and Climate Sciences Department, University of the Free State.

Ncube, B., Twomlow, S.J., Van Wijk, M.T., Dimes, J.P. and Giller, K.E., 2007. Productivity and residual benefits of grain legumes to sorghum under semi-arid conditions in southwestern Zimbabwe. Plant and Soil, 299(1-2), pp.1-15.

Ncube, B., Dimes, J.P., van Wijk, M.T., Twomlow, S.J. and Giller, K.E., 2009. Productivity and residual benefits of grain legumes to sorghum under semi-arid conditions in south-western Zimbabwe: unravelling the effects of water and nitrogen using a simulation model. Field Crops Research, 110(2), pp.173-184.

NWS (National Weather Service), 2005. Composite Analysis Instructions, viewed 04 January 2016, from http://www.nws.noaa.gov/om/csd/pds/PCU4/Composites.

Osborn, T., Barichivich, J., Harris, I., Van Der Schrier, G. and Jones, P., 2017. Monitoring global drought using the self-calibrating Palmer Drought Severity Index [in" State of the Climate in 2016"]. Bulletin of the American Meteorological Society, 98(8), pp.S32-S33.

Pedersen, T.F., 2004. On wind turbine power performance measurements at inclined airflow. Wind Energy: An International Journal for Progress and Applications in Wind Power Conversion Technology, 7(3), pp.163-176.

Peng, S., Huang, J., Sheehy, J.E., Laza, R.C., Visperas, R.M., Zhong, X., Centeno, G.S., Khush, G.S. and Cassman, K.G., 2004. Rice yields decline with higher night temperature from global warming. Proceedings of the National Academy of Sciences of the United States of America, 101(27), pp.9971-9975.

Pidwirny, M., 2006. Actual and Potential Evapotranspiration. Fundamentals of Physical Geography, 2nd Edition. Viewed on 13 March 2015. http://www.physicalgeography.net/ fundamentals/8j.html.

Pielke, R.A., 2001. Influence of the spatial distribution of vegetation and soils on the prediction of cumulus convective rainfall. Reviews of Geophysics, 39(2), 151–177.

Pinheiro, É.F.M., Lima, E., Ceddia, M.B., Urquiaga, S., Alves, B.J. and Boddey, R.M., 2010. Impact of pre-harvest burning versus trash conservation on soil carbon and nitrogen stocks on a sugarcane plantation in the Brazilian Atlantic forest region. Plant and Soil, 333(1-2), pp.71-80.

Pohlert, T., 2016. Non-parametric trend tests and change-point detection. CC BY-ND, 4.

Potgieter, A.B., Everingham, Y.L. and Hammer, G.L., 2003. On measuring quality of a probabilistic commodity forecast for a system that incorporates seasonal climate forecasts. International Journal of Climatology: A Journal of the Royal Meteorological Society, 23(10), pp.1195-1210.

Promburom, P., Jintrawet, A., and Ekasingh, M., 2001. Estimating sugarcane yields with Oy-Thai interface. In Proceedings of the International Society of Sugar Cane Technologists, 81-86. Brisbane, Australia.

Qian, C., Zhou, W., Yang, X.Q. and Chan, J.C., 2018. Statistical prediction of non-Gaussian climate extremes in urban areas based on the first-order difference method. International Journal of Climatology, 38(6), pp.2889-2898.

Ratnam, J.V., Behera, S.K., Masumoto, Y. and Yamagata, T., 2014. Remote effects of El Niño and Modoki events on the austral summer precipitation of southern Africa. Journal of Climate, 27(10), pp.3802-3815.

Rayner, N.A., Parker, D.E., Horton, E.B., Folland, C.K., Alexander, L.V., Rowell, D.P., Kent, E.C. and Kaplan, A., 2003. Global analyses of sea surface temperature, sea ice, and night marine air temperature since the late nineteenth century. Journal of Geophysical Research: Atmospheres, 108(D14), pp.4407-4443.

Richard, Y. and Poccard, I., 1998. A statistical study of NDVI sensitivity to seasonal and interannual rainfall variations in Southern Africa. International Journal of Remote Sensing, 19(15), pp.2907-2920.

Riebeek, H., 2011. Global Warming. http://earthobservatory.nasa.gov/Features/ (accessed on 09 October 2017).

Riffkin, P. and Evans, P.M., 2004, September. Use of resources in 4 cultivars of wheat in the high rainfall zone of south-eastern Australia–protein and water soluble carbohydrates. In New Directions for a Diverse Planet. Proceedings of 4th International Crop Science Congress. Brisbane, Australia.

Ropelewski, C.F. and Halpert, M.S., 1989. Precipitation patterns associated with the high index phase of the Southern Oscillation. Journal of climate, 2(3), pp.268-284.

Ropelewski, C.F. and Halpert, M.S., 1987. Global and regional scale precipitation patterns associated with the El Niño/Southern Oscillation. Monthly weather review, 115(8), pp.1606-1626.

Ropelewski, C.F. and Jones, P.D., 1987. An extension of the Tahiti–Darwin southern oscillation index. Monthly Weather Review, 115(9), pp.2161-2165.

Rosegrant, M.W., Cai, X., Cline, S.A., 2002. World water and food to 2025: dealing with scarcity. International Food Policy Research Institute, Washington, DC.

Rouault, M. and Richard, Y., 2005. Intensity and spatial extent of droughts in southern Africa. Geophysical Research Letters, 32(15702), pp.1-4.

Russell, J.S., 1990. Effect of interactions between available water and solar radiation on sugarcane productivity and the impact of climatic change. Proceedings of the Australian Society of Sugar Cane Technologists, 12, pp.29–38.

Russo, S., Marchese, A.F., Sillmann, J. and Immé, G., 2016. When will unusual heat waves become normal in a warming Africa? Environmental Research Letters, 11(5), p.054016.

SASA (South African Sugar Association), 2013. South African Sugar Industry Directory 2013/14. Durban: South African Sugar Association.

SASA (South African Sugar Association), 2015. South African Sugar Industry Directory 2014/15. Durban: South African Sugar Association.

SAWS (South African Weather Service), 2016. How does ENSO affect South Africa? Available at http://www.weathersa.co.za/learning/climate (accessed on 20 April 2016).

Schlenker, W. and Roberts, M.J., 2009. Nonlinear temperature effects indicate severe damages to US crop yields under climate change. Proceedings of the National Academy of sciences, 106(37), pp.15594-15598.

Schneider, U., Becker, A., Finger, P., Meyer-Christoffer, A., Rudolf, B. and Ziese, M., 2018. GPCC Full Data Monthly Product Version 8 at 0.5°: Monthly Land-Surface Precipitation from Rain-Gauges built on GTS-based and Historical Data.

Schulze, R.E. and Kunz, R.P., 2010. Climate Change and Sugarcane Production Using the Smith Model. Climate Change and the South African Sugarcane Sector: A 2010 Perspective, pp.73-81.

Selvaraju, R. and Baas, S., 2007. Climate variability and change: Adaptation to drought in Bangladesh. A resource book and training guide. Asian Disaster Preparedness Centrer, Food and Agriculture Organisation of the United Nations, Rome.

Singels, A. and Bezuidenhout, C.N., 1999. The relationship between ENSO and rainfall and yield in the South African sugar industry. South African Journal of Plant and Soil, 16(2), pp.96-101.

Singels, A., 2007. A new approach to implementing computer-based decision support for sugarcane farmers and extension staff. The case of My Canesim. In Proceeding of International Society of Sugar Cane Technologists, 26, pp.211-219.

Singels, A., Ferrer, S., Leslie, G.W., McFarlane, S.A., Sithole, P. and Laan, M., 2011. Review of South African sugarcane production in the 2010/2011 season from an agricultural perspective. In Proceedings of the Annual Congress-South African Sugar Technologists' Association, 84, pp.66-83.

Singels, A., Jones, M., Marin, F., Ruane, A. and Thorburn, P., 2014. Predicting climate change impacts on sugarcane production at sites in Australia, Brazil and South Africa using the Canegro model. Sugar Technology, 16(4), pp.347-355.

Sneyers, R., 1990. On the Statistical Analysis of Series of Observations, WMO Technical Note 143.WMO No. 415, TP-103, Geneva, World Meteorological Organization, 192pp.

SSA (Statistics South Africa), 2013. Mid-year 2013 population estimates for provinces available at http://beta2.statssa.gov.za/ (accessed on 20 February 2014).

Stringer, L., Dyer, J., Reed, M. S., Dougill, A. J., Twyman, C., and Mkwambisi, D., 2009. Adaptations to climate change, drought and desertification: insights to enhance policy in southern Africa. Environmental Science and Policy, 12(7), pp.748-65.

Szczypta, C., Calvet, J.C., Albergel, C., Balsamo, G., Boussetta, S., Carrer, D., Lafont, S. and Meurey, C., 2011. Verification of the new ECMWF ERA-Interim reanalysis over France. Hydrology and Earth System Sciences, 15(2), p.647-666.

Tadross, M., Davis, C., Engelbrecht, F., Joubert, A., Archer van Garderen, E., 2011. Regional scenarios of future climate change over southern Africa. In: Davis, C.L. (Ed.), Climate Risk and Vulnerability: A Handbook for Southern Africa. Council for Scientific and Industrial Research, Pretoria, South Africa, 92pp.

Tadross, M.A., Hewitson, B.C. and Usman, M.T., 2005. The inter-annual variability of the onset of the maize growing season over South Africa and Zimbabwe. Journal of Climate, 18(16), pp.3356-3372.

Tallaksen, L.M. and Van Lanen, H.A. eds., 2004. Hydrological Drought: Processes and Estimation Methods for Streamflow and Groundwater, Developments in Water Science, 48, 579pp. Elsevier, Amsterdam.

Taylor, K.E., 2001. Summarizing multiple aspects of model performance in a single diagram. Journal of Geophysical Research: Atmospheres, 106(D7), pp.7183-7192.

Torrence, C. and Compo, G.P., 1998. A practical guide to wavelet analysis. Bulletin of the American Meteorological Society, 79(1), pp.61-78.

Tucker, C.J., Pinzon, J.E., Brown, M.E., Slayback, D.A., Pak, E.W., Mahoney, R., Vermote, E.F. and El Saleous, N., 2005. An extended AVHRR 8-km NDVI dataset compatible with MODIS and SPOT vegetation NDVI data. International Journal of Remote Sensing, 26(20), pp.4485-4498.

Tyson, P.D. and Preston-Whyte, R.A., 2000. The weather and climate of Southern Africa. Oxford University Press, Cape Town, South Africa, 396pp.

Ummenhofer, C.C., Xu, H., Twine, T.E., Girvetz, E.H., McCarthy, H.R., Chhetri, N. and Nicholas, K.A., 2015. How climate change affects extremes in maize and wheat yield in two cropping regions. Journal of Climate, 28(12), pp.4653-4687.

van den Berg, M. and Singels, A., 2013. Modelling and monitoring for strategic yield gap diagnosis in the South African sugar belt. Field Crops Research, 143, pp.143-150.

van der Schrier, G., Barichivich, J., Briffa, K.R. and Jones, P.D., 2013. A scPDSI-based global data set of dry and wet spells for 1901–2009. Journal of Geophysical Research: Atmospheres, 118(10), pp.4025-4048.

Viswanathan, R. and Rao, G.P., 2011. Disease scenario and management of major sugarcane diseases in India. Sugar Technology, 13(4), pp.336-353.

Viswanathan, R., Balamuralikrishnan, M., and Karuppaiah, R., 2007. Sugarcane mosaic in India: a cause of combined infection of sugarcane mosaic virus and sugarcane streak mosaic virus, Sugar Cane International, 25(2), pp.6–14.

Walker, F., 1865. List of the specimens of *lepidopterous* insects in the collection of the British Museum. British Museum (Natural History). Part 32. Supplement, Part 2, pp.632-633.

Wang, H., Murtugudde, R. and Kumar, A., 2016. Evolution of Indian Ocean dipole and its forcing mechanisms in the absence of ENSO. Climate dynamics, 47(7-8), pp.2481-2500.

Wegener, M.K., 1990. Analysis of risk in irrigated sugarcane at Mackay. Proceedings of the Australian Society of Sugar Cane Technologists, 12, pp.45–51.

Weldon, D. and Reason, C.J.C., 2014. Variability of rainfall characteristics over the South Coast region of *South* Africa. Theoretical and Applied Climatology, 115 (1-2), pp.177-185.

Wessels, K.J., Prince, S.D., Malherbe, J., Small, J., Frost, P.E. and VanZyl, D., 2007. Can human-induced land degradation be distinguished from the effects of rainfall variability? A case study in South Africa. Journal of Arid Environments, 68(2), pp.271-297.

White, B., 2000. The importance of climate variability and seasonal forecasting to the Australian economy. In Applications of Seasonal Climate Forecasting in Agricultural and Natural Ecosystems (pp.1-22). Springer, Dordrecht.

Wijngaard, J.B., Tank, A.K. and Können, G.P., 2003. Homogeneity of 20th century European daily temperature and precipitation series. International Journal of Climatology, 23(6), pp.679-692.

WHO (World Health Organization), ed., 2013. Global tuberculosis report 2013, viewed on 12 May 2015 in the website: http://www.who.int/iris/handle/10665.

Xu, J., Powell Jr, A.M. and Zhao, L., 2013. Intercomparison of temperature trends in IPCC CMIP5 simulations with observations, reanalyses and CMIP3 models. Geoscientific Model Development, 6(5), pp.1705-1714.

Yamori, W., Hikosaka, K. and Way, D.A., 2014. Temperature response of photosynthesis in C3, C4, and CAM plants: temperature acclimation and temperature adaptation. Photosynthesis Research, 119(1-2), pp.101-117.

Yaseen, Z.M., Deo, R.C., Hilal, A., Abd, A.M., Bueno, L.C., Salcedo-Sanz, S. and Nehdi, M.L., 2018. Predicting compressive strength of lightweight foamed concrete using extreme learning machine model. Advances in Engineering Software, 115, pp.112-125.

Zhao, D. and Li, Y.R., 2015. Climate change and sugarcane production: potential impact and mitigation strategies. International Journal of Agronomy, 2015 (547386), 10pp.

APPENDICES

Appendix A

This appendix contains results which were found to be important for this study but, due to their length, cannot be afforded space in the results and discussion chapters. The study extensively used 4×4 gridded climate data and global data from FAO, thus it is useful to examine trends in different sugar mill levels in the sugar belt of southeastern Africa. Rainfall data from 14 sugar mills were correlated with sugarcane yield for each mill. There is a strong relationship between these two variables in rain-fed than irrigated regions. This is consistent with findings by Singels, *et al*. (2011).

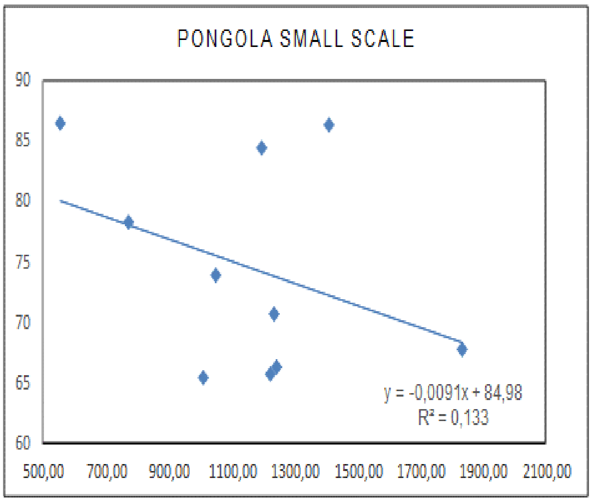

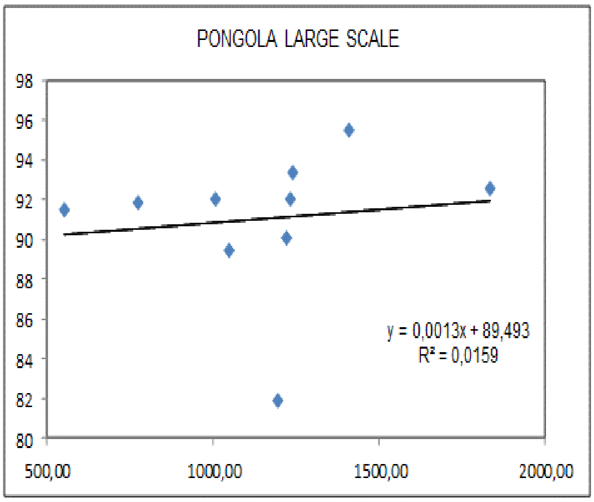

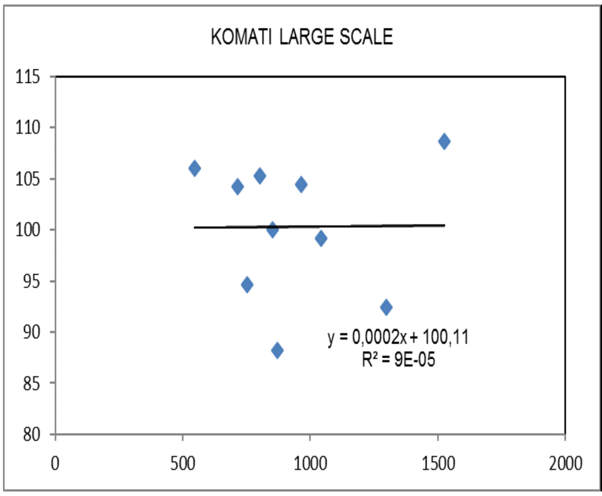

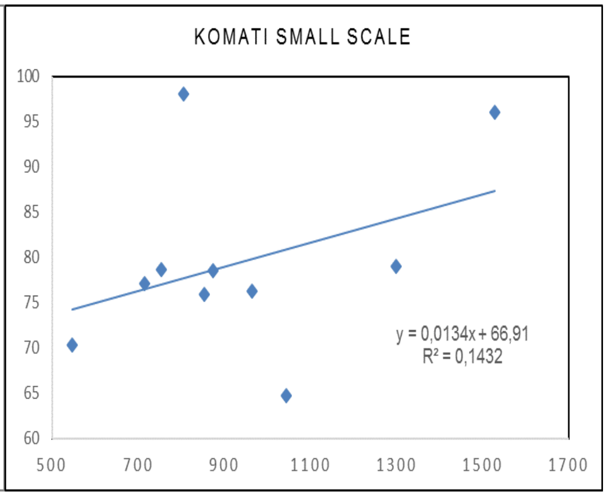

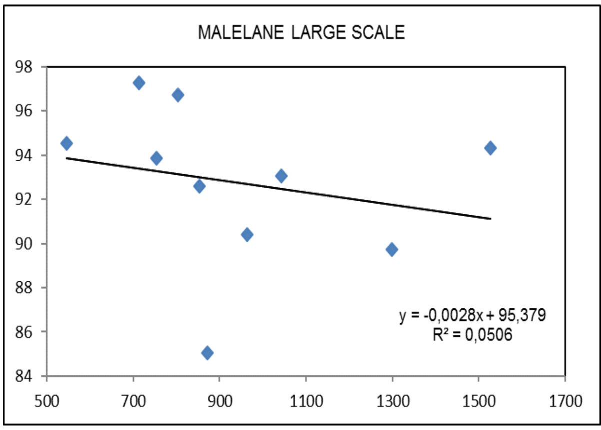
MALELANE LARGE SCALE
y = -0,0028x + 95,379
R² = 0,0506

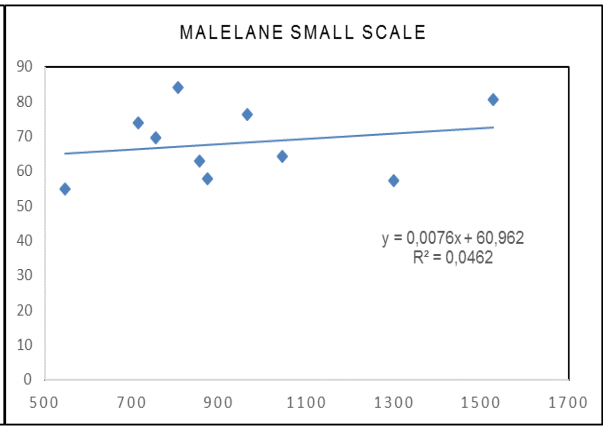
MALELANE SMALL SCALE
y = 0,0076x + 60,962
R² = 0,0462

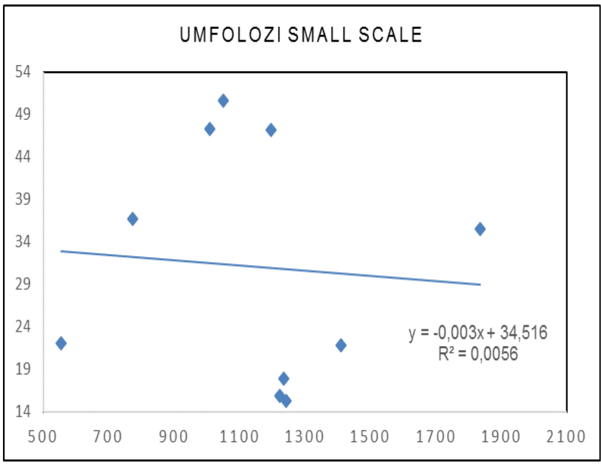
UMFOLOZI SMALL SCALE
y = -0,003x + 34,516
R² = 0,0056

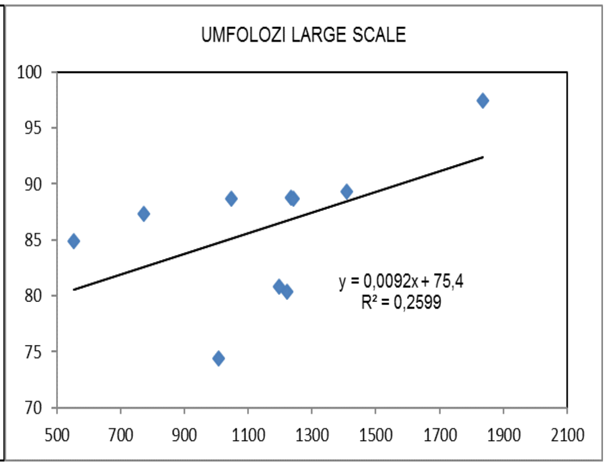
UMFOLOZI LARGE SCALE
y = 0,0092x + 75,4
R² = 0,2599

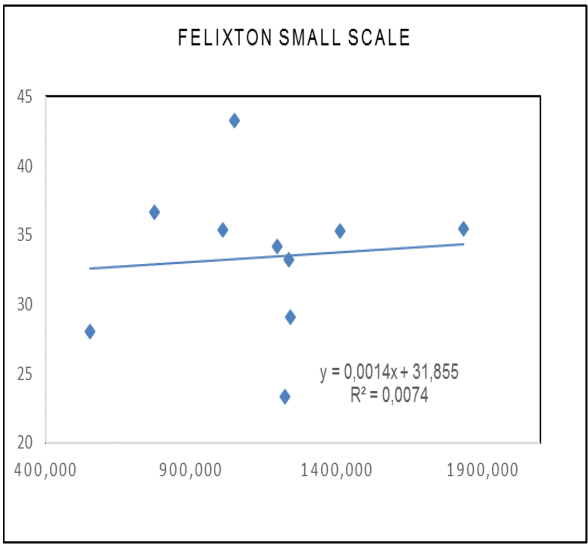
FELIXTON SMALL SCALE
y = 0,0014x + 31,855
R² = 0,0074

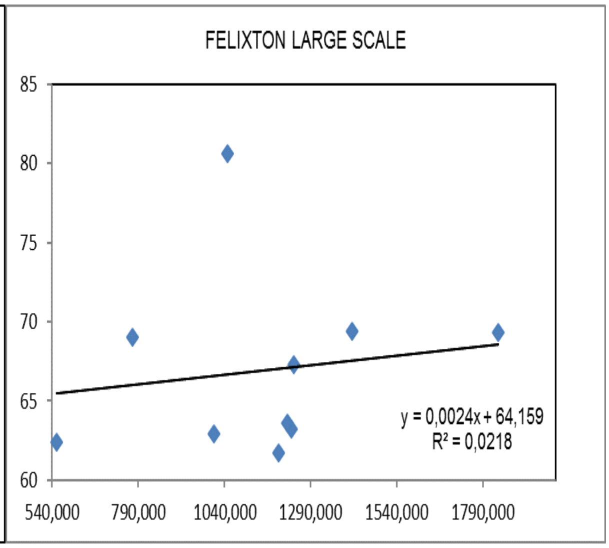
FELIXTON LARGE SCALE
y = 0,0024x + 64,159
R² = 0,0218

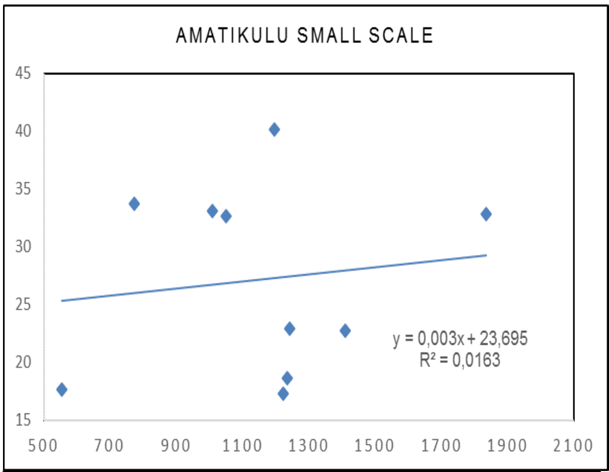
AMATIKULU SMALL SCALE
y = 0,003x + 23,695
R² = 0,0163

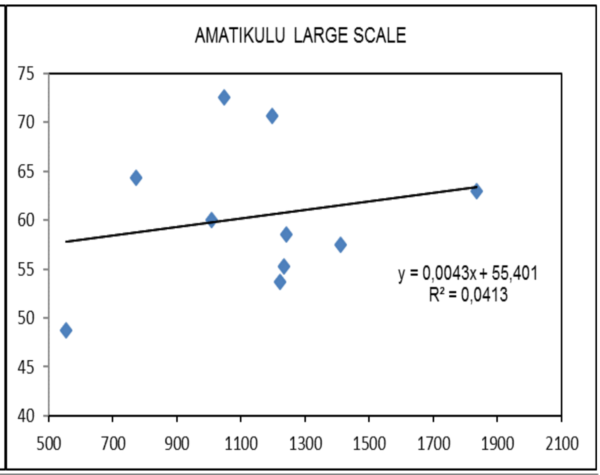
AMATIKULU LARGE SCALE
y = 0,0043x + 55,401
R² = 0,0413

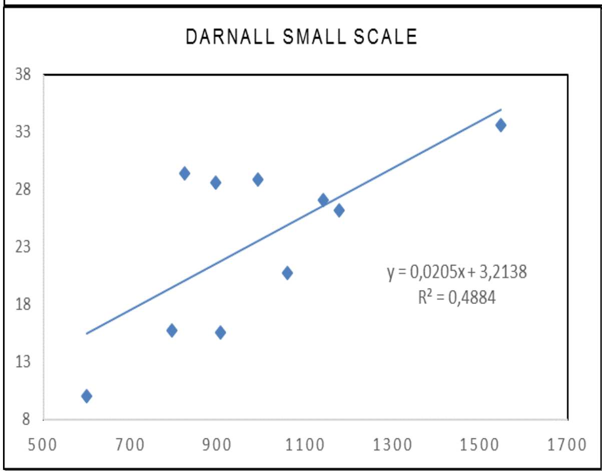
DARNALL SMALL SCALE
y = 0,0205x + 3,2138
R² = 0,4884

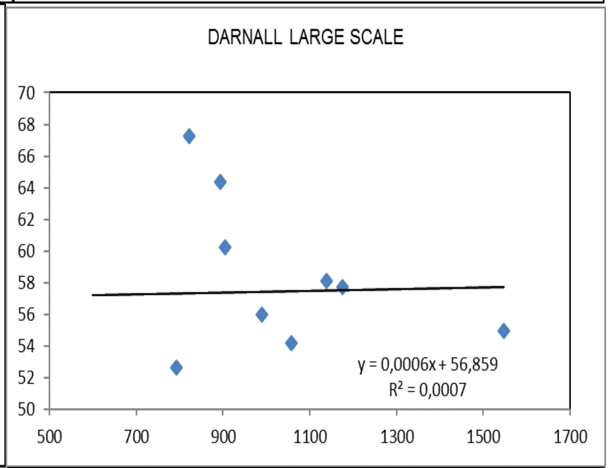
DARNALL LARGE SCALE
y = 0,0006x + 56,859
R² = 0,0007

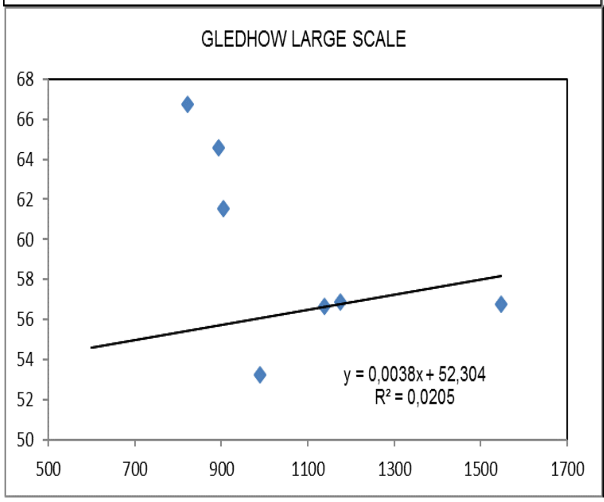
GLEDHOW LARGE SCALE
y = 0,0038x + 52,304
R² = 0,0205

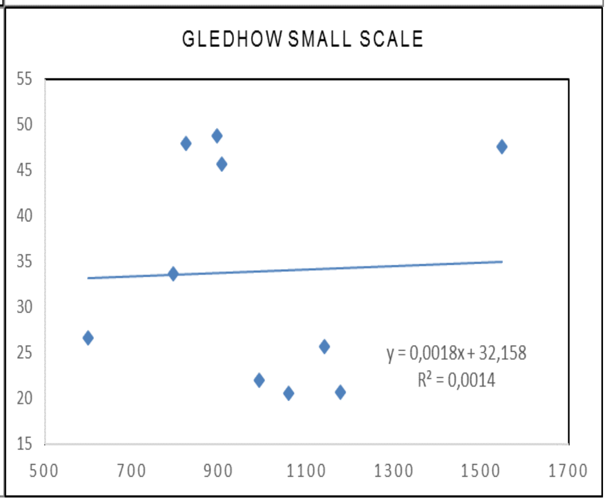
GLEDHOW SMALL SCALE
y = 0,0018x + 32,158
R² = 0,0014

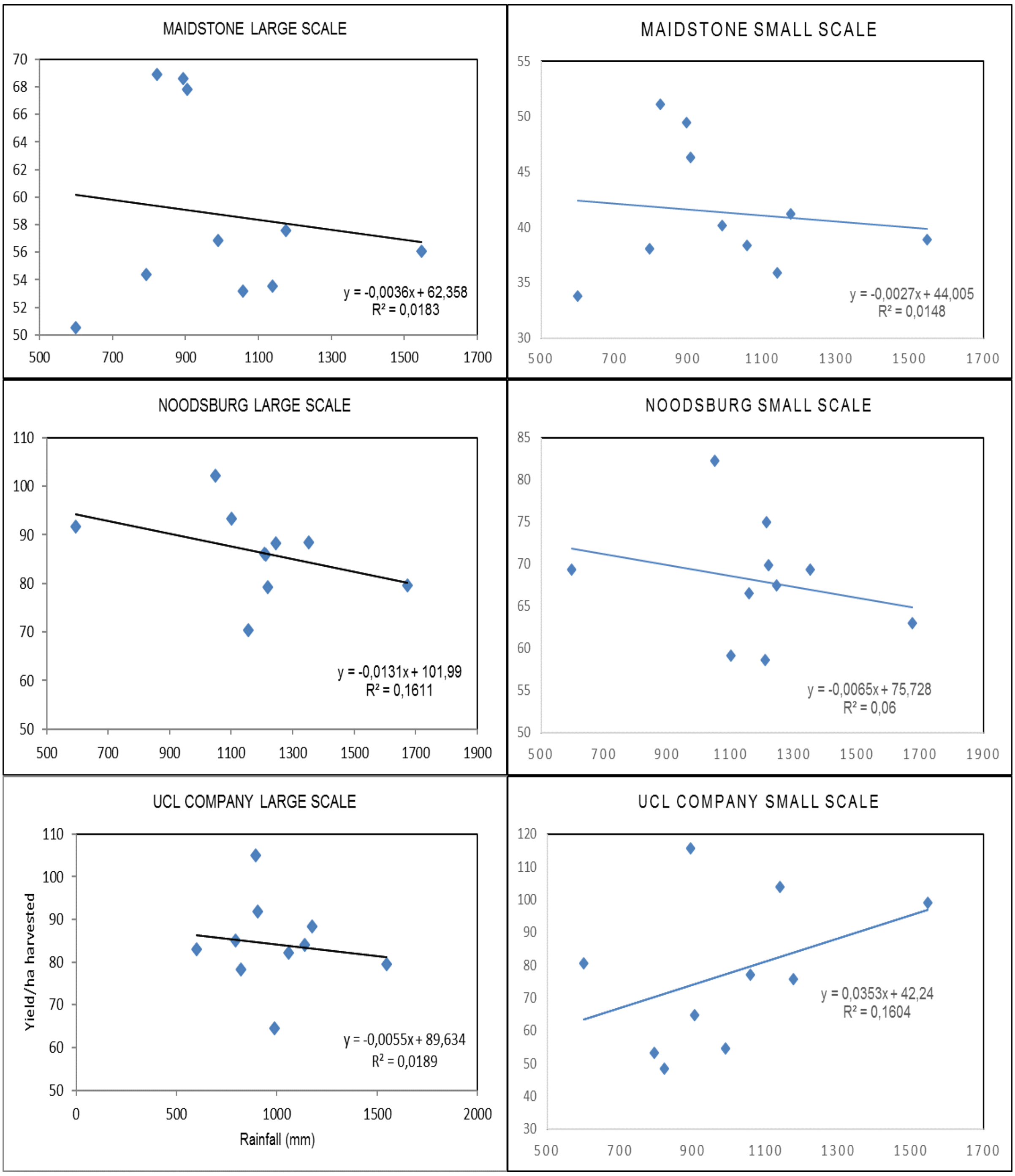
MAIDSTONE LARGE SCALE
y = -0,0036x + 62,358
R² = 0,0183
MAIDSTONE SMALL SCALE
y = -0,0027x + 44,005
R² = 0,0148
NOODSBURG LARGE SCALE
y = -0,0131x + 101,99
R² = 0,1611
NOODSBURG SMALL SCALE
y = -0,0065x + 75,728
R² = 0,06
UCL COMPANY LARGE SCALE
Yield/ha harvested
Rainfall (mm)
y = -0,0055x + 89,634
R² = 0,0189
UCL COMPANY SMALL SCALE
y = 0,0353x + 42,24
R² = 0,1604

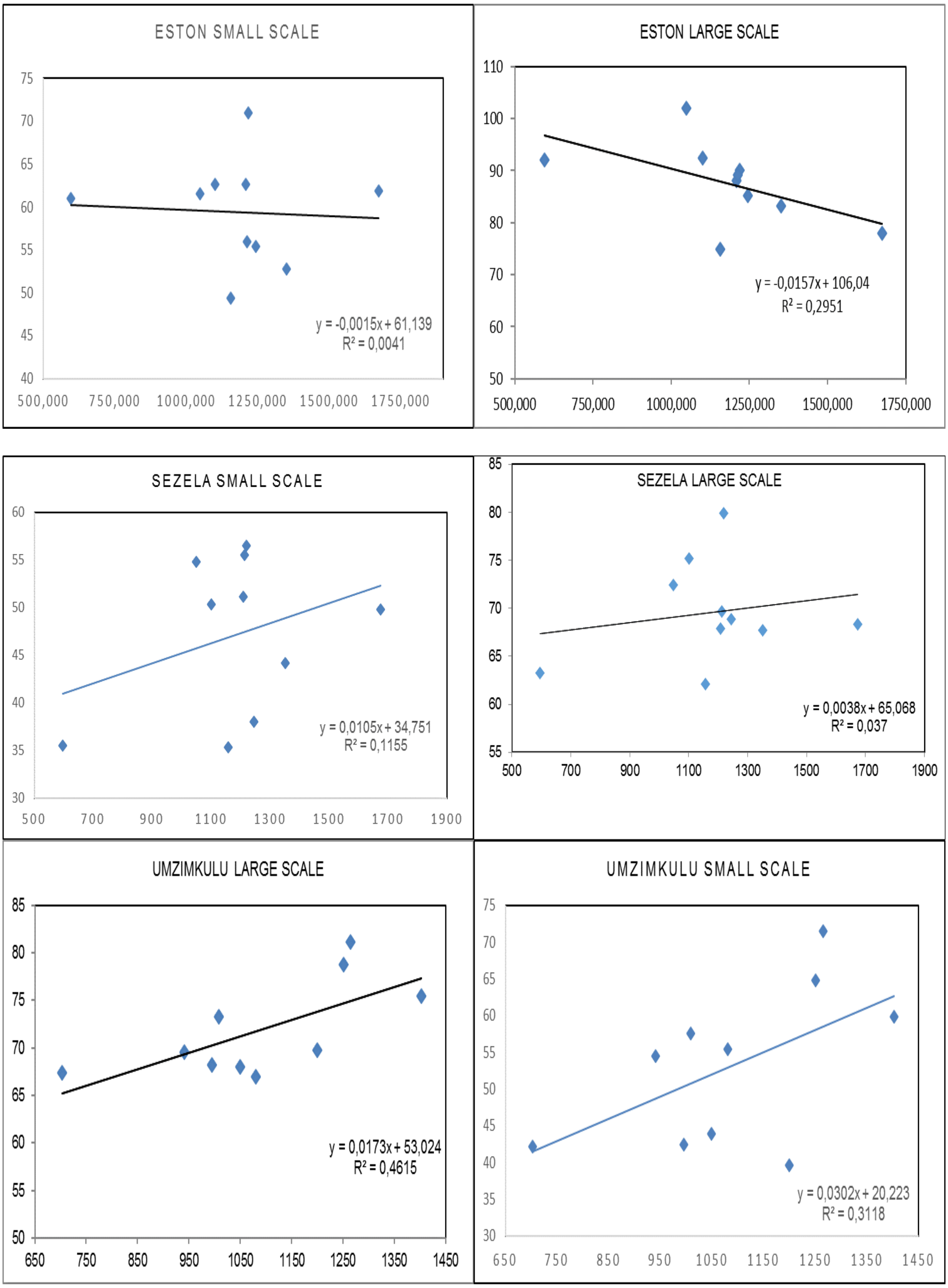

Figure A.1 Scatterplots showing the correlation coefficient (R^2) between rainfall and sugarcane yield for individual sugar mills in South Africa due to data accessibility.

Appendix B

Appendix B presents the comparison between local data and data extracted from the Food and Agriculture Organisation (FAO) of the United Nations (UN). The study found that in most instances the model used in the FAO miscalculates the sugarcane yield values for South Africa but the differences in some seasons are sound, although in some cases (2013 and 2014) the difference exceeds 10 ton/ha, which needs to be modified by referring to local data from the South African Sugar Association. Normally, the last two values in the yield time series are the estimates, and the time series require continuous updating for correct analysis. FAO sugarcane yield data have been used for various sugarcane producing countries (Lobell & Field, 2007; Zhao & Li, 2015).

Table B.1 Comparison between regional and national sugarcane yield data for South Africa to confirm validity of FAO data. The difference of 0 implies that SASA and FAO recorded same sugarcane yield for that season, negative difference means that FAO underestimated the actual yield, and positive difference indicates that FAO underestimated the yield. Bold-black indicate differences which are ≤ -1 *and* $\geq +1$.

SEASONS	SASA YIELD (ton/ha)	FAO YIELD (ton/ha)	DIFFERENCE (FAO-SASA)
1988	74.7	71.7	**-3.0**
1989	73.3	71.9	**-1.4**
1990	68.9	68.3	-0.6
1991	73.5	72.7	-0.8
1992	48.4	48.3	-0.1
1993	40.6	41.7	**1.0**
1994	55.4	55.2	-0.2
1995	61.0	61.2	0.2
1996	69.2	69.9	0.7
1997	73.5	74.7	**1.2**
1998	72.5	72.5	0.0
1999	67.7	67.7	0.0
2000	74.0	74.0	0.0
2001	65.0	65.0	0.0
2002	71.6	71.6	0.0
2003	62.7	62.6	0.0
2004	60.4	60.4	0.0
2005	66.0	66.0	0.0
2006	66.4	66.4	0.0
2007	64.2	64.2	0.0
2008	67.0	67.0	0.0
2009	62.2	67.1	**4.9**
2010	54.9	59.1	**4.2**

Appendix C

The results of trend detection and analysis are presented in this section due to its length. Further discussion is found in the time series analysis of climatic variables and yields (*see* Table 4.1 and Figure 4.10). The potential trend turning points (PTTPs) are also further elaborated on in the same chapter. Here the trends detected are shown for all agro-climatic zones of SA sugar industry.

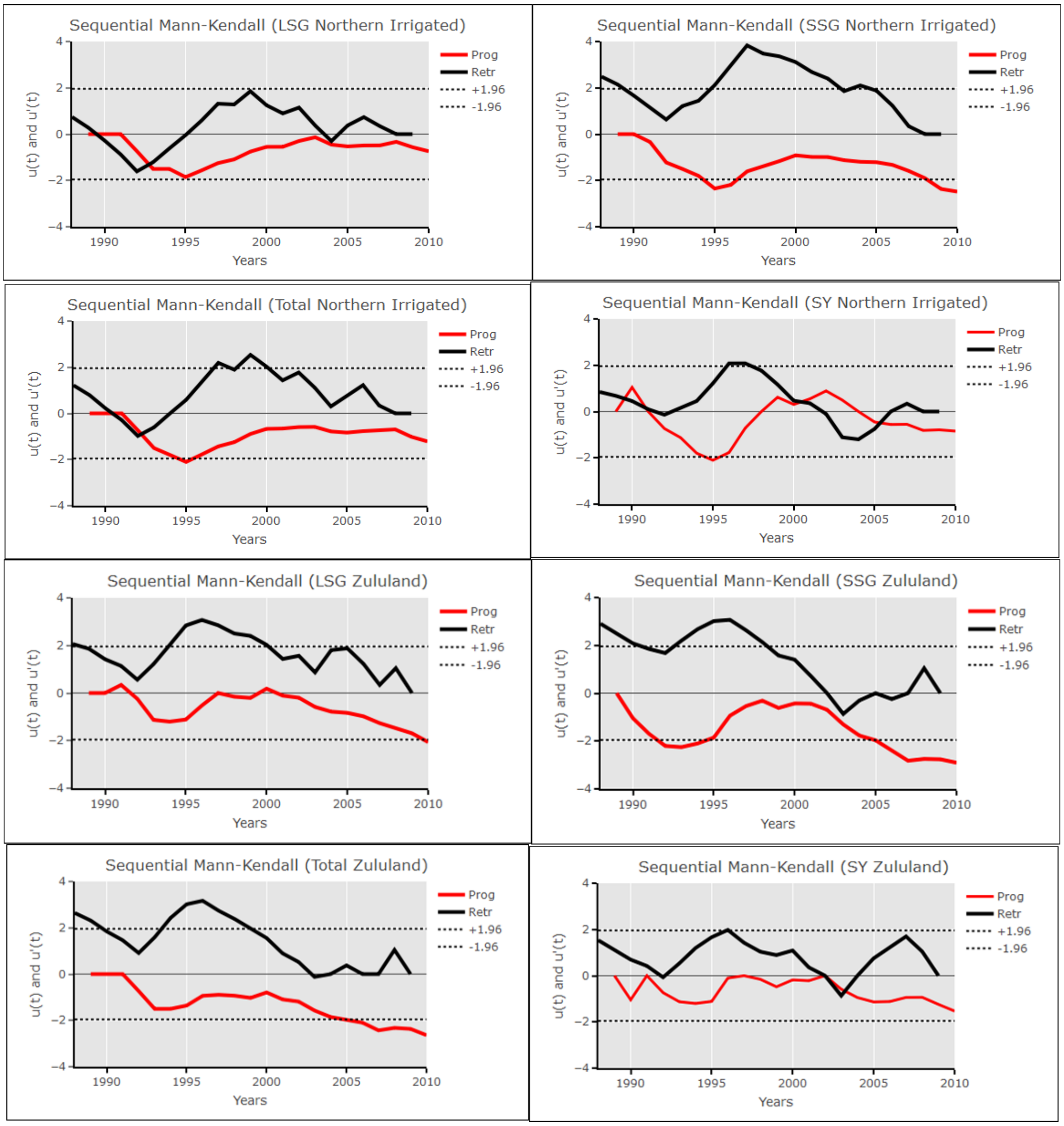

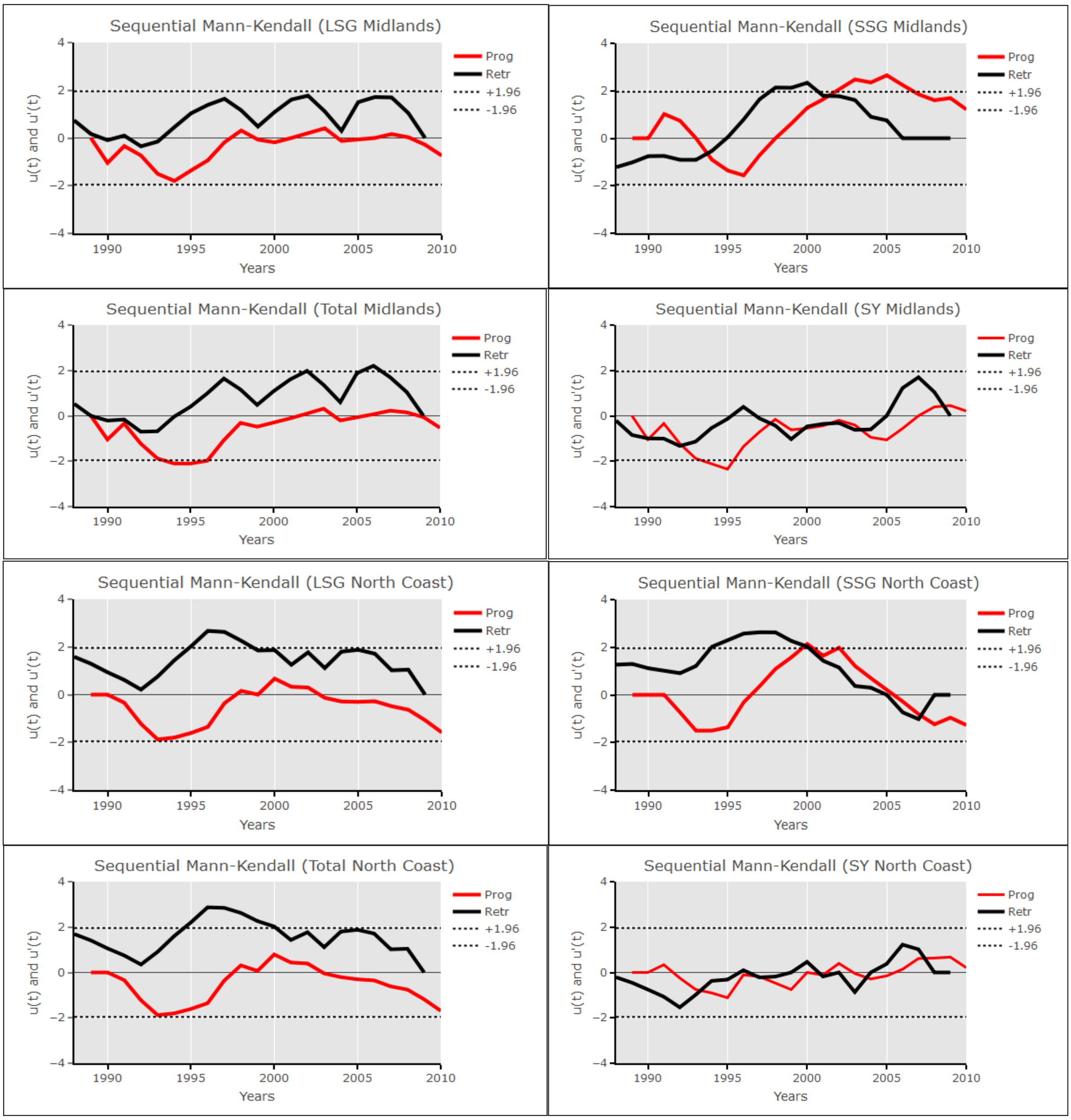
Sequential Mann-Kendall (LSG Midlands)
Sequential Mann-Kendall (SSG Midlands)
Sequential Mann-Kendall (Total Midlands)
Sequential Mann-Kendall (SY Midlands)
Sequential Mann-Kendall (LSG North Coast)
Sequential Mann-Kendall (SSG North Coast)
Sequential Mann-Kendall (Total North Coast)
Sequential Mann-Kendall (SY North Coast)
Prog
Retr
+1.96
-1.96
u(t) and u'(t)
Years
1990
1995
2000
2005
2010

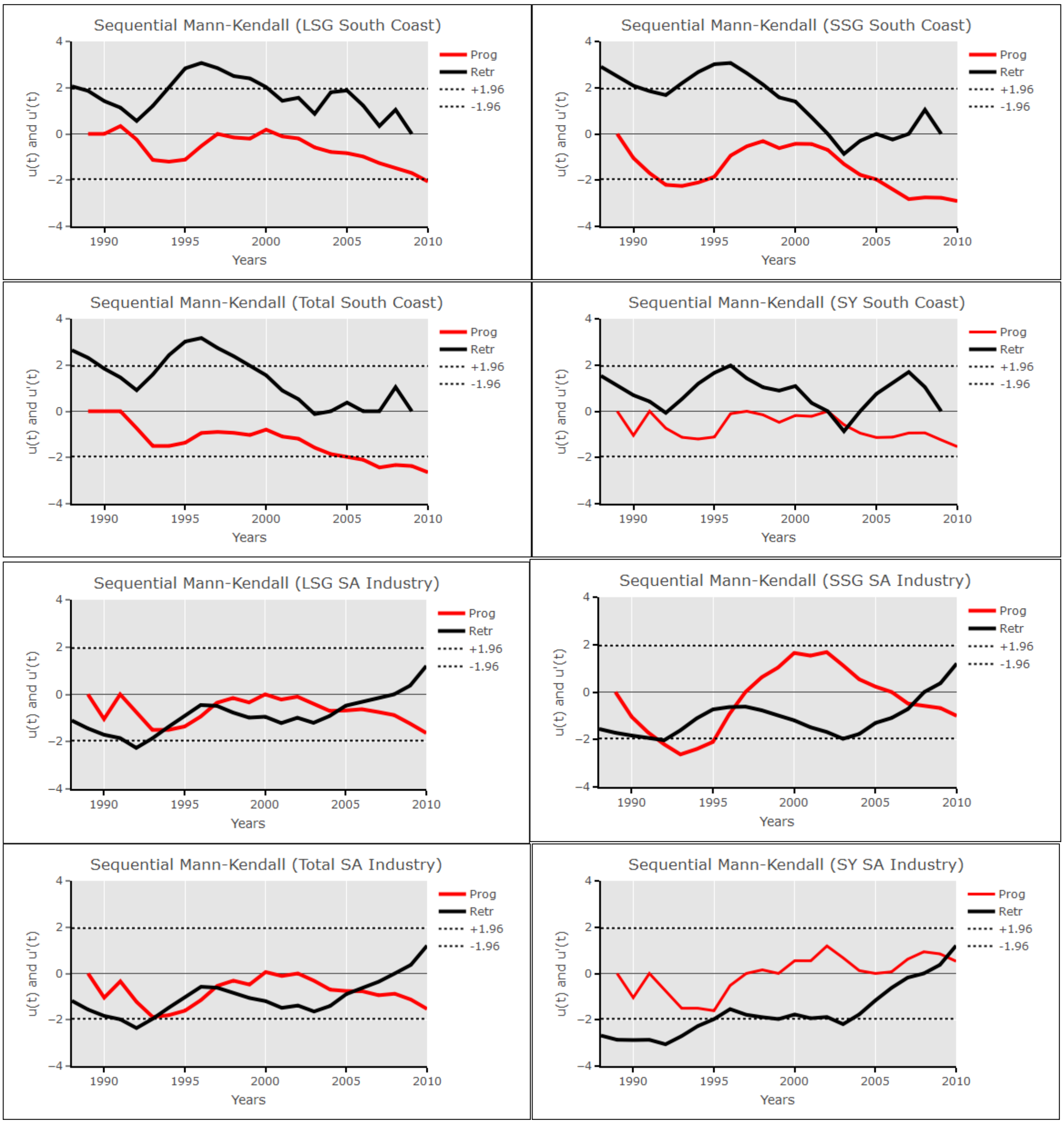

Figure C.1 is similar to Figure 4.10 but here trends are detected for all agro-climatic regions of South Africa (Northern Irrigated, Zululand, Midlands, North Coast and South Coast) on different production scales for the period 1988-2010.

Appendix D

The cross-correlation was performed following the Pearson method which uses the Pearson correlation coefficient (PCC) to explore the statistical linear links between actual sugarcane yields from different spheres of production (LSG, SSG and TOT), potential yields from model simulations, climate variables, and large-scale climate drivers over the study area for the period 1988-2010.

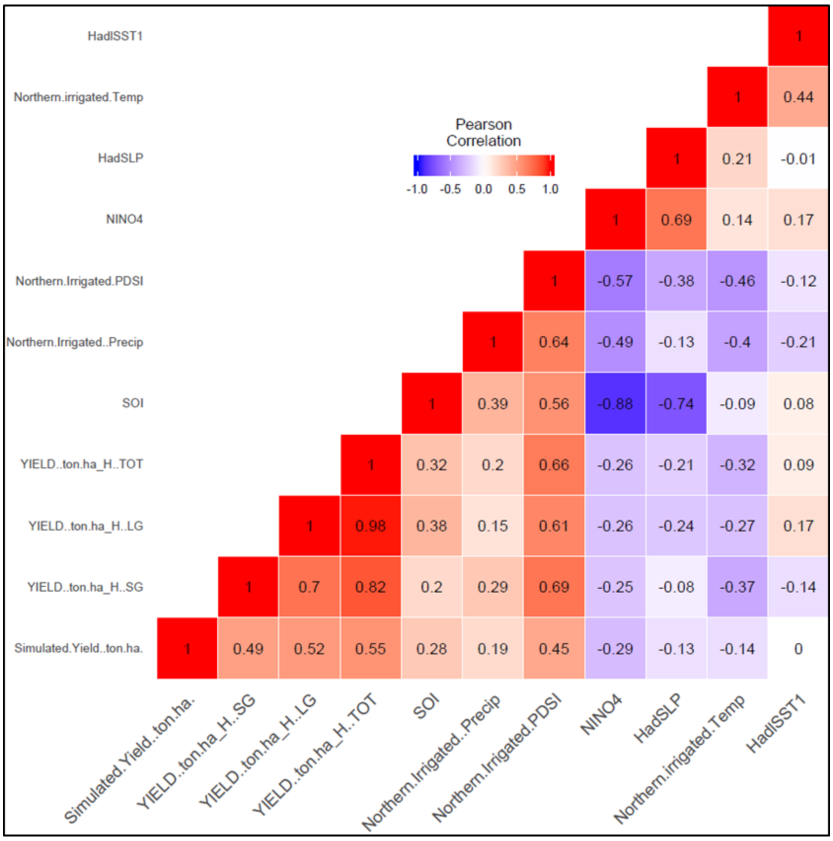

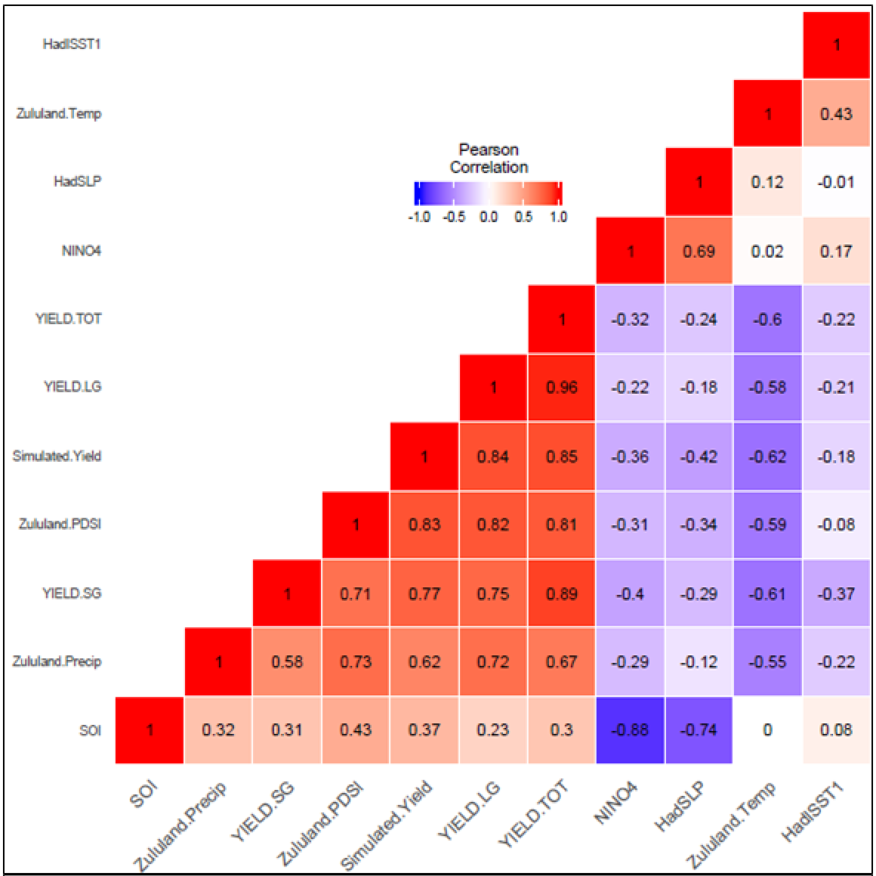

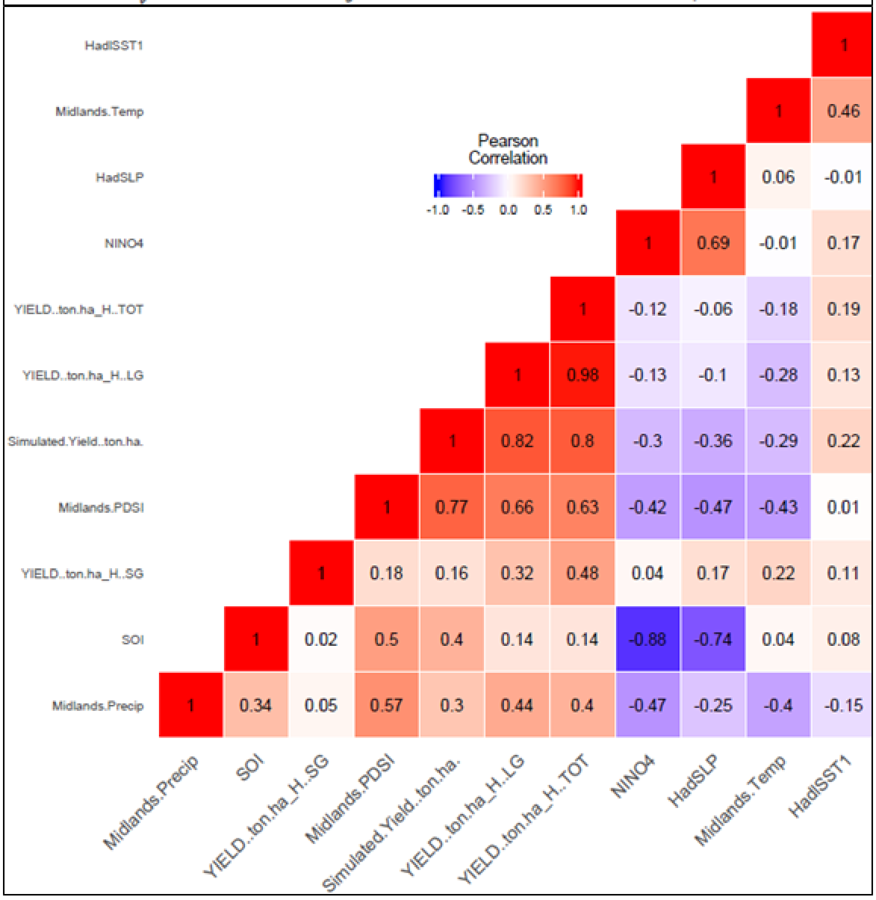

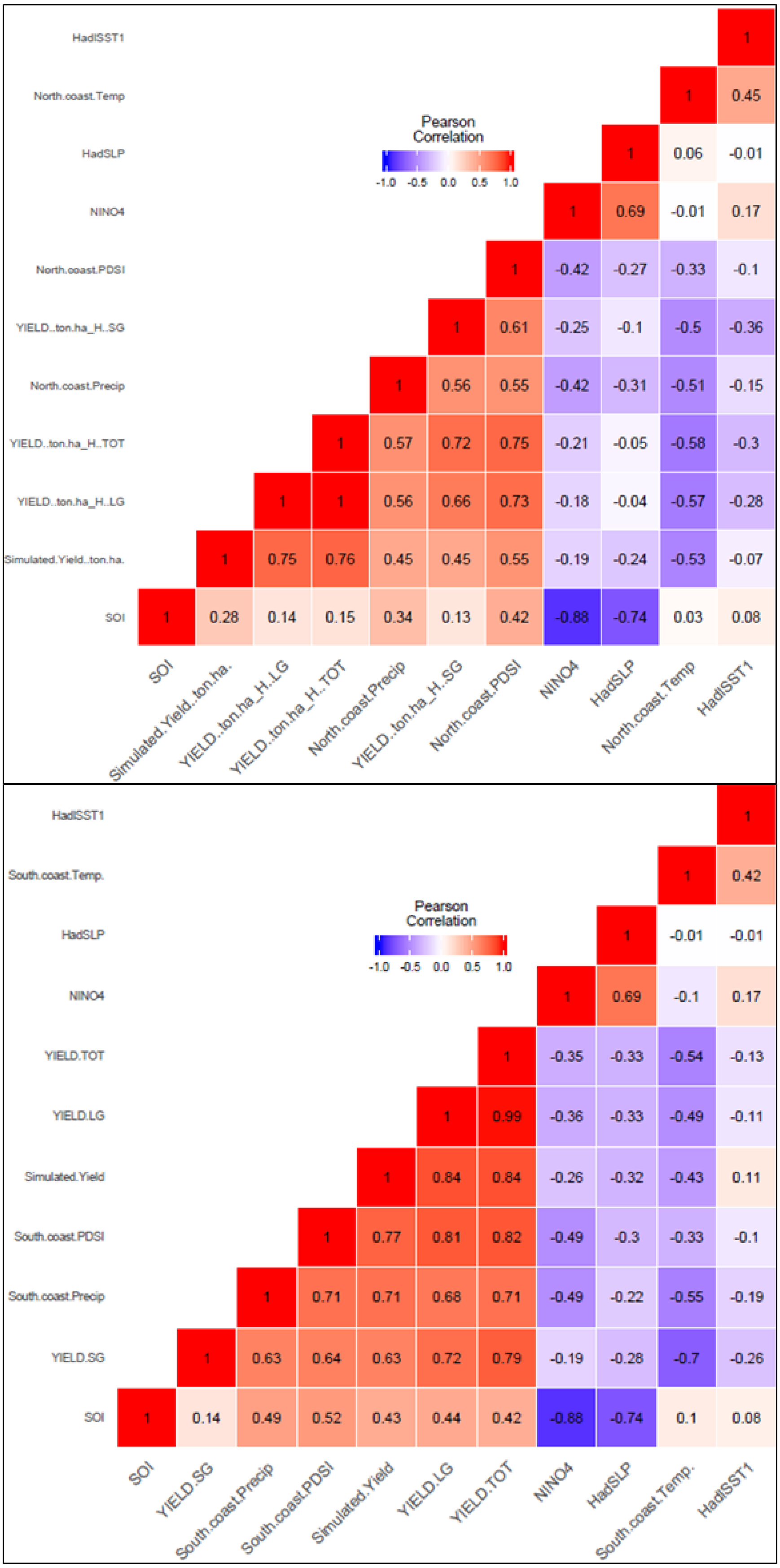
Pearson Correlation
-1.0 -0.5 0.0 0.5 1.0
HadISST1 1
North.coast.Temp 1 0.45
HadSLP 1 0.06 -0.01
NINO4 1 0.69 -0.01 0.17
North.coast.PDSI 1 -0.42 -0.27 -0.33 -0.1
YIELD..ton.ha_H..SG 1 0.61 -0.25 -0.1 -0.5 -0.36
North.coast.Precip 1 0.56 0.55 -0.42 -0.31 -0.51 -0.15
YIELD..ton.ha_H..TOT 1 0.57 0.72 0.75 -0.21 -0.05 -0.58 -0.3
YIELD..ton.ha_H..LG 1 1 0.56 0.66 0.73 -0.18 -0.04 -0.57 -0.28
Simulated.Yield..ton.ha. 1 0.75 0.76 0.45 0.45 0.55 -0.19 -0.24 -0.53 -0.07
SOI 1 0.28 0.14 0.15 0.34 0.13 0.42 -0.88 -0.74 0.03 0.08
SOI
Simulated.Yield..ton.ha.
YIELD..ton.ha_H..LG
YIELD..ton.ha_H..TOT
North.coast.Precip
YIELD..ton.ha_H..SG
North.coast.PDSI
NINO4
HadSLP
North.coast.Temp
HadISST1
Pearson Correlation
-1.0 -0.5 0.0 0.5 1.0
HadISST1 1
South.coast.Temp. 1 0.42
HadSLP 1 -0.01 -0.01
NINO4 1 0.69 -0.1 0.17
YIELD.TOT 1 -0.35 -0.33 -0.54 -0.13
YIELD.LG 1 0.99 -0.36 -0.33 -0.49 -0.11
Simulated.Yield 1 0.84 0.84 -0.26 -0.32 -0.43 0.11
South.coast.PDSI 1 0.77 0.81 0.82 -0.49 -0.3 -0.33 -0.1
South.coast.Precip 1 0.71 0.71 0.68 0.71 -0.49 -0.22 -0.55 -0.19
YIELD.SG 1 0.63 0.64 0.63 0.72 0.79 -0.19 -0.28 -0.7 -0.26
SOI 1 0.14 0.49 0.52 0.43 0.44 0.42 -0.88 -0.74 0.1 0.08
SOI
YIELD.SG
South.coast.Precip
South.coast.PDSI
Simulated.Yield
YIELD.LG
YIELD.TOT
NINO4
HadSLP
South.coast.Temp.
HadISST1

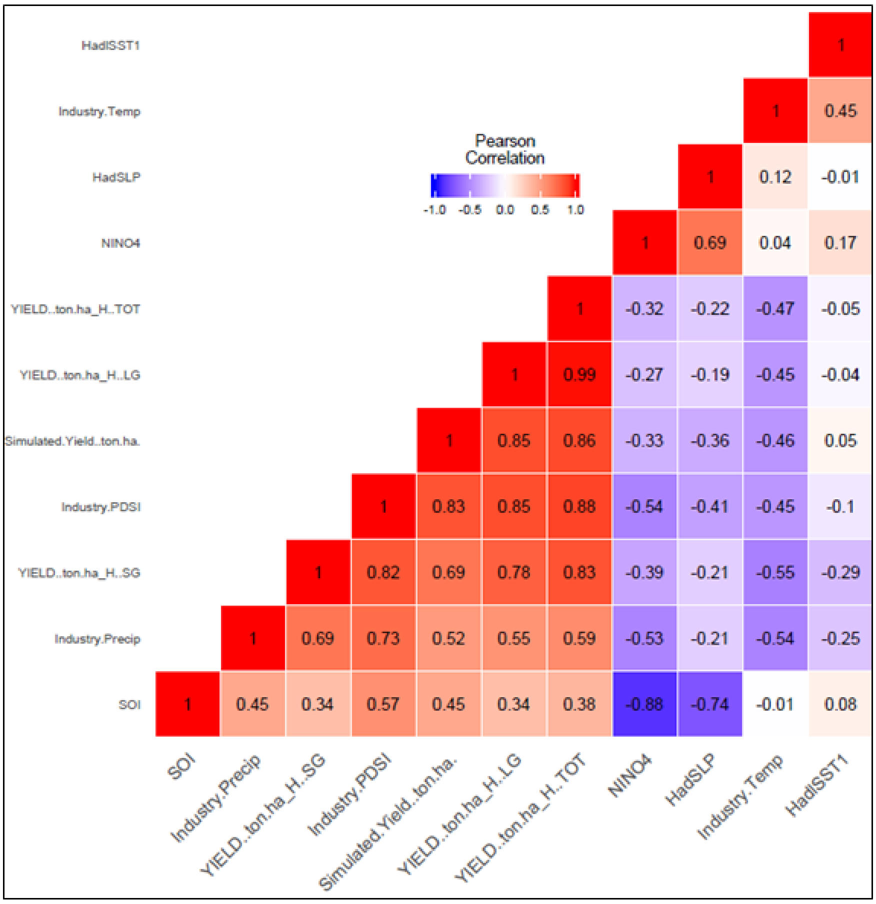

Figure D.1 is similar to Figure 4.12 but for the whole sugar industry of South Africa for the period 1988-2010.

Appendix E

The linear relationship between sugarcane yield and sugarcane-drivers and large-scale climate drivers over SE Africa is illustrated in Table E.1. It can be argued with confidence that rainfall, soil moisture content, surface air temperature and evaporation play an essential role in sugarcane maturing and development through their interdependence, which is integrated in the PDSI. This index (PDSI) is a good proxy for sugarcane yield since it has a strong positive correlation with sugarcane yield and climate (Figure 4.12 and D.1).

Table E.1 is similar to Table 4.3 but for different agro-ecological zones of SA sugar industry where sugarcane yields is a dependant variable and climatic variables and indices are independent variables for the period from 1988-2010.

Northern Irrigated SY					
	Estimate	Std. Error	t-value	p-value	Signif. Codes
(Intercept)	-1.319e+02	2.142e+02	-0.616	0.547	
Northern Irrigated_PDSI	5.078e-02	3.231e-02	1.572	0.137	
Northern Irrigated_Precip	-1.994e-04	2.614e-04	-0.763	0.457	
Northern Irrigated_Temp	-1.750e-03	1.182e-01	-0.015	0.988	
Niño4	-6.162e-02	1.546e-01	-0.399	0.696	
SOI	1.319e-02	1.431e-01	0.092	0.928	
HadISST1	5.320e-02	2.157e-01	0.247	0.809	
HadSLP	1.336e-01	2.115e-01	0.632	0.537	
Northern Irrigated LSG					
	Estimate	Std. Error	t-value	p-value	Signif. Codes
(Intercept)	-7.963e+01	1.136e+02	-0.701	0.4940	
Northern Irrigated_PDSI	4.711e-02	1.713e-02	2.750	0.0149	*
Northern Irrigated_Precip	-2.257e-04	1.386e-04	-1.628	0.1243	
Northern Irrigated_Temp	-5.388e-02	6.266e-02	-0.860	0.4034	
Niño4	1.763e-02	8.195e-02	0.215	0.8326	
SOI	5.649e-02	7.588e-02	0.744	0.4681	
HadISST1	1.137e-01	1.144e-01	0.994	0.3362	
HadSLP	8.161e-02	1.122e-01	0.728	0.4780	
Northern Irrigated SSG					
	Estimate	Std. Error	t-value	p-value	Signif. Codes
(Intercept)	-2.650e+02	2.511e+02	-1.055	0.30808	
Northern Irrigated_PDSI	1.495e-01	3.787e-02	3.947	0.00129	**
Northern Irrigated_Precip	-4.508e-04	3.065e-04	-1.471	0.16197	
Northern Irrigated_Temp	-6.491e-02	1.385e-01	-0.469	0.64612	
Niño4	-1.286e-01	1.812e-01	-0.710	0.48868	
SOI	-1.157e-01	1.678e-01	-0.690	0.50082	
HadISST1	3.196e-02	2.529e-01	0.126	0.90111	
HadSLP	2.667e-01	2.480e-01	1.076	0.29914	

Northern irrigated TOT					
	Estimate	Std. Error	t-value	p-value	Signif. Codes
(Intercept)	-8.019e+01	1.172e+02	-0.684	0.5042	
Northern Irrigated_PDSI	5.694e-02	1.767e-02	3.222	0.0057	**
Northern Irrigated_Precip	-2.361e-04	1.430e-04	-1.651	0.1195	
Northern Irrigated_Temp	-5.268e-02	6.464e-02	-0.815	0.4279	
Niño4	-1.075e-02	8.454e-02	-0.127	0.9005	
SOI	1.430e-02	7.828e-02	0.183	0.8574	
HadISST1	1.070e-01	1.180e-01	0.907	0.3789	
HadSLP	8.231e-02	1.157e-01	0.711	0.4877	

Zululand SY					
	Estimate	Std. Error	t-value	p-value	Signif. Codes
(Intercept)	8.894e+01	8.912e+01	0.998	0.3341	
Zululand_PDSI	4.525e-02	1.495e-02	3.027	0.0085	**
Zululand_Precip	1.759e-05	1.050e-04	0.168	0.8692	
Zululand_Temp	-6.496e-02	6.198e-02	-1.048	0.3112	
Niño4	-7.922e-02	6.477e-02	-1.223	0.2402	
SOI	-8.056e-02	6.705e-02	-1.201	0.2482	
HadISST1	4.734e-02	9.584e-02	0.494	0.6285	
HadSLP	-8.291e-02	8.810e-02	-0.941	0.3616	

Zululand LSG					
	Estimate	Std. Error	t-value	p-value	Signif. Codes
(Intercept)	-1.177e+01	1.185e+02	-0.099	0.92218	
Zululand_PDSI	5.988e-02	1.987e-02	3.013	0.00874	**
Zululand_Precip	1.287e-04	1.396e-04	0.922	0.37104	
Zululand_Temp	-2.395e-02	8.240e-02	-0.291	0.77527	
Niño4	-5.469e-02	8.612e-02	-0.635	0.53495	
SOI	-6.736e-02	8.914e-02	-0.756	0.46155	
HadISST1	-9.051e-03	1.274e-01	-0.071	0.94431	
HadSLP	1.639e-02	1.171e-01	0.140	0.89059	

Zululand SSG					
	Estimate	Std. Error	t-value	p-value	Signif. Codes
(Intercept)	-3.835e+01	2.767e+02	-0.139	0.8916	
Zululand_PDSI	9.239e-02	4.641e-02	1.991	0.0651	.
Zululand_Precip	-2.350e-05	3.259e-04	-0.072	0.9435	
Zululand_Temp	-2.071e-01	1.924e-01	-1.076	0.2987	
Niño4	-3.562e-01	2.011e-01	-1.771	0.0968	.
SOI	-2.558e-01	2.082e-01	-1.229	0.2381	
HadISST1	-7.143e-02	2.976e-01	-0.240	0.8136	
HadSLP	4.748e-02	2.735e-01	0.174	0.8645	

Zululand TOT					
	Estimate	Std. Error	t-value	p-value	Signif. Codes

(Intercept)	-4.778e+01	1.327e+02	-0.360	0.72383	
Zululand_PDSI	6.693e-02	2.226e-02	3.007	0.00885	**
Zululand_Precip	5.167e-05	1.563e-04	0.331	0.74554	
Zululand_Temp	-8.039e-02	9.229e-02	-0.871	0.39749	
Niño4	-1.284e-01	9.646e-02	-1.331	0.20306	
SOI	-9.365e-02	9.984e-02	-0.938	0.36309	
HadlSST1	3.466e-02	1.427e-01	0.243	0.81141	
HadSLP	5.197e-02	1.312e-01	0.396	0.69759	

North Coast SY

	Estimate	Std. Error	t-value	p-value	Signif. Codes
(Intercept)	1.210e+01	2.238e+02	0.054	0.9576	
North Coast_PDSI	3.585e-02	2.269e-02	1.580	0.1349	
North Coast_Precip	2.250e-05	2.485e-04	0.091	0.9291	
North Coast_Temp	-2.975e-01	1.664e-01	-1.789	0.0939	.
Niño4	8.266e-02	1.879e-01	0.440	0.6663	
SOI	1.128e-01	1.723e-01	0.655	0.5227	
HadlSST1	1.589e-01	2.699e-01	0.589	0.5648	
HadSLP	-5.507e-03	2.206e-01	-0.025	0.9804	

North Coast LSG

	Estimate	Std. Error	t-value	p-value	Signif. Codes
(Intercept)	-9.325e+01	1.859e+02	-0.502	0.62318	
North Coast_PDSI	5.824e-02	1.885e-02	3.091	0.00746	**
North Coast_Precip	9.505e-05	2.064e-04	0.460	0.65178	
North Coast_Temp	-1.819e-01	1.382e-01	-1.316	0.20793	
Niño4	1.541e-02	1.561e-01	0.099	0.92268	
SOI	-4.490e-03	1.431e-01	-0.031	0.97539	
HadlSST1	-8.890e-02	2.242e-01	-0.397	0.69728	
HadSLP	1.016e-01	1.833e-01	0.554	0.58747	

North Coast SSG

	Estimate	Std. Error	t-value	p-value	Signif. Codes
(Intercept)	-4.605e+00	2.335e+02	-0.020	0.9845	
North Coast_PDSI	4.679e-02	2.368e-02	1.976	0.0668	.
North Coast_Precip	2.283e-04	2.593e-04	0.880	0.3925	
North Coast_Temp	-1.256e-01	1.736e-01	-0.724	0.4805	
Niño4	-4.963e-02	1.961e-01	-0.253	0.8036	
SOI	-8.794e-02	1.798e-01	-0.489	0.6319	
HadlSST1	-1.580e-01	2.816e-01	-0.561	0.5832	
HadSLP	1.422e-02	2.303e-01	0.062	0.9516	

North Coast TOT

	Estimate	Std. Error	t-value	p-value	Signif. Codes
(Intercept)	-9.250e+01	1.681e+02	-0.550	0.59031	
North Coast_PDSI	5.690e-02	1.705e-02	3.338	0.00449	**
North Coast_Precip	8.276e-05	1.867e-04	0.443	0.66387	

North Coast_Temp	-1.777e-01	1.250e-01	-1.421	0.17567
Niño4	1.217e-03	1.412e-01	0.009	0.99324
SOI	-8.287e-03	1.295e-01	-0.064	0.94981
HadISST1	-8.167e-02	2.028e-01	-0.403	0.69281
HadSLP	1.006e-01	1.658e-01	0.607	0.55317

Midlands SY					
	Estimate	Std. Error	t-value	p-value	Signif. Codes
(Intercept)	-5.212e+01	1.369e+02	-0.381	0.70878	
Midlands_PDSI	6.704e-02	1.891e-02	3.545	0.00294	**
Midlands_Precip	-2.490e-04	1.793e-04	-1.389	0.18518	
Midlands_Temp	-1.022e-01	1.008e-01	-1.014	0.32677	
Niño4	-1.096e-01	1.207e-01	-0.908	0.37808	
SOI	-5.550e-02	1.077e-01	-0.515	0.61383	
HadISST1	2.652e-01	1.638e-01	1.619	0.12633	
HadSLP	5.185e-02	1.349e-01	0.384	0.70618	
Midlands LSG					
	Estimate	Std. Error	t-value	p-value	Signif. Codes
(Intercept)	-1.003e+02	1.749e+02	-0.574	0.5746	
Midlands_PDSI	6.666e-02	2.415e-02	2.760	0.0146	*
Midlands_Precip	-2.003e-05	2.290e-04	-0.087	0.9315	
Midlands_Temp	-2.915e-02	1.287e-01	-0.226	0.8239	
Niño4	-8.398e-02	1.541e-01	-0.545	0.5939	
SOI	-9.834e-02	1.375e-01	-0.715	0.4856	
HadISST1	1.721e-01	2.092e-01	0.822	0.4238	
HadSLP	9.978e-02	1.723e-01	0.579	0.5711	
Midlands SSG					
	Estimate	Std. Error	t-value	p-value	Signif. Codes
(Intercept)	-5.020e+02	3.323e+02	-1.511	0.1516	
Midlands_PDSI	8.646e-02	4.589e-02	1.884	0.0791	.
Midlands_Precip	1.010e-04	4.351e-04	0.232	0.8195	
Midlands_Temp	4.848e-01	2.446e-01	1.982	0.0661	.
Niño4	1.541e-01	2.929e-01	0.526	0.6066	
SOI	1.582e-01	2.614e-01	0.605	0.5540	
HadISST1	-2.581e-01	3.976e-01	-0.649	0.5260	
HadSLP	4.957e-01	3.275e-01	1.514	0.1508	
Midlands TOT					
	Estimate	Std. Error	t-value	p-value	Signif. Codes
(Intercept)	-1.520e+02	1.714e+02	-0.887	0.38909	
Midlands_PDSI	6.975e-02	2.366e-02	2.947	0.00999	**
Midlands_Precip	-2.273e-05	2.244e-04	-0.101	0.92066	
Midlands_Temp	2.512e-02	1.261e-01	0.199	0.84484	
Niño4	-7.562e-02	1.511e-01	-0.501	0.62392	

SOI	-8.013e-02	1.348e-01	-0.595	0.56101	
HadISST1	1.649e-01	2.050e-01	0.804	0.43384	
HadSLP	1.498e-01	1.689e-01	0.887	0.38903	

South Coast SY

	Estimate	Std. Error	t-value	p-value	Signif. codes
(Intercept)	1.982e+02	2.156e+02	0.919	0.37267	
South Coast_PDSI	6.698e-02	2.137e-02	3.135	0.00681	**
South Coast_Precip	2.772e-04	2.712e-04	1.022	0.32282	
South Coast_Temp	-1.464e-01	1.815e-01	-0.806	0.43266	
Niño4	2.844e-01	1.611e-01	1.766	0.09781	.
SOI	1.910e-01	1.498e-01	1.275	0.22185	
HadISST1	2.493e-01	2.266e-01	1.100	0.28855	
HadSLP	-1.945e-01	2.134e-01	-0.911	0.37648	

South Coast LSG

	Estimate	Std. Error	t-value	p-value	Signif. Codes
(Intercept)	8.809e+01	2.111e+02	0.417	0.68242	
South Coast_PDSI	6.931e-02	2.092e-02	3.313	0.00473	**
South Coast_Precip	1.369e-05	2.655e-04	0.052	0.95955	
South Coast_Temp	-1.816e-01	1.777e-01	-1.022	0.32306	
Niño4	1.374e-01	1.577e-01	0.871	0.39731	
SOI	1.274e-01	1.467e-01	0.868	0.39890	
HadISST1	4.206e-02	2.218e-01	0.190	0.85218	
HadSLP	-8.017e-02	2.089e-01	-0.384	0.70657	

South Coast SSG

	Estimate	Std. Error	t-value	p-value	Signif. Codes
(Intercept)	4.728e+02	2.067e+02	2.287	0.0371	*
South Coast_PDSI	5.443e-02	2.048e-02	2.658	0.0179	*
South Coast_Precip	2.224e-04	2.600e-04	0.856	0.4057	
South Coast_Temp	-3.350e-01	1.740e-01	-1.925	0.0734	.
Niño4	-8.572e-02	1.544e-01	-0.555	0.5870	
SOI	-2.739e-01	1.437e-01	-1.907	0.0759	.
HadISST1	1.863e-01	2.172e-01	0.857	0.4047	
HadSLP	-4.602e-01	2.046e-01	-2.249	0.0399	*

South Coast TOT

	Estimate	Std. Error	t-value	p-value	Signif. Codes
(Intercept)	1.329e+02	1.977e+02	0.672	0.51162	
South Coast_PDSI	6.668e-02	1.959e-02	3.404	0.00392	**
South Coast_Precip	4.523e-05	2.486e-04	0.182	0.85807	
South Coast_Temp	-2.015e-01	1.664e-01	-1.211	0.24474	
Niño4	1.125e-01	1.477e-01	0.762	0.45791	
SOI	8.053e-02	1.374e-01	0.586	0.56644	
HadISST1	6.717e-02	2.077e-01	0.323	0.75086	
HadSLP	-1.246e-01	1.956e-01	-0.637	0.53376	

SA Industry SY

	Estimate	Std. Error	t-value	p-value	Signif. codes
(Intercept)	-1.570e+01	1.157e+02	-0.136	0.89391	
Industry_Precip	-1.623e-04	1.910e-04	-0.850	0.40883	
Industry_Temp	-1.198e-01	8.266e-02	-1.449	0.16797	
Industry_PDSI	7.329e-02	1.855e-02	3.951	0.00128	**
Niño4	3.643e-02	8.896e-02	0.409	0.68797	
SOI	5.111e-02	7.952e-02	0.643	0.53012	
HadSLP	1.912e-02	1.144e-01	0.167	0.86947	
HadlSST1	1.434e-01	1.208e-01	1.187	0.25375	

SA Industry LSG

	Estimate	Std. Error	t-value	p-value	Signif. Codes
(Intercept)	-9.322e+01	1.247e+02	-0.748	0.466238	
Industry_Precip	-1.938e-04	2.058e-04	-0.942	0.361149	
Industry_Temp	-7.334e-02	8.905e-02	-0.824	0.423072	
Industry_PDSI	9.206e-02	1.998e-02	4.607	0.000342	***
Niño4	3.244e-02	9.584e-02	0.338	0.739703	
SOI	2.963e-02	8.567e-02	0.346	0.734269	
HadSLP	9.649e-02	1.232e-01	0.783	0.445839	
HadlSST1	5.513e-02	1.301e-01	0.424	0.677821	

SA Industry SSG

	Estimate	Std. Error	t-value	p-value	Signif. codes
(Intercept)	-1.022e+02	1.725e+02	-0.592	0.56248	
Industry_Precip	-1.273e-05	2.846e-04	-0.045	0.96491	
Industry_Temp	-1.075e-01	1.232e-01	-0.873	0.39645	
Industry_PDSI	9.398e-02	2.764e-02	3.400	0.00396	**
Niño4	-3.965e-02	1.326e-01	-0.299	0.76898	
SOI	-2.096e-02	1.185e-01	-0.177	0.86195	
HadSLP	1.082e-01	1.705e-01	0.634	0.53535	
HadlSST1	-6.078e-02	1.800e-01	-0.338	0.74031	

SA Industry TOT

	Estimate	Std. Error	t-value	p-value	Signif. codes
(Intercept)	-1.084e+02	1.132e+02	-0.958	0.353366	
Industry_Precip	-1.987e-04	1.868e-04	-1.064	0.304352	
Industry_Temp	-8.564e-02	8.085e-02	-1.059	0.306244	
Industry_PDSI	9.176e-02	1.814e-02	5.057	0.000142	***
Niño4	1.206e-02	8.701e-02	0.139	0.891565	
SOI	2.697e-02	7.778e-02	0.347	0.733626	
HadSLP	1.113e-01	1.119e-01	0.994	0.335779	
HadlSST1	7.147e-02	1.181e-01	0.605	0.554278	

*Signif. codes: 0 '***' 0.001 '**' 0.01 '*' 0.05 '.' 0.1 ' ' 1 where these numbers from 0-1 are p-values and the order of significance is strongest at* $p - value = 0$ *and denoted with '***' while* $p - value = 1$ *means that the independent variable is not statistically significant.*